UNIVERSITY OF CALIFORNIA

Los Angeles

The Functional Role of ACOT7 in Head and Neck Squamous Cell Carcinoma

A dissertation submitted in partial satisfaction of the

requirements for the degree Doctor of Philosophy

in Oral Biology

by

Zhenning Jin

2021

ABSTRACT OF THE DISSERTATION

The Functional Role of ACOT7 in

Head and Neck Squamous Cell Carcinoma

by

Zhenning Jin

Doctor of Philosophy in Oral Biology

University of California, Los Angeles, 2021

Professor Shen Hu, Chair

The initiation and development of head and neck squamous cell carcinoma (HNSCC) is a complex process, but the underlying mechanisms remain unclear. In this study, we found acyl-CoA thioesterase 7 (ACOT7), a novel metabolic enzyme, was significantly upregulated in HNSCC tumor tissues *versus* the adjacent normal tissues and in HNSCC cell lines *versus* normal human oral keratinocytes (NHOK). HNSCC patients with high ACOT7 expression suffered from unfavorable disease-free and overall survival rates compared to those with low ACOT7 expression, which was also observed in many other types of human cancers. Silencing ACOT7 significantly inhibited the proliferation, migration, invasion, and tumor-sphere formation

of HNSCC cells, whereas overexpressing ACOT7 significantly promoted the proliferation, migration, invasion, and tumor sphere formation of HNSCC cells. Meanwhile, arachidonic acid, the product of ACOT7 enzymatic reaction, also had a promoting effect on the proliferation, colony formation, and migration of HNSCC cells. Furthermore, we demonstrated that MYC transcriptionally upregulated the expression of ACOT7 in HNSCC cells, whereas MYC inhibitor significantly suppressed ACOT7 expression in a dose-dependent manner. Lastly, RNA-sequencing, followed by functional pathway analysis, revealed that p53 signaling was one of the downstream target pathways of ACOT7 in HNSCC cells. Using Western blot analysis and immunofluorescence, we demonstrated that ACOT7 downregulation, through arachidonic acid, significantly prohibited AKT but not phospho-AKT, which in turn inhibited the expression of phospho-MDM2 but not total MDM2 and led to the upregulation of p53 in HNSCC cells. In conclusion, our studies demonstrated the functional significance of ACOT7 and the related regulatory pathway of MYC-ACOT7-AKT-MDM2-p53 axis in promoting HNSCC progression. Our findings revealed novel metabolic mechanisms in HNSCC and target genes with therapeutic interventions.

The dissertation of Zhenning Jin is approved.

Diana V. Messadi

Flavia Q. Pirih

Yong Kim

Shen Hu, Committee Chair

University of California, Los Angeles

2021

TABLE OF CONTENTS

CHAPTER ONE

CHAPTER TWO

LIST OF FIGURES

ACKNOWLEDGEMENTS

This dissertation would not be possible without the generous support and help from many people throughout my Ph.D. study. First and foremost, I would like to thank Dr. Shen Hu for his mentorship, guidance, insight, as well as support. I want to thank my committee members, Dr. Diana Messadi, Dr. Flavia Pirih, and Dr. Yong Kim, for their guidance, advice, and encouragement. It is my great honor to have them as my committee members. I want to thank Mr. Matthew Dingman at the UCLA School of Dentistry, Division of Oral Biology and Medicine, for his assistance with my academic requirements. Many thanks to all the lab mates of Dr. Shen Hu's lab. Last but not least, I would like to acknowledge my family members for their support for my dream of accomplishing my Ph.D. studies.

BIOGRAPHICAL SKETCH	
NAME Jin, Zhenning	**POSITION TITLE** Graduate Student in Division of Oral Biology and Medicine

Education/ Training

INSTITUTION	**DEGREE**	**Completion Date (MM/YYYY))**	**FIELD OF STUDY**
Sichuan University	D.D.S.	06/2016	Dentistry
University of California, Los Angeles	M.S.	06/2019	Oral Biology, Dentistry
University of California, Los Angeles	Ph.D.	*In progress*	Oral Biology, Dentistry

A. Personal Statement

I am currently an Oral Biology Ph.D. student, conducting head and neck cancer research in Dr. Shen Hu's lab at the UCLA School of Dentistry since 2017. As one of the top dental schools worldwide, UCLA School of Dentistry has focused on achieving and maintaining excellence in four main areas: comprehensive dental education, cutting-edge research, quality patient care, and public services. The academic settings in our school have offered me an excellent opportunity to learn new knowledge and biotech skills, write research proposals, design research projects, and write research articles. Before I came to the United States, I graduated from West China School of Stomatology, one of the top dental schools in China. These undergraduate and graduate studies helped me develop my research skills and broaden my basic and clinical knowledge. I have collaborated with my teammates on ~ 15 research projects in the past few years and learned how to conduct a research project independently with feasible methods. The focus of my Ph.D. project is to demonstrate the functional role of the metabolic enzyme ACOT7 in head and neck cancer. My studies may lead to novel targets for therapeutic applications in head and neck cancer.

B. Publications

1. Cui, L., Zhao, X., **Jin, Z.**, Wang, H., Yang, S. F., & Hu, S. (2021). Melatonin modulates metabolic remodeling in HNSCC by suppressing MTHFD1L-formate axis. *J Pineal Res*, 71(4), e12767.
2. **Jin, Z.**, Chai, Y. D., & Hu, S. (2021). Fatty Acid Metabolism and Cancer. *Adv Exp Med Biol*,

1280, 231-241.
3. **Jin, Z.**, Zhao, X., Cui, L., Xu, X., Zhao, Y., Younai, F., & Hu, S. (2020). UBE2C promotes the progression of head and neck squamous cell carcinoma. *Biochem Biophys Res Commun*, 523(2), 389-397.
4. Chen, H., Liu, X., **Jin, Z.**, Gou, C., Liang, M., Cui, L., & Zhao, X. (2018). A three miRNAs signature for predicting the transformation of oral leukoplakia to oral squamous cell carcinoma. *American Journal of Cancer Research*, 8(8), 1403-1413.
5. Zhou, X., Chen, D., **Jin, Z.**, et al. (2017). Investigation of the effect of nuclear factor κB on inflammatory cell recruitment phenotype of oral cancer associated macrophage. *Shanghai Journal of Stomatology*, 26(2): 151-155.
6. Deng Y, Wang C, **Jin, Z.**, et al. (2016). Comparison of the GOHAI and OHIP-14 as Measures of the Oral Health-Related Quality of Life of Middle-aged Population in Southwest China. *International Journal of Stomatology*, 43(6):632-635.

CHAPTER ONE: THE FUNCTIONAL ROLE OF ACOT7 IN HNSCC

1 INTRODUCTION

1.1 Head and neck squamous cell carcinoma (HNSCC)

1.1.1 Prevalence of HNSCC

Head and neck cancer (HNC) is one of the most common malignant cancers globally, leading to severe health issues in many developed and developing countries. Currently, it is the 8th most common cancer affecting men in the United States because of a rising epidemic of oropharynx cancer (tonsil and tongue base) [1]. HNC usually begins in the mucosal surfaces of various anatomical sites in the head and neck, including paranasal sinuses, nasal cavity, oral cavity, tongue, salivary glands, larynx, and pharynx [2]. The most common pathological type of HNC is squamous cell carcinoma (HNSCC). In the United States, the reported cases of HNSCC is approximately 4% of all cancer cases [3]. According to the latest Cancer Statistics, in 2021, scientists estimated that about over 68,000 men and women would be diagnosed with HNC [3]. Males have a significantly higher incidence rate than females, ranging from 2:1 to 4:1 [4]. The incidence rate in patients varies considerably in different regions. For example, nasopharyngeal cancer is more common in Hong Kong. Mouth and tongue cancers are the most common pathological HNSCC types in the Indian subcontinent [5]. Moreover, the incidence is even different in the various ethnic groups. For instance, the incidence rate of laryngeal cancer is

significantly 50% higher in African American men than in white men [6].

1.1.2 Risk factors of HNSCC

Alcohol and tobacco consumption are the two most significant risk factors for HNSCC, accounting for 75% of all HNSCC cases [7]. Most HNSCC cases in the mouth and voice box are developed because of alcohol and tobacco use [8]. Human papillomavirus (HPV) is another important risk factor of HNSCC, which is detected in about 25% of all HNSCC cases, and the infection with HPV, especially HPV type 16, is the leading risk factor for oropharyngeal (OP) squamous cell carcinoma, compared with the HNSCC cases derived from other regions [9, 10]. Other known risk factors for HNSCC include genomic changes, genetic factors, radiation exposure, Epstein-Barr (EB) virus infection, and occupational exposure [11-13].

1.1.3 TNM Staging of HNSCC

The tumor size, node, metastasis (TNM) staging system allows clinicians to categorize tumors of the head and neck region to assess disease status, prognosis, and management [14]. Three categories comprise the TNM staging system. T (tumor) refers to the size and extent of the primary tumor. N (node) refers to the involvement of lymph nodes near the primary tumor. M (metastasis) refers to the absence or presence of distant metastases. The clinical information that can assist staging assessment includes physical exam, radiographic, intraoperative, and pathologic testing [14]. Many changes have been made on the recently published 8th edition TNM classification of the American Joint Committee on Cancer (AJCC) and Union for

International Cancer Control (UICC) cancer staging manuals, reflecting the understanding of the pathophysiology of HNSCC [15]. Other factors, such as biomarkers and molecular studies, have not been included in the staging of HNSCC, which may lead to a more comprehensive guide, if adopted, in the future.

1.1.4 Molecular mechanisms of HNSCC

HNSCC formation is a complex and multistep process involving increased genetic instability, altered expression of oncogenes and tumor suppressor genes, loss of cellular organization, and so on [16]. Research on the molecular and genetic alterations in the pathology of HNSCC will lead to a complete understanding of HNSCC mechanisms and facilitate the development of therapeutic treatment for HNSCC [17]. P53 functions as a tumor suppressor by regulating its downstream pathways, including cell cycle, apoptosis, cellular senescence, and DNA repair and damage prevention [18]. Normal TP53 function is lost in most cancers through gene mutation or genetic deletion. TP53 mutations are significantly associated with short survival time and elevated tumor resistance to radiotherapy and chemotherapy in HNSCC patients [19]. Overexpression of epidermal growth factor receptor (EGFR) was observed in approximately 90% of HNSCC patients, leading to tumorigenicity, therapy resistance, and unfavorable survival rates [20, 21]. The connection between HPV and HNSCC cases has also been established after many years' research [22]. The most common type of HPV is HPV-16, which is detected in 90-95% of HPV-positive cases [23]. Nevertheless, the molecular

mechanisms of HNSCC remain largely unknown. Therefore, it is critical to continue studying the molecular events in HNSCC and discover potential targets for improved therapy of HNSCC patients.

1.1.5 Treatments of HNSCC

Currently, the therapeutic treatments for HNSCC patients include surgery, chemotherapy, radiotherapy, immunotherapy, and molecular-target therapies [24, 25]. The treatment plan for each patient varies depending on the location of the tumor, the stage of cancer, and the patient's age and general health. The main surgery processes of head and neck cancer include laser technology, excision, lymph node dissection or neck dissection, and reconstructive surgery. Approximately 40% of HNSCC patients cases present with early-stage disease, requiring single treatment, such as surgery or radiotherapy [26]. For the advanced stage HNSCC, chemotherapy is commonly used. Palliative chemotherapy and the epidermal growth factor receptor inhibitor, cetuximab, are the main components of treatment for patients with recurrent or metastatic tumor (R/M HNSCC) [1]. Platinum chemotherapy may be combined with cetuximab or 5-fluorouracil, leading to improved overall survival [1]. Other drugs commonly used in treating R/M HNSCC include docetaxel, paclitaxel, cetuximab, capecitabine, pemetrexed, and methotrexate [1]. New therapies, such as mTOR inhibitors, anti-angiogenic agents, and IGF1R inhibitors, are under investigation, which may be suitable for clinical applications in the future [1].

Although there have been numerous advances in HNSCC diagnosis and treatment in the past several years, it remains a long way to go for treating HNSCC patients sufficiently, and the prognosis and survival of HNSCC patients remain poor [27].

1.2 Acyl-CoA thioesterases (ACOTs)

Acyl-CoA thioesterases (ACOTs) are a specific group of enzymes involving fatty acid metabolism. Their function is to catalyze the hydrolysis of acyl-CoAs to free fatty acid and coenzyme A (CoASH), regulating lipid metabolism by keeping the balance between intracellular levels of acyl-CoAs, free fatty acids, and CoASH [28]. The catalytic reactions of different ACOTs are localized in various cellular compartments, such as endoplasmic reticulum, cytosol, mitochondria, and peroxisomes [28]. Till now, 13 mammalian genes have been identified as ACOT superfamily members, which are highly regulated by peroxisome proliferator-activated receptors (PPARs), and other nutritional factors involved in lipid metabolism [29]. Depending on the molecular mass of these enzymes, ACOTs are mainly divided into two distinct types, which are not structurally similar and do not share sequence homology [29-31]. Type I ACOTs are characterized by a molecular weight of approximately 40kDa and their robust response to peroxisome proliferator treatment, while the molecular weight of Type II ACOTs is around 110-150kDa with variable responses to peroxisome proliferators [32]. Type I ACOTs are mainly localized to the cytosol (ACOT1), mitochondria (ACOT2), and peroxisomes (ACOT3-ACOT6) [33, 34]. The oligomeric Type II ACOTs (ACOT7, ACOT8, ACOT9, ACOT11, ACOT12, ACOT13)

have different cellular locations depending on their isoforms [35, 36]. Even though the detailed biochemical characterization of several ACOT family members has been identified, these enzymes are now viewed as vital metabolic regulators in health and diseases [37].

1.3 Acyl-CoA thioesterase 7 (ACOT7)

Acyl-CoA thioesterase 7 (ACOT7) is one of the significant isoforms of the ACOT family, catalyzing the hydrolysis of fatty acyl-CoAs to free fatty acids and CoA-SH. In humans, the coding gene location of ACOT7 is localized in chromosome 1 (1p36.31). This special enzyme, ACOT7, is localized in the cytosol and highly expressed in brain and testis [38, 39]. The primary function of ACOT7 is the hydrolysis of arachidonoyl-CoA (AA-CoA) to arachidonic acid (AA) and CoA [29]. However, its functional role in HNSCC remains unknown. In acute myeloid leukemia, patients with high ACOT7 expression have a poorer prognosis than patients with low ACOT7 expression [40]. The increased expression levels of ACOT7 also indicated unfavorable outcomes in both chemotherapy-only patient group and hematopoietic stem cell transplantation (HSCT) patient group [40]. In addition, neurons have an exceptionally high ACOT7 activity, which represents a critical regulatory point in neural fatty acid metabolism, preventing neurotoxicity by limiting the access of long-chain acyl-CoAs [41]. In the study, ACOT7 KO mice exhibit neurodegeneration and neurological/behavioral deficits, indicating the critical role of ACOT7 in maintaining neuronal fatty acid homeostasis [41]. Lastly, *Jung et al.* pointed out the function of ACOT7 in cell cycle progression by regulating PKCζ–p53–p21 signaling pathway

without a DNA damage response [29]. In breast and lung cancer cells, they also demonstrated a synergistic effect of silencing ACOT7 in combination with either IR or doxorubicin on cancer cell proliferation [29]. ACOT7 overexpression also altered the production of prostaglandins D2 and E2 in macrophages *in vitro*, predicting that it may be a therapeutic target in inflammatory disease [42].

In this chapter, we hypothesize that ACOT7 is overexpressed in HNSCC and promotes the progression of HNSCC. We mainly aim to evaluate the ACOT7 expression in various human cancers, investigate its clinical significance on cancer patients' prognosis, and identify the functional role of ACOT7 in HNSCC. The data from the TCGA and GEO databases were used to analyze the expression levels of ACOT7 in human cancers. X-tile software was applied for clinical significance evaluation. Immunohistochemistry (IHC) of tissue microarray (TMA) sections was performed to investigate the expression levels of ACOT7 in HNSCC and normal tissues. To identify the functional role of ACOT7, we silenced and overexpressed ACOT7 in HNSCC cell lines *in vitro* and identified related effects on the malignant phenotypes, morphology, and cell cycle of HNSCC cells.

2 MATERIALS AND METHODS

Data source and differential expression analysis

The expression levels of ACOT7 in HNSCC and normal tissues were investigated based on the NCBI Gene Expression Omnibus (GEO) (http://www.ncbi.nlm.nih.gov/geo/). The accession numbers from the GEO databases were GSE6791, GSE9844, GSE25099, GSE30784, GSE31056, GSE37991, and GSE74530. The clinical information and RNASeq V2 datasets of cancer patients were obtained from The Cancer Genome Altas (TCGA) databases (https://tcga data.nci.nih.gov/tcga/) to analyze the clinical significance of ACOT7 in cancers. The mRNA expression levels were log2-transformed, and the X-tile software (https://medicine.yale.edu/lab/rimm/research/software.aspx) was applied to determine the best cutoff point to divide the cancer patients into high/low ACOT7 expression groups. Kaplan-Meier overall survival curves were generated for the patients whose follow-up data were available. The log-rank test was used to determine the survival differences between the two groups.

Immunohistochemistry (IHC)

The tissue microarray (TMA) sections were obtained from US Biomax, Inc. (US Biomax, MD, USA) for IHC analyses. Formalin-fixed paraffin-embedded sections were deparaffinized by sequential washing with xylene, 100% ethanol, 95% ethanol, 80% ethanol, and PBS. The sections were incubated with 0.3% H2O2 in methanol for 5 min to quench the endogenous peroxidase activity. The slides were blocked in PBS with 5% BSA for 30 min and then incubated

overnight with a 1:50 dilution of anti-ACOT7 primary antibody (Invitrogen, CA, USA) at 4°C. After sections were washed with PBS, they were incubated with horseradish peroxidase (HRP)-conjugated goat anti-rabbit IgG (Invitrogen, CA, USA) for 2 h at room temperature.

Cell culture

UMSCC1, UMSCC6, UMSCC23, UM1, and UM2 cell lines were cultured in the Dulbecco's modified eagle medium (DMEM) (Life Technologies, CA, USA) supplemented with 10% fetal bovine serum (FBS) (Life Technologies, CA, USA), penicillin (100U/ml) and streptomycin (100μg/ml) (Life Technologies, CA, USA). Normal human oral keratinocytes (NHOKs) were cultured in EpiLife medium supplemented with the human keratinocyte growth supplement (Invitrogen, CA, USA). The temperature was controlled at 37 °C, and the CO_2 concentration was set 5% in a humidified cell culture incubator. The medium was changed every two days, and the cells were passaged when reaching 90-95% confluence. UMSCC1 and UMSCC6 cell lines were selected as *in vitro* models in this project. Both UMSCC1 and UMSCC6 cell lines are HPV negative.

siRNA transfection

UMSCC1 and UMSCC6 cells were plated in the 6-well plates before transfection. Cancer cells were transfected with siRNAs (Sigma-Aldrich, MO, USA) using the RNAiMAX transfection reagent (Invitrogen, CA, USA) following the manufacturer's protocols. siRNA (Sigma-Aldrich, MO, USA) was mixed with the transfection reagent, respectively, and added to the cell culture

medium. siCTRL (Sigma-Aldrich, MO, USA) was used as the negative control. After 48-72 h incubation following the transfection, the cells were collected for further experiments.

Production of ACOT7 lentiviral vectors

Lenti-ORF clone of ACOT7 (mGFP-tagged)-human acyl-CoA thioesterase 7 (ACOT7) was obtained from OriGene Technologies, Inc. (OriGene, MD, USA). Lentiviral vectors and packaging vectors were transfected into 293 FT cells. The viral supernatant from the cell culture was harvested 48 h and 72 h after transfection. After being combined and filtered through a 0.45 μm filter to remove cellular debris, the lentivirus was stored at -80°C for further use, and the titer of lentivirus was determined. The empty vector was packaged as a negative control. The cancer cells were infected with the lentivirus at a multiplicity of infection of 5. Following 48-72 h incubation, the transfected cells were collected for further experiments.

MTT assay

After serum starvation for 24 h, the collected cells were seeded into a 96-well plate at a density of 4,000 cells per well in 100 μl complete medium. After incubating the cells overnight, at the indicated time points of the following days, 20 μl of MTT (Sigma-Aldrich, MO, USA) dissolved in PBS at 5 mg/ml was added into each well. Following 4 h incubation at 37 °C, the supernatant was discarded, and the precipitate was dissolved in 200 μl of dimethyl sulfoxide (DMSO, Sigma-Aldrich, MO, USA). The absorbance was read using a Synergy VT microplate reader (BioTek Instruments, VT, USA) at 570 nm after being resolved. The assay was repeated

in triplicate.

Cell colony formation assay

Cells were collected and resuspended in the complete DMEM and then plated into 6-well plates at a density of 3,000 cells per well in a 2 ml medium. After incubation at 37 °C for 14 days, the cells were washed three times with PBS (Life Technologies, CA, USA), fixed with 3.7% formaldehyde (Fisher Scientific, PA, USA), and stained with 0.1% crystal violet for 30 min (Fisher Scientific, PA, USA). Cells were photographed and counted using the Image J software (Fiji Version, National Institutes of Health, MD, USA). The assay was repeated in triplicate.

5-ethynyl-2'-deoxyuridine assay

The Click-iT EdU Cell Proliferation Kit (Invitrogen, CA, USA) was used to evaluate cell proliferation. According to the manufacturer's imaging protocol, the cells were plated on coverslips at the desired density and incubated overnight. On the next day, the cells were treated with 10 mM EdU solution for 2 h at 37 °C and fixed with 3.7% formaldehyde in PBS for 15 mins at room temperature. After being washed twice with 3% BSA in PBS, the cells were treated with 0.5% Triton X-100 (Sigma-Aldrich, MO, USA) in PBS for 20 min. Following washed twice with 3% BSA in PBS, the cells were incubated with 0.5 ml of Click-iT® reaction cocktail in each well protected from light for 30 min at room temperature. Hoechst 33342 solution (the final concentration is 5 μg/ml, Invitrogen, CA, USA) in PBS was applied to stain the cell nuclear for 30 min at room temperature. Images were captured under a REVOLVE 4 upright, inverted,

brightfield, fluorescent microscope (Echo Laboratories, CA, USA). The assay was repeated in triplicate.

Immunofluorescence (IF)

HNSCC cells were fixed using 3.7% paraformaldehyde (Fisher Scientific, PA, USA) in PBS pH 7.4 for 15 min at room temperature. After rinsing with 1x ice-cold PBS 3 times for 5 min each, the coverslips were treated with 0.5% Triton X-100 (Sigma-Aldrich, MO, USA) in PBS at room temperature for 20 min. Following repeat the washing steps, the coverslips were blocked with 10% serum (Invitrogen, CA, USA) from the species the secondary antibody for 1h. The fixed cells were incubated in the diluted antibody in blocking buffer in a humidified chamber for 1-1.5 h (1.5h: Proteintech Inc. antibody) at room temperature or overnight at 4°C. On the next day, following the 3 times PBS washing steps, the coverslips were rinsed in the secondary antibody in blocking buffer at room temperature for 1 h in a dark, moist environment. 0.1-1 µg/mL Hoechst 33342 solution (Thermo Scientific, CA, USA) or DAPI (DNA stain) (Thermo Scientific, CA, USA) was applied for nuclear staining steps. Images were captured under a REVOLVE 4 fluorescent Microscope (Echo Laboratories, CA, USA). The assay was repeated in triplicate.

Migration assay

The migration assay was performed using the Transwell chambers (Corning, NY, USA). After 24 h serum starvation, the cells were collected, resuspended in the serum-free DMEM

medium, and added to the upper chamber of Transwell inserts (the final concentration is 1×10^5 cells/well). DMEM with 10% FBS was used as a chemoattractant in the lower chamber. After 24 h, the cells migrating through the membrane were fixed and stained with 0.1% crystal violet for 30 min (Fisher Scientific, PA, USA). The cell numbers per well under light microscopy (Echo Laboratories, CA, USA) in various random fields were calculated using the Image J software (Fiji Version, National Institutes of Health, MD, USA). The assay was repeated in triplicate.

Transwell Matrigel invasion assay

The Transwell Matrigel-coated chambers (Corning, NY, USA) were used to assess the cellular invasive ability. After 24 h starvation, the HNSCC cells (5×10^5 cells/well) were trypsinized, resuspended in the serum-free medium, and added to the upper chamber of the Transwell inserts. DMEM supplemented with 10% FBS was used in the lower chamber to serve as a chemoattractant. Following 48 h incubation, cells invaded through the membrane were fixed and stained with 0.1% crystal violet solution. The cell numbers of the invaded area per field under light microscopy in four random fields were counted using the Image J software. The assay was repeated in triplicate.

Cell cycle analysis

HNSCC cancer cells were siRNA treated or lentivirus treated as described above. The cells were fixed overnight with 75% alcohol. After washed and resuspended in PBS with 1% BSA (Invitrogen, CA, USA) and 0.1% Triton X-100 (Sigma-Aldrich, MO, USA). After finishing all the

steps, 1 µl of FxCycle™ Violet stain (Invitrogen, CA, USA) was added to the sample tubes and mixed well. Following 30 min incubation, the cellular samples were investigated with a flow cytometer (Attune NxT Flow Cytometer, Invitrogen, CA, USA) at 405 nm excitation with a 450/50 bandpass filter. The assay was repeated in triplicate.

Tumor sphere formation assays

UMSCC1 and UMSCC6 cells were cultured in 24-well ultra-low attachment plates at a density of 3,000 cells per well for the tumor sphere assays. Cells were cultured in serum-free DMEM/F12 (Invitrogen, CA, USA) supplemented with 1% B27 supplement (Gibco, NY, USA), 1% N2 supplement (Gibco, NY, USA), penicillin (100U/ml), and streptomycin (100µg/ml) (Life Technologies, CA, USA), human recombinant epidermal growth factor (EGF; 20ng/ml, Gemini Bio, CA, USA), and human recombinant basic fibroblast growth factor (bFGF; 10ng/ml, Gemini Bio, CA, USA), in a humidified 5% CO2 incubator at 37°C. Fresh EGF and bFGF were added to the culture plates every 2 days, and the serum-free medium was changed every other day until the tumor spheres formed. Spheres were counted 1-2 weeks after plating. The assay was repeated in triplicate.

Western blotting

Protein was collected in the RB buffer and was separated with 4-12% Bis-Tris NuPAGE gel. The separated protein in the gel was transferred onto nitrocellulose membrane (Santa Cruz Biotech, CA, USA) via the Trans-blot SD semi-dry transfer cell (Bio-rad, CA, USA). The

membranes were blocked with 5% non-fat milk (Santa Cruz Biotech, CA, USA) within 1 x TBST buffer for 1 h at room temperature. After blocking, the membranes were incubated with the primary antibodies at 4°C overnight. On the second day, after being incubated with the secondary antibodies (Cytiva™ technologies, MA, USA) for 1 h at room temperature, the membranes were detected with the ECL-plus Western blotting detection reagent kit (Cytiva™ technologies, MA, USA). The primary antibodies in this project were listed in supplementary data.

Statistical analysis

Experiments were performed in triplicates in this study unless stated otherwise. Most of the data were calculated as the mean ± standard deviation and analyzed by the independent samples t-test using the GraphPad Prism (version 9, GraphPad Software Inc., CA, USA). Kaplan-Meier method and log-rank test were performed to analyze the differences in survival rates. P values < 0.05 were considered statistically significant.

3 RESULTS

3.1 Transcriptomic analysis of HNSCC and matched normal tissues

3.1.1 ACOT7 is overexpressed in HNSCC

According to the metabolic enzyme analysis between HNSCC cancer patients and normal tissue samples by RNA sequencing, the levels of ACOT7 were found to be significantly higher in HNSCC than normal tissues (****P<0.0001) **(Figure 1A)**. In addition, compared to adjacent control tissues, the expression level of ACOT7 was significantly higher in HNSCC tissues based on eight independent datasets (TCGA-HNSC, GSE 6791, GSE 9844, GSE 25099, GSE 30784, GSE 31056, GSE 37991, GSE 74530) (**P<0.01, ***P<0.001, ****P<0.0001) **(Figure 1B)**. According to the expression analysis in dataset GSE 30784, ACOT7 gene expression was also correlated with HNSCC dysplasia.

3.1.2 ACOT7 is overexpressed in other types of cancers

Based on the TCGA datasets, we also found that compared to the normal controls, ACOT7 was significantly overexpressed in other cancers, including bladder urothelial carcinoma (BLCA), breast invasive carcinoma (BRCA), cervical squamous cell carcinoma, and endo-cervical adenocarcinoma (CESC), cholangiocarcinoma (CHOL), colon adenocarcinoma (COAD), esophageal carcinoma (ESCA), kidney renal clear cell carcinoma (KIRC), liver hepatocellular carcinoma (LIHC), lung adenocarcinoma (LUAD), lung squamous cell carcinoma

(LUSC), pheochromocytoma and paraganglioma (PCPG), prostate adenocarcinoma (PRAD), stomach adenocarcinoma (STAD), stomach and esophagus adenocarcinoma (STES), thyroid cancer (THCA), and uterine corpus endometrial carcinoma (UCEC) ($P<0.001$, $P<0.0001$) **(Figure 2)**.

3.1.3 ACOT7 overexpression is associated with poor prognosis in HNSCC

Based on the TCGA datasets of HNSCC, a significantly worse overall survival rate was observed in the HNSCC patients with high ACOT7 expression than those with low ACOT7 expression ($P=0.0054$) **(Figure 3A)**. The definition of disease-free survival is the time from randomization to recurrence of tumor or death, which is a direct measure of the clinical benefit. After analyzing the data from the TCGA-HNSCC datasets, we found a significantly worse disease-free survival rate in the high ACOT7 expression patient group than that in the low ACOT7 expression patient group ($P=0.0072$) **(Figure 3A)**.

3.1.4 ACOT7 overexpression is associated with poor prognosis in other types of cancers

Besides, high ACOT7 expression was significantly associated with a worse disease-free survival rate in BRCA, CESC, LUAD, LUSC, kidney renal papillary cell carcinoma (KIRP), and sarcoma (SARC) **(Figure 3B)**. Meanwhile, high ACOT7 expression was significantly correlated to a more unfavorable overall survival rate in BLCA, BRCA, KIRP, LUAD, LUSC, and SARC **(Figure 3C)**.

3.1.5 Expression levels of ACOT families in HNSCC

ACOTs are a group of enzymes catalyzing the hydrolysis of activated fatty acids to their corresponding non-esterified (free) fatty acid and coenzyme A (CoASH) [36]. Based on the data from TCGA datasets, the expression levels of ACOT1, ACOT2, ACOT4, ACOT8, ACOT11 between the HNSCC patients' samples and normal controls showed no difference **(Figure 4)**. Our results also revealed that the expression levels of ACOT9 and ACOT13 were significantly increased in HNSCC cancer tissues compared to normal control tissues (****P<0.0001) **(Figure 4)**. However, the ACOT6 expression was considerably lower in HNSCC tissues when compared to the control tissues (****P<0.0001) **(Figure 4)**.

3.1.6 Expression levels of ACOT7 in HNSCC cells

To investigate the potential involvement of ACOT7 in HNSCC progression, we analyzed the expression levels of ACOT7 in HNSCC cell lines, UMSCC1, UMSCC6, UMSCC23, UM1, UM2 and a normal cell line, NHOK **(Figure 5A)**. To test if the exogenous growth factors in the culture condition affect the expression levels of ACOT7, we added epidermal growth factor (EGF) and basic fibroblast factor (FGF) to the culture media for HNSCC cell lines. Our results showed that it was EGF, but not FGF, that induced the ACOT7 expression (****P<0.0001) **(Figure 5B)** in the HNSCC cells. In addition, the localization of ACOT7 in UMSCC1 and UMSCC6 cells was indicated by immunofluorescence **(Figure 5C)**.

3.1.7 ACOT7 is overexpressed in head and neck cancer tissues

The expression levels of ACOT7 on the tissue microarray (TMA) sections of HNSCC and normal tissues were examined by IHC. The results revealed that the staining intensity of ACOT7 in head and neck cancer patients was significantly higher compared to the normal tissues **(Figure 6A)**. Preliminary analysis of the effect of clinicopathologic parameters on ACOT7 expression were also performed **(Figure 6B)**.

3.2 ACOT7 plays a pro-carcinogenic role in HNSCC

3.2.1 ACOT7 downregulation inhibits malignant phenotypes of HNSCC cells *in vitro*

Downregulation of ACOT7 was achieved by transfecting ACOT7 siRNAs (siACOT7#1 and siACOT7#2) into UMSCC1 and UMSCC6. Western Blotting results demonstrated the significant downregulation of ACOT7 expression in siACOT7-treated cells compared to siCTRL-transfected cells (****P<0.0001) **(Figure 7A)**. Immunofluorescence results also revealed that the fluorescence intensity was decreased following ACOT7 downregulation in both UMSCC1 and UMSCC6 cell lines **(Figure 7B)**.

To evaluate the effect of silencing ACOT7 on cancer cell proliferation, MTT, colony formation, and EdU assays were performed. MTT assay demonstrated that the proliferation ability of UMSCC1 and UMSCC6 cells with siACOT7 knockdown was significantly lower compared to the control cells (****P<0.0001) **(Figure 8A)**. After 14-day incubation in the 6-well culture plates, there were significantly fewer colonies formed by siACOT7-treated cells than those by siCTRL-treated cells (****P<0.0001) **(Figure 8B)**. Additionally, the percentage of EdU

positive cells was significantly decreased following ACOT7 downregulation in the UMSCC cell lines (***P<0.001) **(Figure 8C).**

Cell cycle analysis with flow cytometry was performed to determine whether the inhibitory of ACOT7 knockdown on HNSCC cell proliferation is related to cell-cycle control. Silencing ACOT7 was found to significantly downregulate the enrichment of the cells in the S phase (**P<0.01) **(Figure 8D)**.

Transwell migration assays were performed to measure the migration ability of UMSCC1 and UMSCC6 cells with ACOT7 knockdown. Following the fixing and staining steps, our results showed that fewer siACOT7-treated UMSCC1 or UMSCC6 cells were crossing the transwells than the siCTRL-treated UMSCC1 or UMSCC6 cells (****P<0.0001) **(Figure 9A)**.

Matrigel invasion assays were performed to investigate if ACOT7 knockdown inhibits the invasion capability of UMSCC cells. Compared with the cells transfected with siCTRL, the UMSCC1 or UMSCC6 cells transfected with siACOT7 showed significantly decreased numbers of invaded cells crossing the transwells (****P<0.0001) **(Figure 9B)**.

We also observed that ACOT7 downregulation changed the morphology of cancer cells, leading to the failure of the cells attached to the surface of the petri dish **(Figure 10A)**. In addition, the tumor sphere formation assays showed that silencing ACOT7 impaired the UMSCC cells' ability to form tumor spheres (**P<0.01) **(Figure 10B)**.

3.2.2 ACOT7 upregulation promotes malignant phenotypes of HNSCC cells *in vitro*

Lenti-ORF clone of ACOT7 (mGFP-tagged, OriGene Technologies) was used to overexpress the protein in UMSCC1 and UMSCC6 cells. ACOT7 overexpressing lentivirus (ACOT7 OV) was constructed by transfecting the clone into 293 FT cells using the packaging vectors **(Figure 11A)**. Various MOI (the ratio of the number of transducing lentiviral particles to the number of cells) numbers were tested (****P<0.0001) **(Figure 11B)**. Both UMSCC1 and UMSCC6 cells were successfully infected with lentiviral particles, and the expression levels of ACOT7 proteins were significantly increased after lenti-ACOT7 infection (****P<0.0001) **(Figure 11C)**.

MTT, colony formation, and EdU assays were performed to evaluate ACOT7 overexpression on HNSCC cell proliferation. MTT assays showed that the proliferation ability of UMSCC1 and UMSCC6 cells was enhanced after lenti-ACOT7 infection (**P<0.01, ***P<0.001) **(Figure 12A)**. After being incubated in the 6-well culture plates for 14 days, cells with ACOT7 overexpression showed more vital colony-forming ability compared to cells infected with the control lentivirus (****P<0.0001) **(Figure 12B)**. Meanwhile, ACOT7 overexpression led to a significantly higher percentage of EdU positive HNSCC cells (****P<0.0001) **(Figure 12C)**. According to the results of the cell-cycle analysis via flow cytometry, ACOT7 overexpression in UMSCC1 and UMSCC6 slightly elevated the enrichment of the cells in the S phase (*P<0.05) **(Figure 12D)**.

The Transwell migration assays indicated that the ACOT7-overexpressing cells had significantly higher migration capacity than the control cells (***P<0.001) **(Figure 13A)**. Meanwhile, compared to the control cells, both UMSCC1 and UMSCC6 cells with ACOT7 overexpression showed significantly higher invasion potential (***P<0.001) **(Figure 13B)**.

Last, the tumor sphere assays demonstrated that overexpression of ACOT7 in HNSCC cells significantly enhanced the cellular ability to form tumor spheres when compared to the control cells (***P<0.001) **(Figure 14)**.

4 DISCUSSION

The tumorigenesis of HNSCC is a complicated process involving many molecular events, leading to the tumor amplification under an uncontrollable condition. Oncogenes are known to be correlated with the initiation and development of cancer. However, the detailed mechanisms underlying tumor progression remain unclear [43]. ACOT7 is a critical metabolic enzyme belonging to the acyl-coenzyme family [44]. The encoded protein hydrolyzes arachidonoyl-CoA (AA-CoA) to arachidonic acid (AA) and CoA [35]. In this chapter, we have demonstrated that the expression levels of ACOT7 in head and neck tumor tissues are significantly higher compared to the normal tissues based on various datasets from publicly accessible databases. Additionally, the HNSCC patients with higher ACOT7 expression suffered unfavorable disease-free survival and overall survival. Meanwhile, we also analyzed the data of many other types of cancers from the TCGA database, revealing that ACOT7 may also function as a promoter of cancer progression in many other cancers.

The Cancer Genome Atlas (TCGA) is a large-scale cancer genomics program that has harvested and made available genomic sequence, expression, methylation, and copy number variation data on over 20,000 primary cancer and matched normal samples from 33 cancer types [45, 46]. The Gene Expression Omnibus (GEO) (https://www.ncbi.nlm.nih.gov/geo/) is an international publicly accessible database repository for high-throughput microarray, next-generation sequencing, as well as other formats of functional genomic datasets [47]. GEO also

offers several web-based tools and strategies for users to query, analyze, and visualize data [48]. Public access to TCGA and GEO databases helps us better understand the differential gene expression and their clinical significance in cancer. The target gene in this project, ACOT7, was overexpressed in HNSCC tissues compared to the paired normal tissues based on both TCGA and GEO datasets. By analyzing TCGA datasets, we have also found that ACOT7 was significantly overexpressed in 16 other major human cancers and associated with unfavorable clinical outcomes of 12 other human cancers. These findings suggest that ACOT7 upregulation is a common event in human cancers, and ACOT7 overexpression, in general, may lead to unfavorable clinical outcomes.

Compared to the normal epithelial cells, the expression levels of ACOT7 were significantly higher in HNSCC cell lines. Meanwhile, the growth medium for NHOKs contained necessary growth factors EGF and FGF. We hypothesized here that these growth factors may affect the expression levels of ACOT7 in HNSCC cells. Our studies demonstrated that EGF, but not FGF, induced the expression levels of ACOT7 in HNSCC cells. Our IHC analysis of TMA tissue sections also demonstrated that the ACOT7 expression was significantly higher in HNSCC tissues compared to the normal tissues, further implicating the tumor-promoting role of ACOT7 in HNSCC. In addition, effective downregulation of ACOT7 in HNSCC cells significantly suppressed the cell proliferation, migration, invasion, and tumor sphere formation ability. Silencing ACOT7 also changed the cell morphology, detaching the cells from the surface of the

culture dish. Meanwhile, transfecting HNSCC cells with ACOT7 overexpression lentivirus induced the cell proliferation, migration, invasion, and tumor sphere formation capacity. These findings suggest that ACOT7 may play an essential functional role in promoting tumorigenesis in HNSCC. To the best of our knowledge, this is the first study to explore the functional role of ACOT7 in HNSCC.

Acyl-CoA thioesterases are a group of enzymes catalyzing the hydrolysis of acyl-CoA thioesters to non-esterified fatty acid and CoA, which are mainly divided into two separate groups depending on their weight and mass. Some of Acyl-ACOTs are involved in cancer metabolism. For instance, the critical isoform, ACOT1, was associated with poor prognosis in gastric adenocarcinoma [49]. Chenming Ni *et al.* found that ACOT4 played an oncogenic role in pancreatic ductal carcinoma (PDAC), promoting solid tumor formation *in vivo*. Phosphorylation of ACOT4 at S392 by AKT prevented ACOT7 degradation *in vitro* via HSPA1A binding, promoting pancreatic tumorigenesis [50]. ACOT8 and ACOT11 were discovered as novel biomarkers involving metabolic pathways in clear cell renal cell carcinoma (ccRCC) [51]. ACOT12 gain- and loss-of-function studies indicated that ACOT12 suppressed hepatocellular carcinoma (HCC) metastasis and regulated the cellular acetyl-CoA levels and histone acetylation [52].

Previously, ACOT7 was found to function as a critical gene in gastric cancer (GC) patients and to control the cancer progression via the long non-coding RNA NMRAL2P [53]. In

dedifferentiated thyroid cancer (DDTC), significant enrichment of several metabolic genes, including ACOT7, was observed, which was also found to correlate with poorer clinical outcomes [54]. In lung cancer, Liu, Kuan-Ting *et al.* demonstrated upregulation of ACOT7, ACOT11, ACOT13 expression and their association with poor patients' overall survival. However, the induced endoplasmic reticulum (ER) stress could not alter the expression levels of these genes [55]. ACOT7 was also found among the list of the microarray analysis of differentially expressed genes regulating lipid metabolism in melanoma progression [56]. ACOT7 was also observed as mitochondrial-related prognostic biomarkers associated with primary bile acid biosynthesis and tumor microenvironment of hepatocellular carcinoma (HCC) [57]. Lastly, ACOT7 was shown to be responsive to genotoxic stresses such as ionizing radiation (IR) and the anti-cancer drug doxorubicin in time- and dose-dependent manners [29]. Jung, S. *et al.* demonstrated that, in human breast carcinoma and lung carcinoma cell lines *in vitro*, ACOT7 depletion induced cell cycle arrest via activating PKCζ–p53–p21 signaling pathway [29]. These findings suggest that ACOT7 may be a powerful gene for promoting tumorigenesis in HNSCC. Although multiple studies have proved the clinical significance of ACOT7 in several types of cancers, the molecular mechanisms of ACOT7 involved in the initiation and progression of cancers remain largely unknown.

CHAPTER TWO: FUNCTIONAL ROLE OF MYC-ACOT7-AA-AKT-MDM2-P53 AXIS IN HNSCC

1 INTRODUCTION

1.1 MYC and human cancer

MYC, which is overexpressed in many human cancers, has been identified as an oncogene contributing to the progression of 40% of human cancers [58]. In the human genome, the encoding MYC gene localizes in chromosome 8. It controls the downstream genes via binding to the Enhancer box (E-box) sequences, which functions as an important protein binding site [59]. The CANNTG consensus sequences of the E-box are known as the canonical E-boxes [59]. As a master regulator, MYC induces DNA replication and selective gene expression amplification, promoting cell growth and proliferation [60]. MYC may regulate altered metabolic reprogramming during tumorigenesis, involving the biogenesis of ribosomes and mitochondria and the regulation of glucose and glutamine metabolism [58, 61].

In HNSCC, MYC plays a critical role, and its expression is correlated with the patients' poor prognosis [62]. MYC assists tumor chemoresistance, in which suppressing MYC enhanced cisplatin-induced apoptosis in HNSCC cells [63]. MYC is also proved to regulate fatty acid metabolism [64]. Studies have shown that inhibition of MYC is accompanied by the accumulation of intracellular lipid droplets in tumor cells as a direct consequence of mitochondrial dysfunction [65]. It was demonstrated that MYC and HIF-1 regulated glucose

metabolism, such as pyruvate kinase (PKM2), lactate dehydrogenase A (LDHA), and pyruvate dehydrogenase kinase 1 (PDK1), favoring the conversion of glucose to glycolysis [58]. PAK2-c-Myc-PKM2 axis was found to regulate the aerobic glycolysis, proliferation, and chemotherapeutic resistance of HNSCC cells through the Warburg effect [66]. Even though the roles of MYC are well known to some extent, studies are still needed to elucidate its molecular functions in the initiation and progression of HNSCC.

1.2 Arachidonic acid (AA)

Arachidonic acid (AA) is the product of the ACOT7 catalytic reaction, a crucial molecule with functional roles in cell signaling, regulation of cell proliferation, and activation of metabolic enzymes [42]. The major release of AA is derived from activating phospho-lipases$_2$ (PLA_2), one of the important enzymes involved in fatty acid hydrolysis [67]. As one of the dietary n-6 cis polyunsaturated fatty acids, AA may enter the cell membrane, forming the cell membrane phospholipids [68, 69]. Alternatively, AA may be metabolized by the cyclooxygenase, lipoxygenase, and cytochrome P450 pathways into many other metabolites, such as eicosanoids, possessing potent biological activities [70].

The studies on the functional role of AA in cancer are limited. Many cancers and pre-cancerous lesions depend on switching membrane-bound AA to eicosanoids for survival, growth, and spread, indicating that minimizing membrane AA content may be a potential strategy for controlling cancer [71].In breast cancer, it is demonstrated that AA induces NFκB-

DNA binding activity via PI3K-AKT dependent pathway, mediating FAK activation, adhesion, and migration *in vitro* [68]. High levels of palmitic acid (PA) or AA can stimulate cancer progression [72]. In prostate cancer (CaP) cell line, adding extra AA upregulated the transendothelial migration of PC3-GFP cells through inducing an important molecule, ephrin receptor A2 (EphA2), to mediate the functions of AKT, Src, and focal adhesion kinase (FAK) pathways [73]. Although functions of AA in several types of cancers have been identified, it is not known how AA is involved in the progression of HNSCC.

1.3 AKT-MDM2-p53 axis

AKT, a protein serine/threonine kinase, plays a significant role in regulating cell death and apoptosis [74]. AKT activation through the phosphatidylinositide 3'-OH kinase (PI3K) signaling cascade efficiently inhibits apoptosis stimulated by death stimuli [74]. Several AKT substrates have been identified to assist the function of this kinase in inducing cell proliferation and blocking apoptosis.

P53 is significant in DNA damage-induced apoptosis and cell cycle arrest in response to cellular stress and the activation of other oncogenes, protecting the body from the harm of damaged cells [75, 76]. Murine double minute (MDM2), a ubiquitin ligase for p53, plays a central role in the stability of p53, which inhibits the activation of p53 corresponding to cellular stresses [77]. The whole process is that MDM2, by targeting p53 for ubiquitination, permits the export of p53 from the nucleus to the cytoplasm, allowing p53 degradation by proteasomes [78]. Under

normal circumstances, p53 is maintained at low levels by continuous ubiquitination and degradation [76].

MDM2 serves as a downstream substrate of AKT, the function of which is to promote p53 ubiquitination by phosphorylation [76]. AKT phosphorylates MDM2 at Ser166 and Ser186. HER-2/neu-mediated resistance to DNA damage agents required AKT activation, the upregulation of MDM2-mediated ubiquitination, and p53 degradation [79]. Pharmacologically blocking PI3K/AKT signaling or AKT can prevent the nuclear entrance of MDM2, increasing cellular levels of p53 and augmenting p53 transcription activity [80]. All these findings highlight the significance of AKT as the potential upstream regulator of the MDM2-p53 axis.

1.4 The correlation between AA and AKT

It is reported that in prostate cancer, arachidonic acid (AA) induces phosphatidylinositol 3-kinase signaling and enhances 11 different gene expressions [81]. In MDA-MB-231 breast cancer cells, AA may promote cell migration and invasion *in vitro* through a PI3K/AKT-dependent pathway [68]. In mouse embryonic stem cells, through the cooperation of PI3K/AKT/mTOR, MAPK signaling pathways, AA was also observed to mediate short time-period hypoxia-induced expression of G(1) phase cyclins D(1) and E, and CDK2 and CDK4 [82].

All the evidence above suggested that there might be a connection between AA, the product of ACOT7 catalytic reaction, and the AKT-MDM2-p53 axis. Therefore, in Chapter II, we hypothesize that MYC activates ACOT7 in HNSCC cells, which in turn regulates AKT-MDM2-

p53 axis, promoting HNSCC progression. We used CHIP assay to validate direct binding of MYC to ACOT7 gene promoter and luciferase reporter assay to demonstrate MYC induces the promoter activity of ACOT7. RNA-seq analysis following ACOT7 downregulation in HNSCC cells was used to determine the significantly downregulated and upregulated genes in HNSCC cells and to identify the downstream signaling pathways. Western blotting and immunofluorescence were used to validate the genes involving the novel metabolic pathway.

2 MATERIALS AND METHODS

Preparation of MYC inhibitor and AA solution

Small-molecular-weight MYC inhibitor (10058-F4, $C_{12}H_{11}NOS_2$, MilliporeSigma, Burlington, MA, USA) was dissolved in dimethyl sulfoxide (DMSO, Sigma-Aldrich, Saint Louis, MO, USA) following the manufacturer's instruction. MYC inhibitor solution and AA solutions (MP Biomedicals Inc., CA, USA) were diluted in complete culture medium to obtain different final concentrations for experiments.

Chromatin Immunoprecipitation (CHIP)

A magnetic bead chromatin immunoprecipitation (ChIP) kit (Millipore, Burlington, MA, USA) was utilized to investigate the binding between MYC and ACOT7 promoter region in UMSCC1 and UMSCC6 cells. Cells were grown into 100% confluency in 10 cm plates and treated with 1% formaldehyde to cross-link proteins and DNA. Untreated formaldehyde was quenched using glycine. Following the steps of washing twice with 20 ml ice-cold PBS, the plates were scaped for cell collection. Cell lysis buffer and nuclear lysis buffer were applied. Samples were sonicated using Tekmar sonic disruptor to shear DNA and create crosslinked fragments of about 200-1000 base pairs in length.

Immunoprecipitation of crosslinked protein and DNA was carried out with a slurry of protein A magnetic beads and 5 µg of an appropriate primary antibody. Negative control, normal IgG

antibody, and MYC antibody (Santa Cruz Biotech, CA, USA) were used for immunoprecipitations. All the samples were treated with an overnight incubation at 4℃ with rotation.

Protein/DNA complexes were eluted from the protein A magnetic beads using a series of elution buffers. Crosslinks were reversed by incubation in CHIP elution buffer with proteinase K at 62°C for 2 h. DNA was purified using spin columns and a series of buffers to produce a purified DNA eluate. DNA samples were subjected to Real-time PCR (RT-PCR) targeting the promoter sequence of ACOT7. The sequence of the ACOT7 promoter is listed in the supplementary data.

Real-time PCR

The complementary DNA levels were amplified with SYBR™ Green PCR Master Mix (Applied Biosystems, CA, USA) in the 96-well QuantStudio™ 3 Real-Time PCR System (Life Technologies, CA, USA). The running sequence was as follows: polymerase activation at 95°C for 2 min, denaturation at 95°C for 15 sec and extension at 60°C for 1 min, and a final melting curve from 60°C to 95°C. Actin was used as the internal control for mRNA analysis respectively. Triplicate reactions were performed in separate experiments. The fold changes were calculated according to the $2^{-\Delta\Delta Ct}$ method.

Luciferase reporter assay

To test whether MYC induces the ACOT7 promoter activity, head and neck cancer cells were co-transfected in white 96-well plates for different conditions with ACOT7 promoter reporter vector constructs (Active Motif, Inc., CA, USA), Empty reporter vector constructs (Active Motif, Inc., CA, USA), MYC overexpression plasmid DNA (Addgene, MA, USA), and MYC inhibitor (10058-F4, $C_{12}H_{11}NOS_2$, Millipore Sigma, MA, USA) using Lipofectamine 2000 reagent (Invitrogen, CA, USA) following the manufacturer's instructions.

After 48 h incubation, LightSwitch™ Luciferase Assay Kit (Active Motif, Inc., CA, USA) was applied to measure luciferase activity. 100 µl assay solution was directly added to each sample well in a white 96-well plated. The plates were covered and protected from light. After incubating for 30 min at room temperature, the luminescence signal in each well was measured for 2000 ms in a plate luminometer (SpectraMax iD3, CA, USA).

RNA sequencing

UMSCC1 and UMSCC23 cells were lysed 48 hours after siRNA transfection, and the total RNA was isolated with the Quick-RNA Miniprep Kit (Zymo Research, CA, USA) following the manufacture instructions. For quality control, concentration and purity were checked by the NanoDrop 8000 (Thermo Scientific, DE, USA), and integrity was checked by the Agilent 2200 TapeSatation (Agilent, CA, USA).

For library preparation, a total amount of 1 µg RNA per sample was used as the input material. According to the manufacturer's instructions, sequencing libraries were generated

using NEBNext Ultra II Directional RNA Library Prep Kit (NEB, USA). The workflow consisted of mRNA capture, cDNA generation, and end repair to generate blunt ends, A-tailing, adaptor ligation, and PCR amplification. Different adaptors were used for multiplexing samples in one lane. The library quality was assessed on the Agilent Bioanalyzer 2100 system (Agilent, CA, USA). The cluster of the index-coded samples was performed on a cBot Cluster Generation System using PE Cluster Kit cBot-HS (Illumina) following the company's protocols. After cluster generation, the library preparations were sequenced on an Illumina platform (Illumina, MA, USA). Reference genome and gene model annotation files were obtained directly from the genome website browser (NCBI/NCSC/Ensembl). Paired-end clean reads were aligned to the reference genome using the Spliced Transcripts Alignment to a Reference (STAR) software. DESeq2 R package [83] was applied for the differential expression analysis between the two groups. Benjamini and Hochberg's approach was used to adjust the resulting *P* values. In this project, genes showing altered expression with P-value <0.05 and more than 2-fold changes were considered differentially expressed.

Pathway analysis

The Gene Set Enrichment Analysis (GSEA) was used to identify groups of genes enriched in UMSCC1 and UMSCC23 knockdown and control groups. The GSEA analysis tool (version 4.1.0) was downloaded from the Broad Institute website (http://software.broadinstitute.org/gsea/index.jsp). Curated gene sets of the Kyoto Encyclopedia

of Genes and Genomes (KEGG) pathways were downloaded from the Board Institute's Molecular Signatures Database [84]. Fcros R package was used for pre-treating the gene expression data with modifying P value and fold change together. Those pathways with no correlation with head and neck cancer were excluded. Both small (<5 genes) and large gene sets (>500 genes) were excluded from the final analysis. The Morpheus software generated heatmap from the Broad Institute Website (https://software.broadinstitute.org/morpheus/).

3 RESULTS

3.1 Arachidonic acid (AA) affects HNSCC cell phenotypes

Colony formation assays were performed to analyze the effect of exogenous AA on the cell proliferation ability of HNSCC cells. Exogenous AA was added every two days, and cells were incubated for 14 days. The results revealed that the cells cultured in the wells with extra AA formed more colonies in a dose-dependent manner, compared to the negative control groups (**P<0.01) **(Figure 15A).**

Similarly, after adding extra AA into the lower chamber as a chemoattractant, UMSCC1 and UMSCC6 cells were induced to migrate through the migration transwells (****P<0.0001) **(Figure 15B)**. These observations indicated that AA, the product of the ACOT7 enzymatic reaction, impacted the malignant phenotypes of HNSCC cells *in vitro*.

3.2 MYC functions as the upstream regulator of ACOT7

3.2.1 MYC is predicted as the upstream regulator of ACOT7

The CANNTG consensus sequences of the E-box are known as the canonical E-boxes of MYC [59]. We used various tools to predict the transcription factor of ACOT7 and discovered that MYC was a potential upstream regulator. Moreover, the consensus sequence of transcription factor binding in ACOT7 was found to be CACGTG, which belongs to the canonical E-boxes of MYC. Our prediction results suggest that MYC may serve as the transcription factor

for ACOT7 in HNSCC cells.

3.2.2 MYC binds to the ACOT7 promoter region in HNSCC

To determine whether MYC binds to the ACOT7 promoter region, CHIP assays were performed using an anti-MYC antibody according to a standardized protocol. The DNA enrichment within the immunoprecipitated samples was then measured by RT-PCR, and analysis was performed by comparing the data from the anti-MYC immunoprecipitated samples against the background signal of the negative control to calculate the enrichment fold. Compared to the negative controls, there is a significantly higher enrichment of DNA fragments of ACOT7 promoter in the anti-MYC immunoprecipitated samples for UMSCC cell lines (****P<0.0001) **(Figure 16A)**.

Luciferase reporter assays were performed to further validate the regulation of MYC on ACOT7 using ACOT7 gene promoter reporter vector plasmid, empty reporter vector, pCDNA3-HA-HA-humanCMYC, and MYC inhibitor. Our results demonstrated that when ACOT7 gene promoter and pCDNA3-HA-HA-humanCMYC were co-transfected in UMSCC cells, the luciferase activities were significantly higher than those transfected only with ACOT7 gene promoter or empty reporter vector (****P<0.0001) **(Figure 16B)**. Meanwhile, when the ACOT7 gene promoter was transfected, and the MYC inhibitor was simultaneously added to the culture plates, the luciferase activities were significantly suppressed concerning the other two groups (***P<0.001) **(Figure 16B)**.

3.2.3 MYC regulates the expression levels of ACOT7 in HNSCC

To further study if MYC regulates the expression level of ACOT7, we measured the protein expression of ACOT7 after adding MYC inhibitor (10058-F4). The Western Blotting results showed that the expression levels of ACOT7 were significantly suppressed in a dose-dependent manner following the inhibitor treatment (**P<0.01) **(Figure 17A)**.

However, if we upregulated the MYC expression *via* transfecting head and neck cancer cells with overexpression plasmid, the protein expression level of ACOT7 was significantly increased (**P<0.01) **(Figure 17B)**.

3.3 Identification of potential downstream targets of ACOT7 in HNSCC

3.3.1 RNA-sequencing (RNA-seq) analysis

To identify the potential downstream targets of ACOT7 in HNSCC cells, a genome-wide expression analysis with RNA-seq was performed on HNSCC cells transfected with siACOT7 **(Figure 18A)**. Total RNAs isolated from the UMSCC cells treated with siCTRL or siACOT7 were subjected to RNA-seq analysis. The expression Venn diagram presents the number of genes that are uniquely expressed with each group (either siACOT7 or siCTRL). The overlapping regions show the number of genes that are co-expressed in two groups **(Figure 18B)**. Compared to the siCTRL-treated cells, a total of 4,455 upregulated and 3,897 downregulated transcripts were found to be at significantly differential levels in siACOT7-treated UMSCC1 cells

(Figure 18C-18D). For a similar RNA-seq analysis of UMSCC23 cells with ACOT7 knockdown, a total of 3,624 upregulated and 3,432 downregulated transcripts were discovered to be significantly different between the two groups **(Figure 18E-18G)**.

3.3.2 Gene Ontology (GO) analysis

Gene Ontology (GO) analysis is a significant bioinformatics classification system to unify the presentation of gene properties across all species, including three main branches, cellular component (CC), molecular function (MF), and biological process (BP) **(Figure 19A)**. In the BP branch, regulation of protein stability, proteasomal protein catabolic process, negative regulation of cellular protein catabolic process, response to endoplasmic reticulum stress, and cofactor biosynthetic process were the top 5 ranked biological processes in UMSCC1 cells **(Figure 19B)**. In the CC branch, centrosome, midbody, focal adhesion, cell-substrate adherents' junction, and spindle were the top 5 ranked cellular components following ACOT7 downregulation in UMSCC1 cells **(Figure 19C)**. In the MF branch, adhesion binding, cell adhesion molecule binding, protein serine/threonine kinase activity, small GTPase binding, and guanyl ribonucleotide binding were the top 5 ranked molecular functions after ACOT7 downregulation in UMSCC1 cells **(Figure 19D)**.

3.3.3 Gene set enrichment analysis (GSEA)

After excluding those pathways unrelated to head and neck cancer, GSEA showed that the differentially expressed genes were enriched in the cell cycle, p53 signaling pathway,

endocytosis, protein processing in endoplasmic reticulum, cellular senescence, and mTOR signaling pathway **(Figure 20A-20C)**. We also conducted the RNA-seq analysis in the UMSCC23 cells following ACOT7 downregulation and discovered that the differentially expressed genes were enriched in cell cycle, lysosome, p53 signaling pathway, cellular senescence, HIF-1 signaling pathway, and mTOR signaling pathway **(Figure 20D)**.

3.4 The MYC-ACOT7-AA-AKT-MDM2-p53 axis in HNSCC

Both RNA-seq analysis of UMSCC1 and UMSCC23 cell lines following ACOT7 knockdown revealed that the p53 signaling pathway was activated, suggesting that p53 signaling may be a potential downstream pathway of ACOT7. Our Western blot analysis showed that silencing ACOT7 decreased the expression level of AKT but not phospho-AKT (***P<0.001). This, in turn, suppressed the expression level of phospho-MDM2 but not total MDM2 (***P<0.001) and induced p53 expression (****P<0.0001), which was consistent with our findings based on the RNA-seq **(Figure 21A)**. Using immunofluorescence, we proved the significant downregulation of AKT and phospho-MDM2 following silencing ACOT7 in UMSCC1 and UMSCC6 cells **(Figure 21B-21C)**. Meanwhile, transfecting UMSCC cells with ACOT7 overexpression lentivirus led to the upregulation of AKT expression (****P<0.0001) **(Figure 21D)**.

Since previous studies indicated that AA may regulate AKT expression, we investigated the effect of exogenous AA on the expression of AKT in HNSCC cells. Indeed, when the HNSCC cells were treated with AA, we observed a dose-dependent effect of AA on the expression levels

of AKT (***P<0.001, ****P<0.0001) **(Figure 22)**

These results have demonstrated the functional significance of MYC-ACOT7-AKT-MDM2-p53 axis in UMSCC1 and UMSCC6 p53 wildtype HNSCC cell lines. UM1 and UM2 cell lines, which are p53-overexpressing cell lines, were used in this project for further investigation. After transfecting UM1 and UM2 cells with siACOT7, the expression levels of AKT, but not phospho-AKT, were decreased (***P<0.001). The expression levels of phospho-MDM2, but not MDM2, were suppressed (****P<0.0001), and the expression levels of p53 were induced following ACOT7 downregulation (**P<0.01). These results were consistent with our findings in UMSCC1 and UMSCC6 cell lines **(Figure 23)**.

The expression levels of other important molecules involved in MYC-ACOT7-AKT-MDM2-p53 axis were also changed after silencing ACOT7. Inhibiting ACOT7 suppressed the expression levels of PI3KCA (PI3-Kinase P110 Subunit Alpha), and the expression levels of phospho-mTOR, but not mTOR, and induced the expression levels of PTEN (****P<0.0001) **(Figure 24)**, which warrants further investigation.

Collectively, our studies have demonstrated the functional significance of MYC-ACOT7-AKT-MDM2-p53 axis in HNSCC progression, and ACOT7 plays an important role in promoting HNSCC progression **(Figure 25)**.

4 DISCUSSION

In this chapter, we demonstrated that AA, the product of ACOT7 enzymatic reaction, promoted malignant phenotypes of HNSCC cells *in vitro*, indicating it may mediate ACOT7, promoting HNSCC progression. Next, by using bioinformatics tools to predict potential transcription factors, we found that MYC may be the upstream regulator of ACOT7. The predicted consensus sequence, CACGTG, belongs to the canonical E-boxes of MYC. The results of luciferase reporter and CHIP assays revealed that MYC bound to the ACOT7 gene promoter region and induced the promoter activity of ACOT7 gene in HNSCC cells.

RNA-seq analysis of HNSCC cells with siACOT7 knockdown was applied to investigate the downstream pathway of ACOT7. In total, 4,455 significantly upregulated genes and 3,897 significantly downregulated genes were identified in the UMSCC1 cells following ACOT7 downregulation. Based on Gene ontology analysis of RNA-seq data, we found the significantly altered genes were enriched with molecular functions, e.g., adhesion binding, cell adhesion molecule binding, and protein serine/threonine kinase activity, cellular components, e.g., midbody, focal adhesion, and cell-substrate adherents' junction, and biological processes, e.g., regulation of protein stability, response to endoplasmic reticulum stress, and proteasomal protein catabolic processes. Followed by functional pathway analysis of the RNA-seq data, we found that knockdown of ACOT7 in HNSCC cells deactivated important gene pathways, including cell cycle, p53 signaling, and mTOR signaling. Particularly, AKT-MDM2-p53 axis was

demonstrated to be a crucial downstream pathway of ACOT7 in HNSCC cells. By using Western blot analysis and immunofluorescence, we demonstrated that ACOT7, through the action of AA, significantly upregulated AKT but not phospho-AKT, which in turn promoted the expression of phospho-MDM2 but not total MDM2 in HNSCC cells. This eventually led to significantly reduced expression of p53 in HNSCC cells. Our *in vitro* studies demonstrated the functional significance of MYC-ACOT7-AKT-MDM2-p53 axis in tumor development/progression of HNSCC.

The MYC oncogene is overexpressed in many human cancers, contributing to the development and progression of various human cancers. It has a central role in almost every aspect of the oncogenic process, orchestrating proliferation, apoptosis, differentiation, metabolism, signal transduction, and stem cell biology [85, 86]. MYC functions as a transcriptional factor cooperating with its cofactor, MAX, a helix-loop=helix zipper protein [87]. Heterodimerization of MYC-MAX permits an induced-fit complex to recognize the E-box sequences of genes and regulate the transcription processes of the target genes [88]. MYC was found to be important in cell cycle control via stimulating the genes encoding the critical positive cell cycle regulators, including CDKs, cyclins, and E2F transcription factors [89]. MYC involves antagonizing cell cycle inhibitors' activity, such as p21 and p27, through different mechanisms [90, 91]. In eukaryotic cells, MYC can induce genes directly related to DNA replication through the origin recognition complex (ORC), essential for DNA replication [92]. Furthermore, it is

demonstrated that MYC plays a role in controlling genes encoding MCM (minichromosome maintenance) proteins, responsible for correct DNA replication initiation and elongation [93]. MYC was also closely correlated with cell apoptosis. MYC overexpression was always accomplished with the rearrangements in the BCL-2 locus and BCL-2 overexpression functions as promoters of MYC-mediated transformation in human cancers [94]. Last, MYC plays an important regulatory role in metabolic reprogramming pathways, including fatty acid oxidation and pyruvate oxidation via the TCA cycle to the glycolytic as well as glutaminolytic pathways in T cell reprogramming [95]. Our present study demonstrated a new function of MYC in regulating ACOT7 to promote HNSCC progression.

As a member of the omega-6 poly-unsaturated fatty acids, AA is involved in tumor progression via the transformation into prostaglandin E2 [96, 97]. It may participate in crucial biological processes such as growth, development, and lipid metabolism as a precursor of numerous lipid mediators [96]. AA depends on the mechanism of being metabolized by three different distinct enzyme systems, cyclooxygenases, lipoxygenases, and cytochrome P450, to generate a wide range of biologically active fatty acid mediators [98]. Xin, Chunxia, *et al.* demonstrated that the cytosolic phospholipase A2 (cPLA2)-AA-cyclooxygenase-2 (COX-2) pathway was closely associated with lung cancer [99]. In human prostate cancer (PCa) cells, AA promoted prostate cancer cell growth, but it had to be metabolized through the 5-lipoxygenase (5-HETE) pathway to produce 5-HETE series of eicosatetraenoids for its growth stimulatory

effects [97]. AA may also modulate the crosstalk between prostate carcinoma and bone stromal cells, suggesting that AA accumulated in bone marrow might influence the formation of PCa-derived metastatic lesions [100]. These findings, together with ours, demonstrate that AA may also play an important role in tumor progression.

AKT is a critical serine-threonine kinase involved in cell metabolism, proliferation, motility, and survival [101]. Overexpression of AKT has been observed in a variety of human cancers, such as breast, lung, ovarian, pancreatic, and gastric carcinoma [102]. The increased activity and dysregulation of AKT kinases can result in activated growth signals, which is a common feature of tumors [103]. AKT can modulate apoptosis directly or indirectly. The direct function is to regulate the phosphorylation events or interactions with cell death actors, while the indirect role is to mediate the transcriptional responses to apoptotic stimuli [104]. Zhou H *et al.* demonstrated that AKT promoted cell survival and inhibited apoptosis by suppressing pro-apoptotic proteins (such as Bad and Caspase-9) at a post mitochondrial level, and active AKT overexpression rescued cells from apoptosis [105, 106]. Based on our findings, ACOT7 upregulated the expression of AKT in HNSCC cells, which may promote survival and inhibit apoptosis of HNSCC cells.

The tumor suppressor p53 has a significant role in inducing apoptosis, cell cycle arrest, DNA repair, senescence, and angiogenesis, preventing the propagation of damaged cells [75, 107]. p53 activation arrests cells at the G2/M phases and provides checkpoint function, such as

preventing DNA replication when the mitotic spindle is disrupted [108]. In mammalian cells, p53 increases the gene expression involved in various apoptosis signaling and execution steps, including BH3 domain-only proapoptotic proteins, death receptors, and apoptosis execution factors [109]. p53 may also have a functional role in metabolic disorders. In most cell types, p53 supports oxidative phosphorylation (OXPHOS) over glycolysis, while its deficiency contributes to metabolic reprogramming through a more glycolytic profile in cancer cells [110]. Meanwhile, p53 metabolic activities had a crucial role in lipid homeostasis, including lipid transport and storage in fatty acid synthesis, as well as fatty acid oxidation [110, 111]. Lastly, p53 is commonly inhibited when the AKT pathway is activated [112]. Based on our RNA-seq data, p53 was upregulated following ACOT7 downregulation. From our Western blotting results, knockdown of ACOT7 inhibited the expression of AKT whereas upregulated the expression of p53 in HNSCC cells. Meanwhile, overexpression of ACOT7 upregulated the expression of AKT and inhibited the expression of p53 in HNSCC cells. These results suggest that AKT-p53 may be a downstream signaling pathway of ACOT7 in HNSCC cells.

MDM2, a product of a proto-oncogene that inactivates p53, is overexpressed in a large number of human cancers [112]. MDM2 can influence the transcriptional activity of p53 via binding to the N-terminal transactivation domain of p53 and preventing the interactions between other necessary proteins and p53 [112]. On the other hand, Yoko Ogawara *et al.* revealed that AKT did not affect the mRNA expression levels of p53 but promoted the degradation of p53

protein. This is due to AKT enhancing the phosphorylation of MDM2 at Ser 166 and Ser 186, increasing its interaction with p300 and allowing p53 ubiquitination [76, 79]. As discussed above, the AKT-MDM2-p53 axis is a crucial regulating pathway in cancer cell survival and apoptosis, and our results suggest that ACOT7 promotes the proliferation and inhibits the apoptosis of HNSCC cells via the regulation of the AKT-MDM2-p53 signaling pathway.

5 CONCLUSIONS

ACOT7, a critical metabolic enzyme, was found to promote HNSCC progression in this study. ACOT7 was significantly overexpressed in HNSCC tissues *versus* normal tissues based on RNA-seq analysis and IHC analysis of HNSCC TMA sections. More importantly, ACOT7 was found to be significantly associated with the overall and disease-free survival of HNSCC patients. In addition, knockdown of ACOT7 in HNSCC cells significantly inhibited the cell proliferation, migration, invasion, and colony-formation/tumor sphere-formation capabilities, and *vice versa*.

Mechanistically, MYC was found to upregulate ACOT7 expression in HNSCC cells while ACOT7 upregulated the expression of AKT, which in turn phosphorylated MDM2 and inhibited the expression of p53 in HNSCC cells. Our study revealed the functional significance of MYC-ACOT7-AKT-MDM2-p53 axis and novel metabolic mechanisms in HNSCC and may provide novel targets for therapeutic intervention in HNSCC.

6 CLINICAL PERSPECTIVES

Our study has revealed the functional role of a critical metabolic enzyme, ACOT7, in HNSCC progression, indicating its clinical utility for potential diagnosis or prognosis. Since ACOT7 is significantly overexpressed in HNSCCs, it may serve as a biomarker for HNSCC detection. Our studies also found that overexpression of ACOT7 was significantly associated with unfavorable survival in HNSCC patients. Meanwhile, according to the data from the GSE30784, the expression levels of ACOT7 were correlated with tumor dysplasia. These findings suggest that ACOT7 may serve as a biomarker for HNSCC prognosis. Last, the recognition of the ACOT7 function in HNSCC may provide valuable guidance for the selection of precision therapeutic approach. For the HNSCC patients with significant overexpression of ACOT7, therapeutic approaches targeting ACOT7 may be used for potential treatment.

FIGURE CAPTION

Figure 1. ACOT7 is overexpressed in HNSCC. (A) Based on RNA-seq analysis of metabolic enzymes, ACOT7 expression was found to be significantly higher in HNSCC tissues compared to the normal tissues. (B) The levels of ACOT7 were significantly higher in HNSCC tissues compared with the normal tissues in various independent studies (TCGA-HNSC, GSE 6791, GSE 9844, GSE 25099, GSE 30784, GSE 31056, GSE 37991, GSE 74530 ($P<0.0001$).

Figure 2. ACOT7 is overexpressed in other types of cancers. Based on the data available from the TCGA database, we found the expression levels of ACOT7 were significantly increased in human cancer tissues, including bladder urothelial carcinoma (BLCA), breast invasive carcinoma (BRCA), cervical squamous cell carcinoma, and endo-cervical adenocarcinoma (CESC), cholangiocarcinoma (CHOL), colon adenocarcinoma (COAD), esophageal Carcinoma (ESCA), kidney renal clear cell carcinoma (KIRC), liver hepatocellular carcinoma (LIHC), lung adenocarcinoma (LUAD), lung squamous cell carcinoma (LUSC), pheochromocytoma and paraganglioma (PCPG), prostate adenocarcinoma (PRAD), stomach adenocarcinoma (STAD), stomach and esophagus adenocarcinoma (STES), thyroid cancer (THCA), and uterine corpus endometrial carcinoma (UCEC).

Figure 3. ACOT7 overexpression is associated with poor prognosis in HNSCC and other types of cancers. (A) HNSCC patients within higher ACOT7 expression suffered worse long-term overall survival ($P=0.0054$) and disease-free survival ($P=0.0072$). (B) Higher ACOT7

expression was associated with poorer disease-free survival rates in many other types of cancers, including BRCA, CESC, LUAD, LUSC, kidney renal papillary cell carcinoma (KIRP), and sarcoma (SARC). (C) ACOT7 overexpression was also related to unfavorable overall survival rates in BLCA, BRCA, KIRP, LUAD, LUSC, and SARC.

Figure 4. Expression levels of ACOT families in HNSCC. Based on the data from TCGA databases, the expression levels of ACOT1, ACOT2, ACOT4, ACOT6, ACOT8, ACOT9, ACOT11, and ACOT13 were compared between HNSCC and normal tissues.

Figure 5. Expression levels of ACOT7 in HNSCC cell lines. (A) The expression levels of ACOT7 in HNSCC cell lines, UMSCC1, UMSCC6, UMSCC23, UM1, UM2, and normal cell line, NHOK, were presented (n=3). (B) The extra growth factor in the culture medium may affect the expression levels of ACOT7. After adding exogenous epidermal growth factor (EGF) and basic fibroblast factor (FGF) to the cell culture medium, we found that EGF, but not FGF, induced the ACOT7 expression in HNSCC cells (n=3). (C) Immunofluorescence analysis of ACOT7 in UMSCC1 and UMSCC6 cells (n=3).

Figure 6. Immunohistochemical analysis of ACOT7 in HNSCC. (A) Immunohistochemical analysis indicated that the expression levels of ACOT7 were significantly higher in head and neck tumor tissues (n=152) than adjacent normal tissues (n=38). (B) Preliminary analysis of the effect of clinicopathologic parameters on ACOT7 expression (n=152).

Figure 7. Effective knockdown of ACOT7 in HNSCC cell lines. (A) Western Blotting analysis

demonstrated effective downregulation of ACOT7 in UMSCC1 and UMSCC6 cells with siRNA (n=3) (****P<0.0001). (B) Fluorescence intensity was decreased following ACOT7 downregulation in the HNSCC cell lines (n=3).

Figure 8. Downregulation of ACOT7 inhibits HNSCC cell proliferation. (A) The MTT results showed that the OD values of UMSCC cells transfected with siACOT7 were significantly lower compared to the control groups at all time points except for the first day (n=5) (****P<0.0001). (B) The average well surface colony areas were significantly lower for the ACOT7 knockdown groups (n=3) (****P<0.0001). (C) The percentage of EdU positive cells was significantly decreased following ACOT7 downregulation in UMSCC cell lines (n=3) (***P<0.001). (D) Cell cycle analysis demonstrated that silencing ACOT7 significantly decreased the enrichment of the cells in the S phase (n=3) (**P<0.01).

Figure 9. Downregulation of ACOT7 suppresses HNSCC cell migration and invasion. (A) The migration capability of ACOT7 knockdown groups was significantly suppressed. The average migrated cell numbers were lower in the knockdown groups compared to the negative control groups (n=3) (****P<0.0001). (B) The mean invaded cell numbers of ACOT7 knockdown groups were significantly lower than the control ones (n=3) (****P<0.0001).

Figure 10. Downregulation of ACOT7 affects HNSCC cell morphology and sphere formation ability. (A) Following ACOT7 downregulation, the morphology of cancer cells was altered, and the cells were not able to attach to the surface of the culture plates (n=3). (B)

Silencing ACOT7 weakened tumor-sphere formation ability of the HNSCC cells (n=3) (**P<0.01).

Figure 11. Effective overexpression of ACOT7 in HNSCC cell lines. (A) ACOT7 overexpressing lentivirus (Lenti-ORF clone of ACOT7 (mGFP-tagged)-Human acyl-CoA thioesterase 7) was constructed by transfecting the clone into 293 FT cells. (B) Various MOI (the ratio of the number of transducing lentiviral particles to the number of cells) numbers were tested for the overexpression experiments (n=3). (C) Western Blotting analysis demonstrated effective upregulation of ACOT7 in UMSCC cell lines (n=3) (****P<0.0001).

Figure 12. Upregulation of ACOT7 enhances HNSCC cell proliferation. (A) MTT assays showed that the proliferation ability of UMSCC1 and UMSCC6 cells was enhanced after lenti-ACOT7 infection (n=5) (**P<0.01, ***P<0.001). (B) The average well surface colony areas were significantly higher for the ACOT7 overexpression groups (n=3) (****P<0.0001). (C) The percentage of EdU positive cells was significantly increased following the lentivirus transfection (n=3) (****P<0.0001). (D) Cell cycle analysis demonstrated that silencing ACOT7 slightly activated the enrichment of the cells in the S phase (n=3) (*P<0.05).

Figure 13. Upregulation of ACOT7 induces HNSCC cell migration and invasion. (A) The migration capability of ACOT7-overexpression cells was significantly enhanced. The average migrated cell numbers were higher in the overexpression groups compared to the negative control groups (n=3) (****P<0.0001). (B) The mean invaded cell numbers of ACOT7

overexpression groups were significantly increased following lentivirus transfection (n=3) (****P<0.0001).

Figure 14. Upregulation of ACOT7 increases HNSCC tumor-sphere formation ability. ACOT7 upregulation significantly promoted the tumor-sphere formation of the HNSCC cells (n=3) (***P<0.001).

Figure 15. Arachidonic acid (AA) affects HNSCC cell phenotypes. (A) The UMSCC cells cultured in the wells with exogenous AA formed more colonies in a dose-dependent manner than the negative control groups (n=3) (**P<0.01). (B) Exogenous AA attracted more cells to migrate through the migration transwells (n=3) (****P<0.0001).

Figure 16. MYC directly binds to the ACOT7 promoter region in HNSCC cells. (A) Compared to the negative control groups, there was a significantly higher enrichment of DNA fragments of ACOT7 promoter in the anti-MYC immunoprecipitated groups in both UMSCC cell lines (n=3) (****P<0.0001). (B) Luciferase reporter assays showed that pCDNA3-HA-HA-humanCMYC significantly induced the luciferase activity compared to the scramble control (n=5) (****P<0.0001), while MYC inhibitor significantly suppressed the luciferase activity (n=5) (***P<0.001).

Figure 17. MYC regulates ACOT7 expression in HNSCC cells. (A) ACOT7 expression was significantly suppressed in a dose-dependent manner following the inhibitor treatment (n=3) (**P<0.01). (B) The protein expression levels of ACOT7 were significantly increased following

overexpression plasmid transfection (n=3) (**P<0.01).

Figure 18. RNA-seq analysis of HNSCC cells following ACOT7 downregulation. (A) Validation of sufficient ACOT7 knockdown in the HNSCC cells (n=3). (B) The expression Venn diagram of RNA-seq analysis. The overlapping regions showed the number of co-expressed genes in two groups. (C) Volcano plot was generated to visualize DEGs, and red or blue dots in the plots indicated significantly upregulated or downregulated genes, respectively. Compared to the siCTRL-treated cells, a total of 4,455 upregulated and 3,897 downregulated transcripts were found to be significantly aberrantly expressed in siACOT7-treated UMSCC1 cells. (D) Heatmap was used to visualize the distribution of DEGs following ACOT7 inhibition. Previous RNA-seq analysis in UMSCC23 samples. Expression Venn diagram (E), Volcano plot (F), and Heatmap (G). (n=3).

Figure 19. Gene Ontology (GO) analysis. Gene Ontology (GO) analysis was used to identify enriched gene properties in the HNSCC cells with ACOT7 knockdown (A), including three main branches, biological process (B), cellular component (C), and molecular function (D). (n=3).

Figure 20. Gene set enrichment analysis (GSEA) and the top enriched pathways following ACOT7 downregulation. (A) The KEGG pathway analysis following silencing ACOT7 in UMSCC1 cells. The results showed the two important enriched pathways following ACOT7 downregulation with statistical significance, cell cycle (B) and p53 signaling pathway (C). (D) KEGG pathway analysis of the RNA-seq results of UMSCC23 cells (n=3).

Figure 21. ACOT7 regulates AKT-MDM2-p53 axis in UMSCC1 and UMSCC6 cells (WT p53). (A) Silencing ACOT7 decreased the expression level of AKT, but not phospho-AKT (***P<0.001), which in turn suppressed the expression levels of phospho-MDM2 but not total MDM2 (***P<0.001) and induced p53 expression (****P<0.0001) (n=3). Immunofluorescence results showed the significant downregulation of AKT (B) and phospho-MDM2 (C) following silencing ACOT7 in UMSCC1 and UMSCC6 cells (n=3). (D) Transfection of ACOT7 overexpression lentivirus led to the significant upregulation of AKT expression (n=3) (****P<0.0001).

Figure 22. AA affects the expression levels of AKT in UMSCC1 and UMSCC6 cells. A dose-dependent regulation of AKT expression by exogenous AA was found in HNSCC cells (n=3) (***P<0.001, ****P<0.0001).

Figure 23. ACOT7 regulates AKT-MDM2-p53 axis in UM1 and UM2 cells (p53-overexpression). After transfecting UM1 and UM2 cells with siACOT7, the expression levels of AKT, but not phospho-AKT, were decreased (***P<0.001). The expression levels of phospho-MDM2, but not total MDM2, were suppressed (****P<0.0001), while the expression levels of p53 were induced following ACOT7 downregulation (**P<0.01) (n=3).

Figure 24. ACOT7 regulates other important molecules related to AKT-MDM2-p53 axis in UMSCC1 and UMSCC6 cells. Inhibiting ACOT7 suppressed the expression levels of PI3KCA (PI3-Kinase P110 Subunit Alpha) and the expression levels of phospho-mTOR, but not mTOR,

and induced the upregulation of PTEN expression (n=3) (****P<0.0001).

Figure 25. A proposed model of the MYC-ACOT7-AKT-MDM2-p53 axis in tumor development of HNSCC.

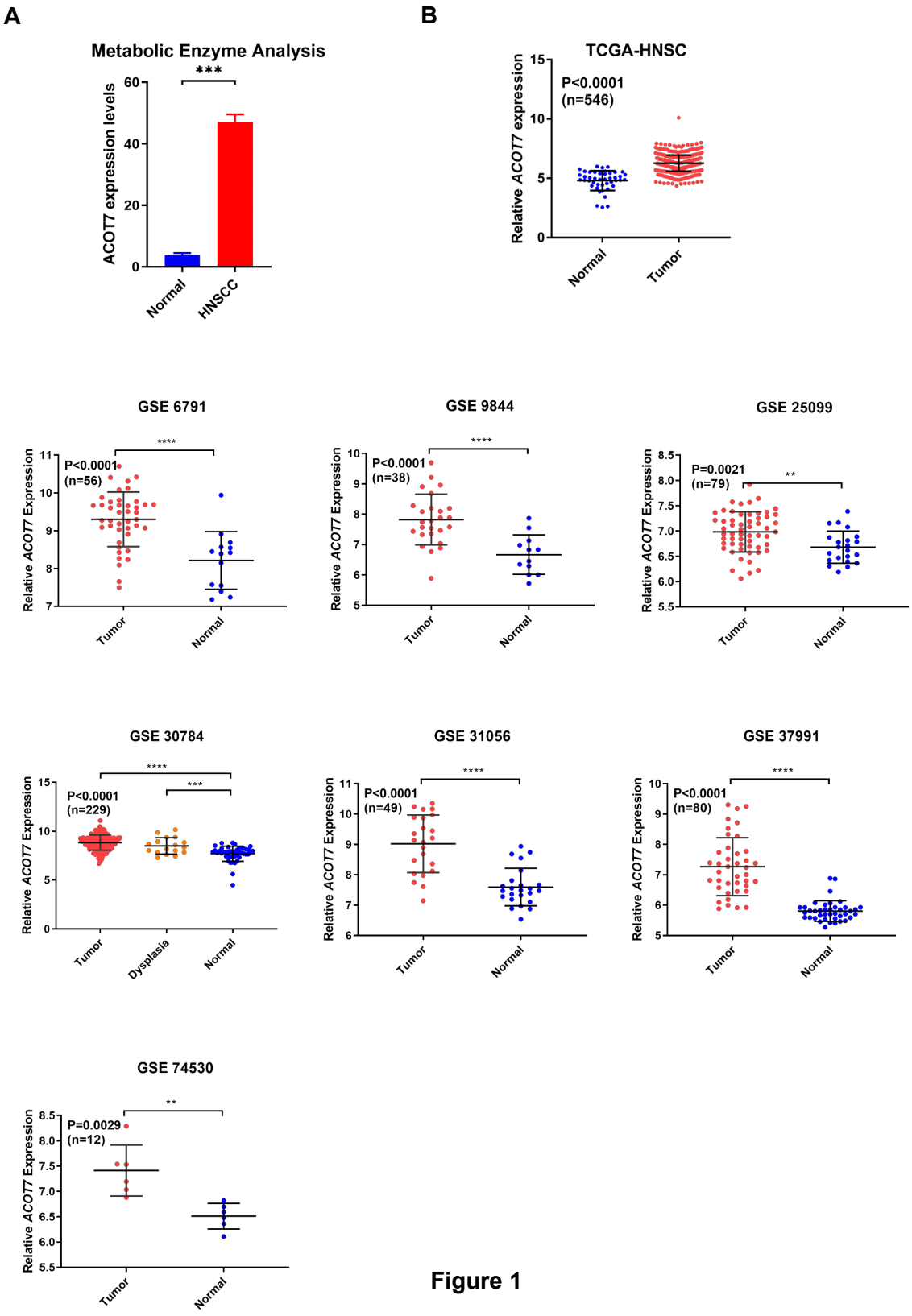
A
Metabolic Enzyme Analysis
***
ACOT7 expression levels
60
40
20
0
Normal
HNSCC
B
TCGA-HNSC
P<0.0001
(n=546)
Relative ACOT7 expression
15
10
5
0
Normal
Tumor
GSE 6791
P<0.0001
(n=56)
****
Relative ACOT7 Expression
Tumor
Normal
GSE 9844
P<0.0001
(n=38)
****
Relative ACOT7 Expression
Tumor
Normal
GSE 25099
P=0.0021
(n=79)
**
Relative ACOT7 Expression
Tumor
Normal
GSE 30784
P<0.0001
(n=229)
****
***
Relative ACOT7 Expression
Tumor
Dysplasia
Normal
GSE 31056
P<0.0001
(n=49)
****
Relative ACOT7 Expression
Tumor
Normal
GSE 37991
P<0.0001
(n=80)
****
Relative ACOT7 Expression
Tumor
Normal
GSE 74530
P=0.0029
(n=12)
**
Relative ACOT7 Expression
Tumor
Normal

Figure 1

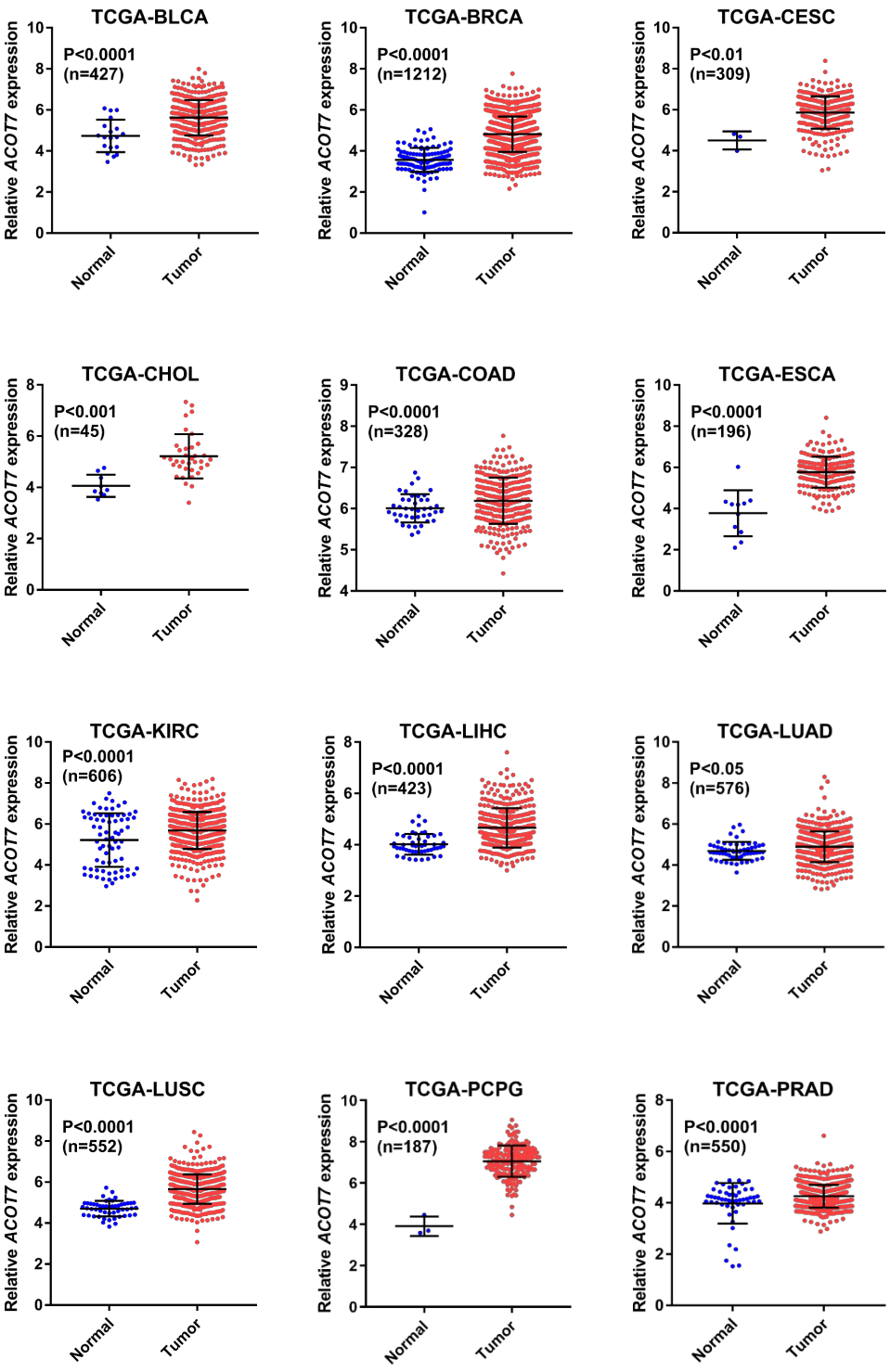
TCGA-BLCA
P<0.0001
(n=427)
TCGA-BRCA
P<0.0001
(n=1212)
TCGA-CESC
P<0.01
(n=309)
TCGA-CHOL
P<0.001
(n=45)
TCGA-COAD
P<0.0001
(n=328)
TCGA-ESCA
P<0.0001
(n=196)
TCGA-KIRC
P<0.0001
(n=606)
TCGA-LIHC
P<0.0001
(n=423)
TCGA-LUAD
P<0.05
(n=576)
TCGA-LUSC
P<0.0001
(n=552)
TCGA-PCPG
P<0.0001
(n=187)
TCGA-PRAD
P<0.0001
(n=550)
Relative ACOT7 expression
Normal
Tumor

Figure 2

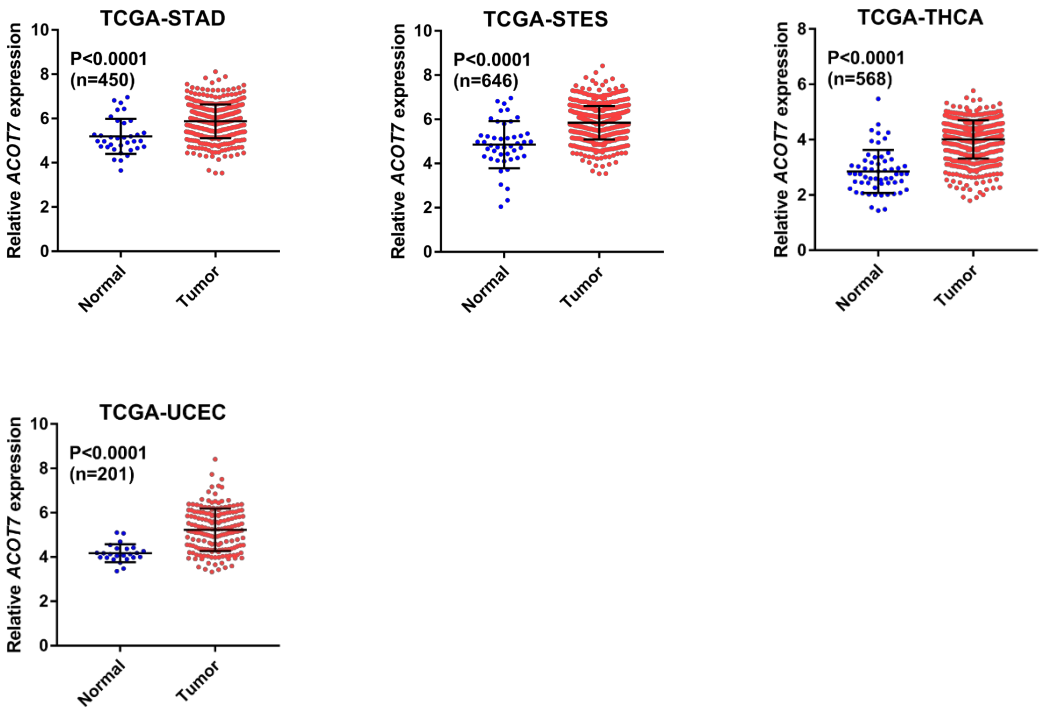
TCGA-STAD
P<0.0001
(n=450)
TCGA-STES
P<0.0001
(n=646)
TCGA-THCA
P<0.0001
(n=568)
TCGA-UCEC
P<0.0001
(n=201)
Relative ACOT7 expression
Normal
Tumor

Figure 2

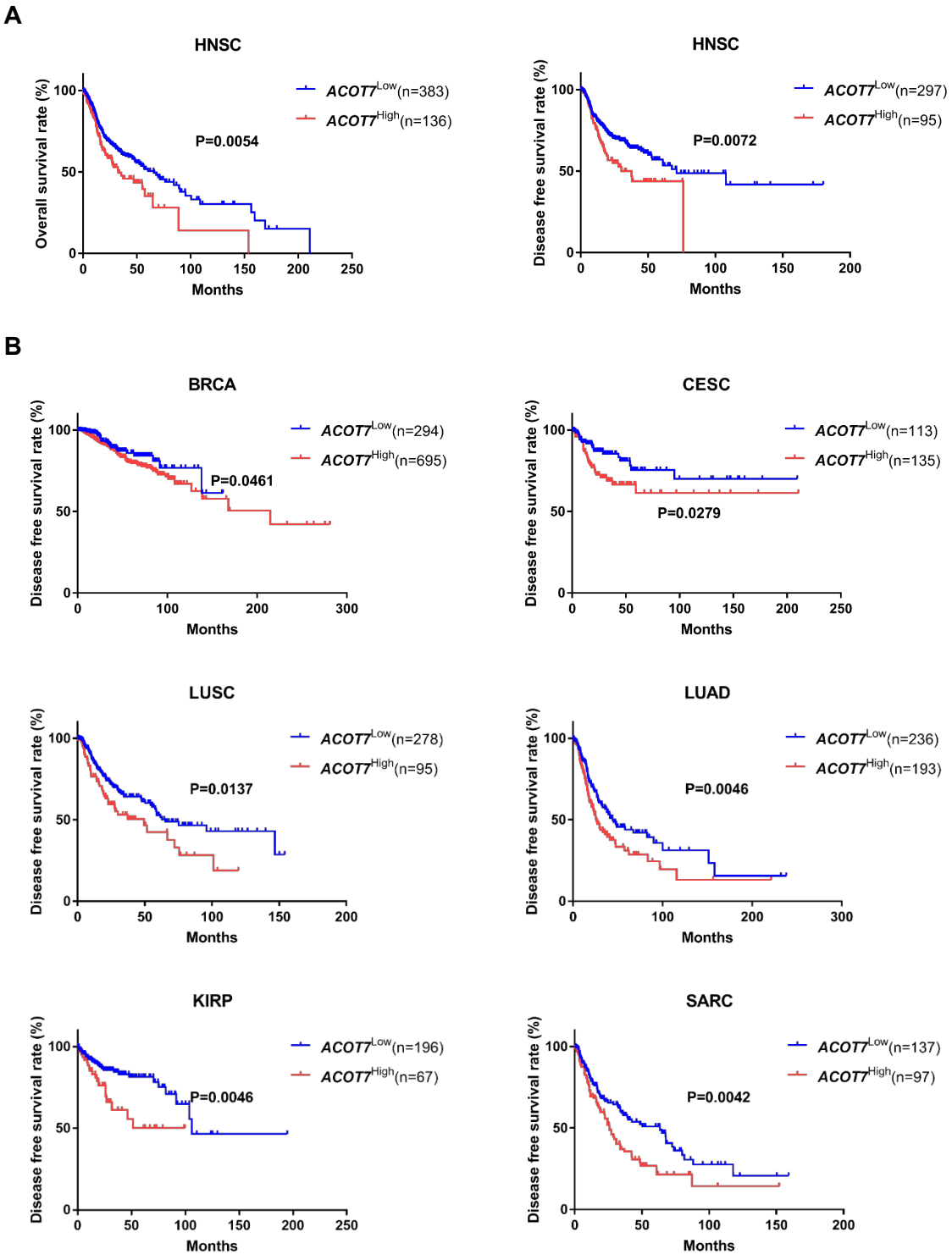
A
HNSC
Overall survival rate (%)
ACOT7Low(n=383)
ACOT7High(n=136)
P=0.0054
Months
HNSC
Disease free survival rate (%)
ACOT7Low(n=297)
ACOT7High(n=95)
P=0.0072
Months
B
BRCA
Disease free survival rate (%)
ACOT7Low(n=294)
ACOT7High(n=695)
P=0.0461
Months
CESC
Disease free survival rate (%)
ACOT7Low(n=113)
ACOT7High(n=135)
P=0.0279
Months
LUSC
Disease free survival rate (%)
ACOT7Low(n=278)
ACOT7High(n=95)
P=0.0137
Months
LUAD
Disease free survival rate (%)
ACOT7Low(n=236)
ACOT7High(n=193)
P=0.0046
Months
KIRP
Disease free survival rate (%)
ACOT7Low(n=196)
ACOT7High(n=67)
P=0.0046
Months
SARC
Disease free survival rate (%)
ACOT7Low(n=137)
ACOT7High(n=97)
P=0.0042
Months

Figure 3

C

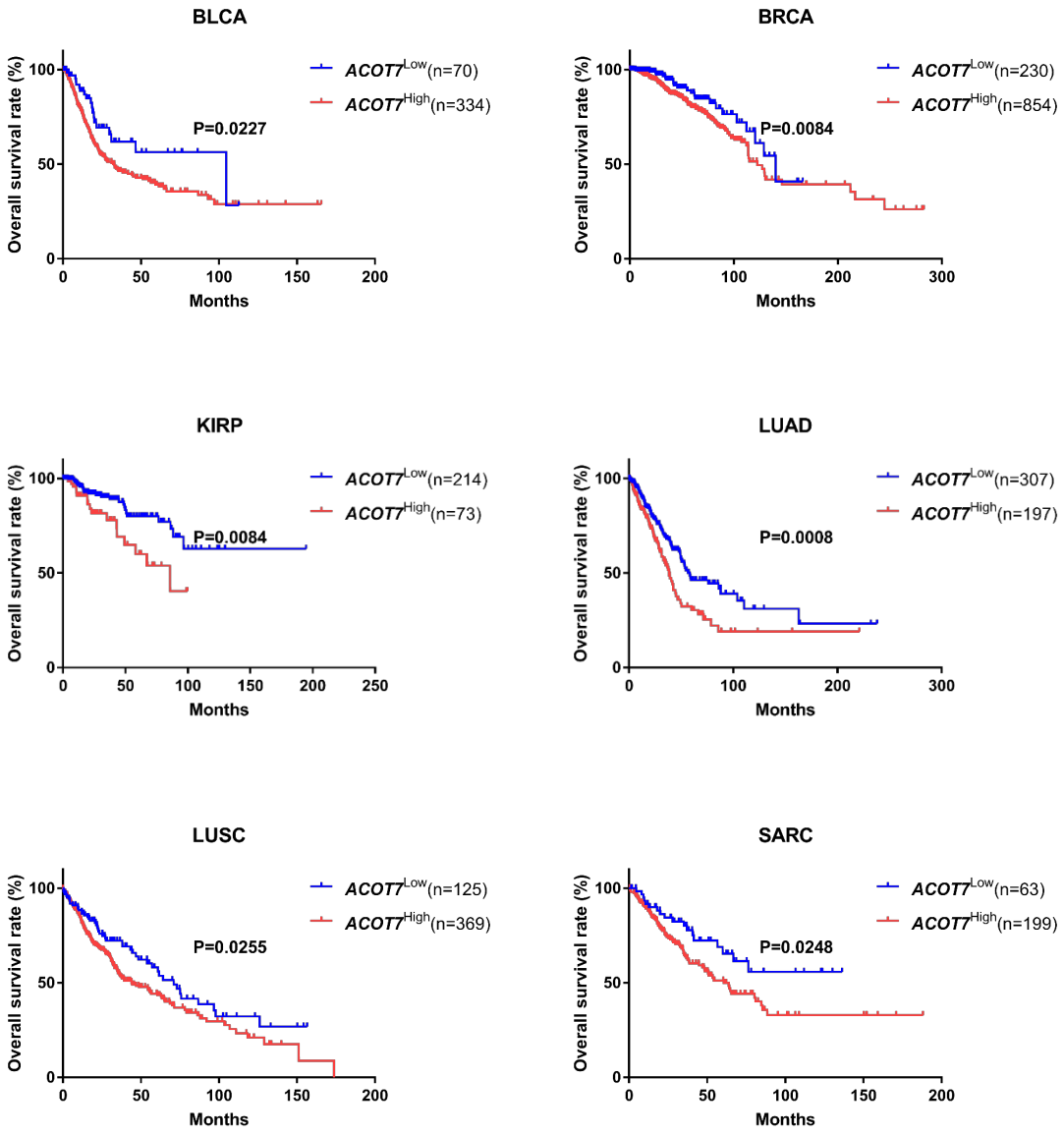
BLCA
Overall survival rate (%)
ACOT7Low(n=70)
ACOT7High(n=334)
P=0.0227
Months
BRCA
ACOT7Low(n=230)
ACOT7High(n=854)
P=0.0084
KIRP
ACOT7Low(n=214)
ACOT7High(n=73)
P=0.0084
LUAD
ACOT7Low(n=307)
ACOT7High(n=197)
P=0.0008
LUSC
ACOT7Low(n=125)
ACOT7High(n=369)
P=0.0255
SARC
ACOT7Low(n=63)
ACOT7High(n=199)
P=0.0248

Figure 3

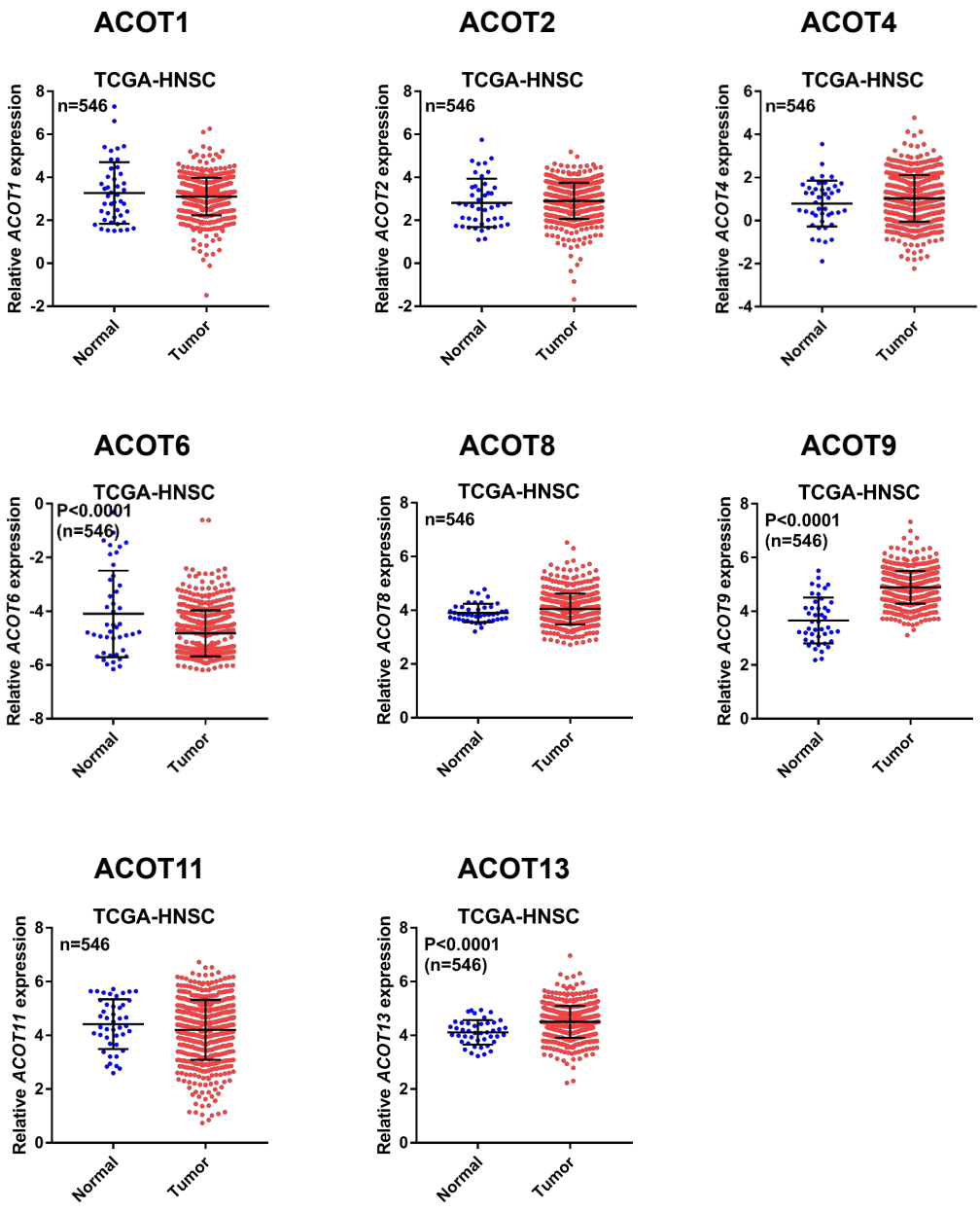
ACOT1
TCGA-HNSC
n=546
Relative ACOT1 expression
Normal
Tumor
ACOT2
TCGA-HNSC
n=546
Relative ACOT2 expression
Normal
Tumor
ACOT4
TCGA-HNSC
n=546
Relative ACOT4 expression
Normal
Tumor
ACOT6
TCGA-HNSC
P<0.0001
(n=546)
Relative ACOT6 expression
Normal
Tumor
ACOT8
TCGA-HNSC
n=546
Relative ACOT8 expression
Normal
Tumor
ACOT9
TCGA-HNSC
P<0.0001
(n=546)
Relative ACOT9 expression
Normal
Tumor
ACOT11
TCGA-HNSC
n=546
Relative ACOT11 expression
Normal
Tumor
ACOT13
TCGA-HNSC
P<0.0001
(n=546)
Relative ACOT13 expression
Normal
Tumor

Figure 4

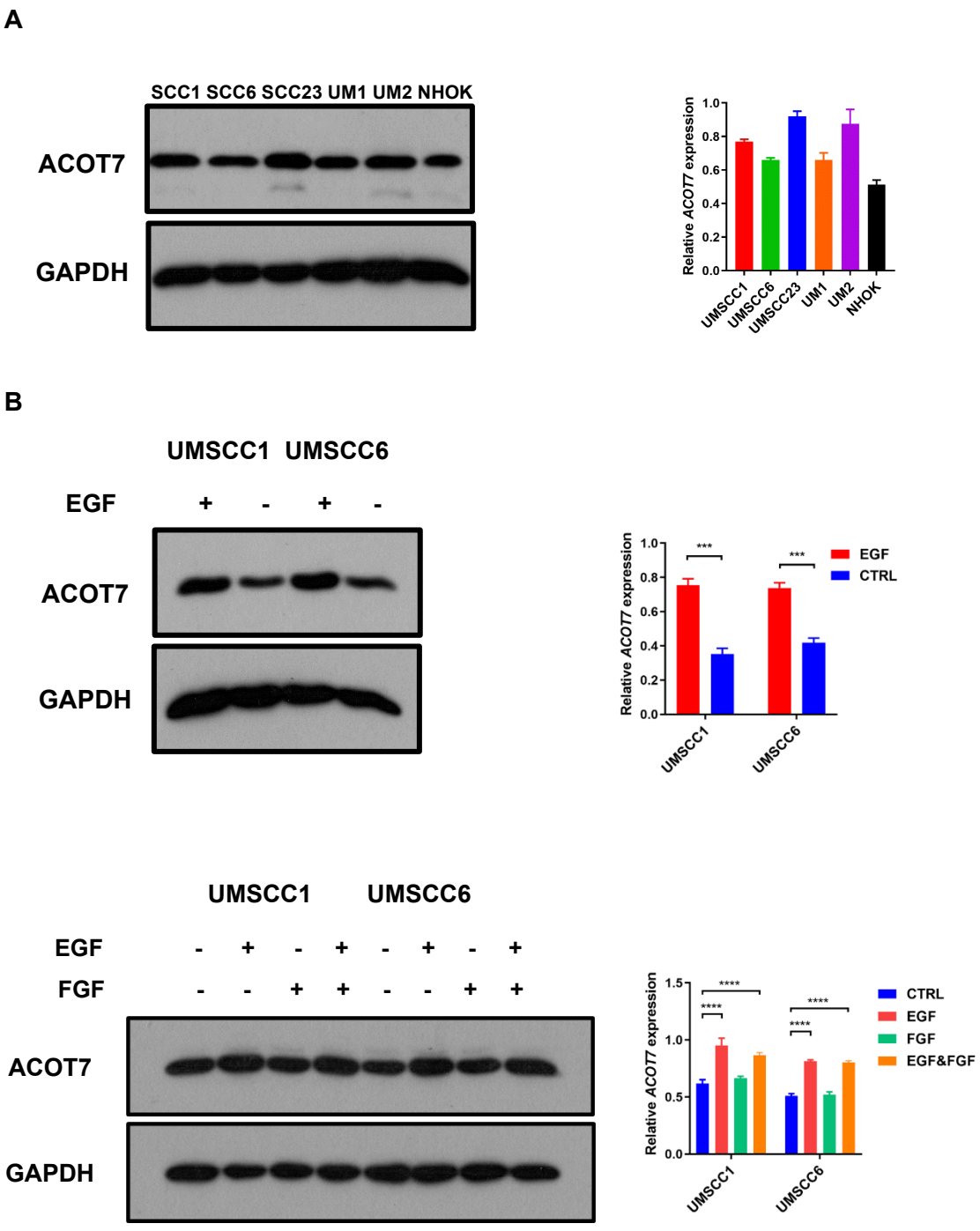
A
SCC1 SCC6 SCC23 UM1 UM2 NHOK
ACOT7
GAPDH
Relative ACOT7 expression
1.0
0.8
0.6
0.4
0.2
0.0
UMSCC1
UMSCC6
UMSCC23
UM1
UM2
NHOK
B
UMSCC1 UMSCC6
EGF + - + -
ACOT7
GAPDH
Relative ACOT7 expression
***
***
EGF
CTRL
UMSCC1
UMSCC6
UMSCC1 UMSCC6
EGF - + - + - + - +
FGF - - + + - - + +
ACOT7
GAPDH
Relative ACOT7 expression
****
****
****
****
CTRL
EGF
FGF
EGF&FGF
1.5
1.0
0.5
0.0
UMSCC1
UMSCC6

Figure 5

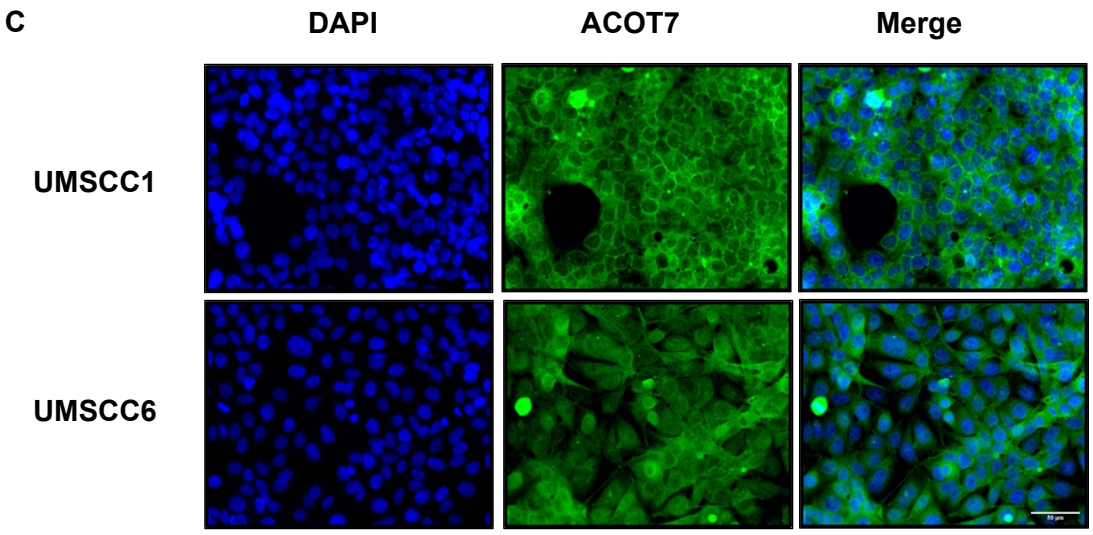

Figure 5

A

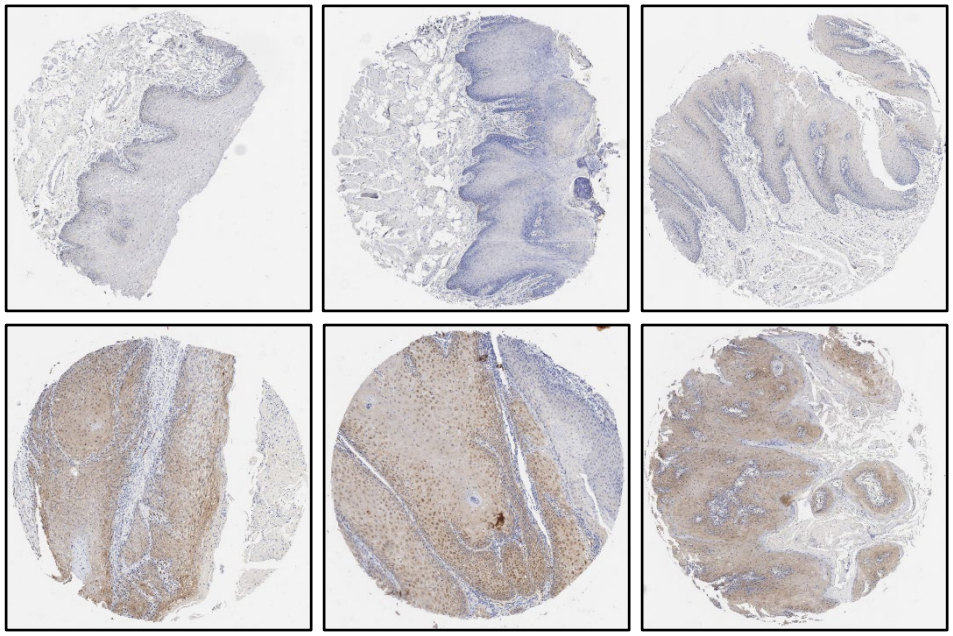

B

Age (y)	
Median(range)	57 (28-95)
Sex (%)	
Male	126
Female	26
Tumor stage (%)	
I	9.87% (15)
II	34.21% (52)
III	23.68% (37)
IVA	21.05% (32)
IV	7.89% (12)
ND	2.63% (4)

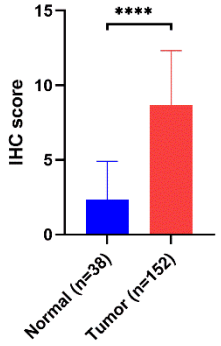

Figure 6

A

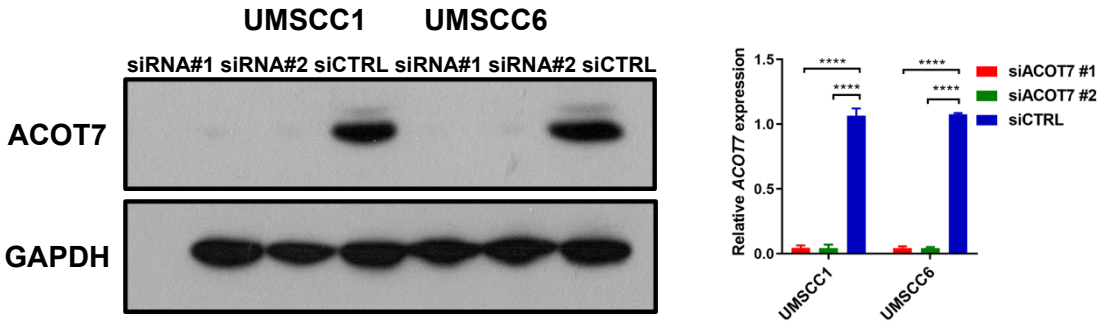
UMSCC1
UMSCC6
siRNA#1 siRNA#2 siCTRL siRNA#1 siRNA#2 siCTRL
ACOT7
GAPDH
Relative ACOT7 expression
1.5
1.0
0.5
0.0
****
****
****
****
siACOT7 #1
siACOT7 #2
siCTRL
UMSCC1
UMSCC6

Figure 7

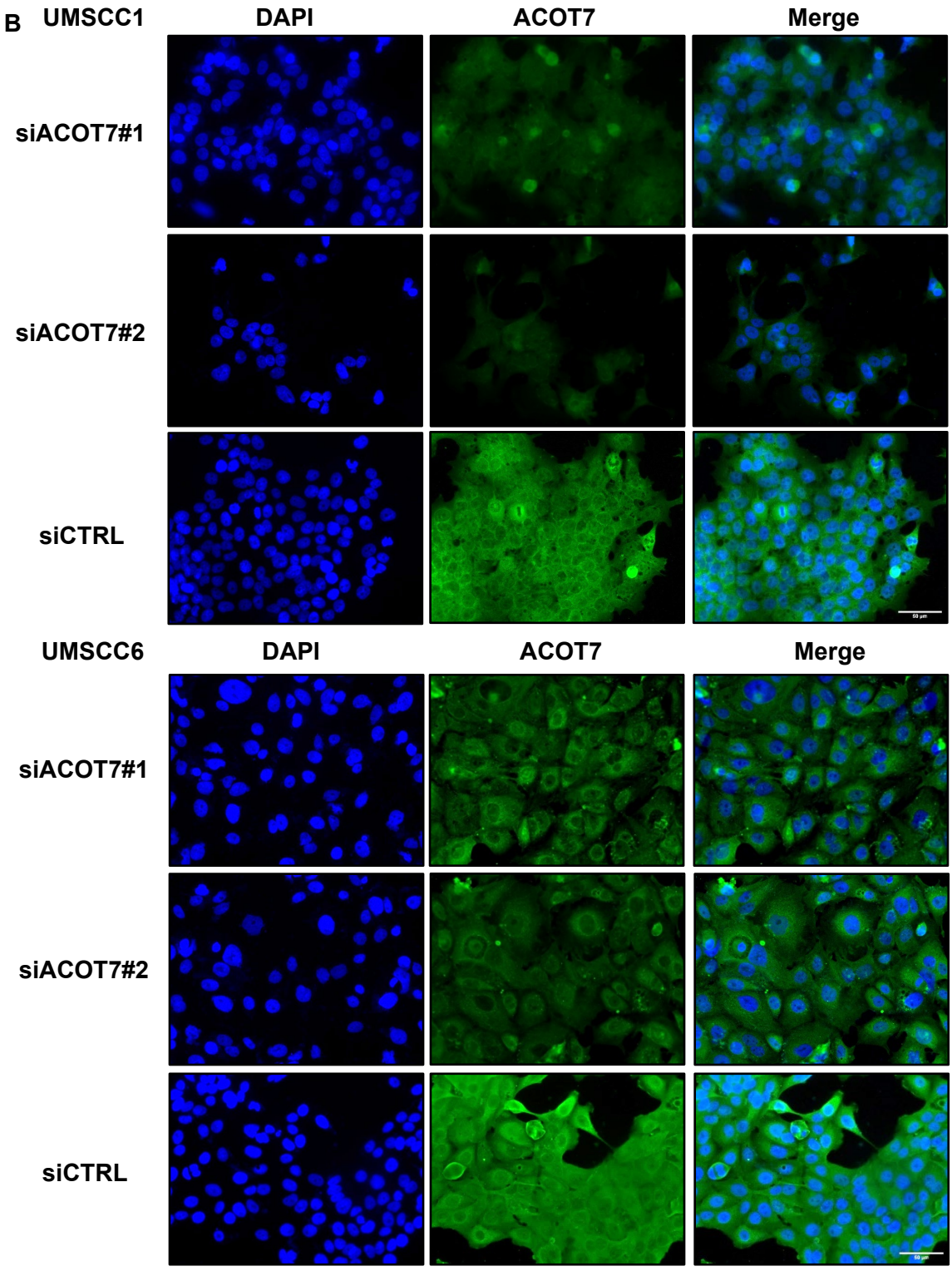
B
UMSCC1
DAPI
ACOT7
Merge
siACOT7#1
siACOT7#2
siCTRL
UMSCC6
DAPI
ACOT7
Merge
siACOT7#1
siACOT7#2
siCTRL

Figure 7

A

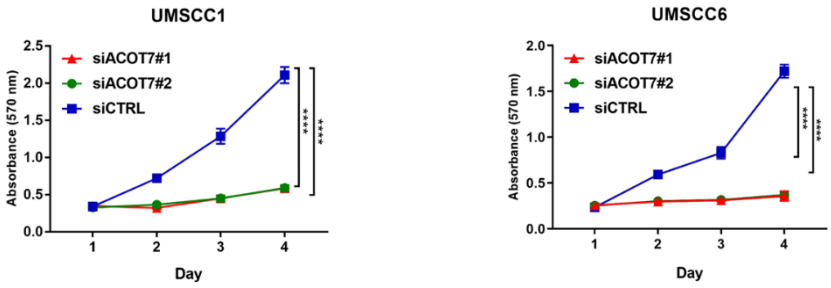
UMSCC1
siACOT7#1
siACOT7#2
siCTRL
Absorbance (570 nm)
Day
UMSCC6
siACOT7#1
siACOT7#2
siCTRL
Absorbance (570 nm)
Day

B

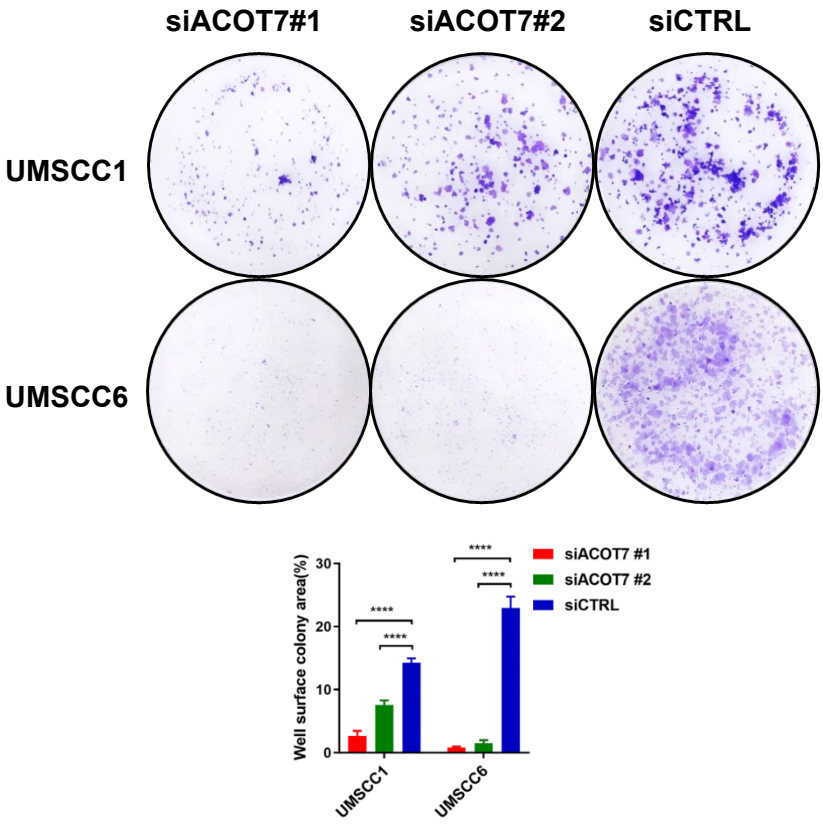
siACOT7#1
siACOT7#2
siCTRL
UMSCC1
UMSCC6
Well surface colony area(%)
siACOT7 #1
siACOT7 #2
siCTRL
UMSCC1
UMSCC6

Figure 8

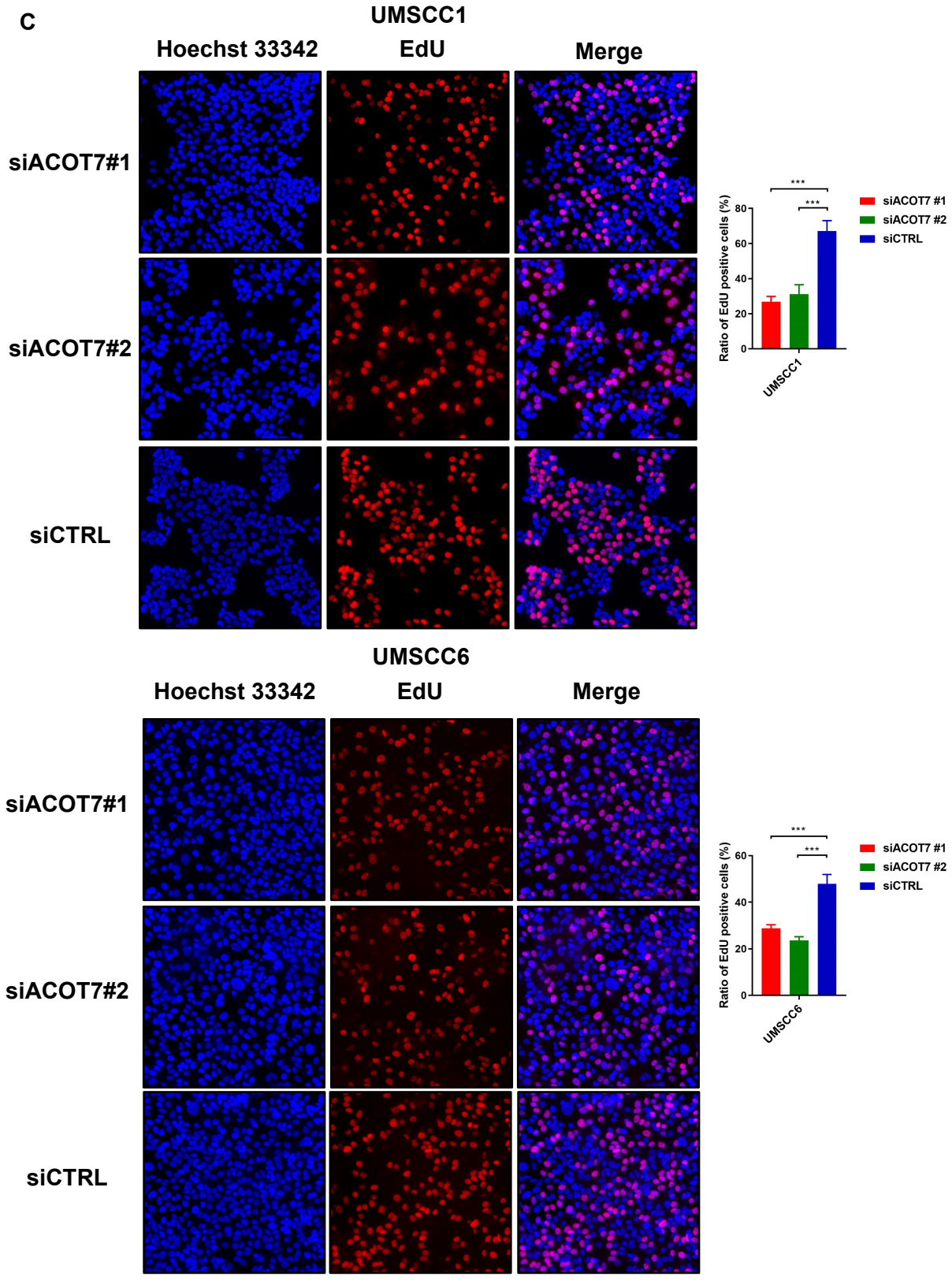
C
UMSCC1
Hoechst 33342
EdU
Merge
siACOT7#1
siACOT7#2
siCTRL
Ratio of EdU positive cells (%)
UMSCC1
siACOT7 #1
siACOT7 #2
siCTRL
UMSCC6
Hoechst 33342
EdU
Merge
siACOT7#1
siACOT7#2
siCTRL
Ratio of EdU positive cells (%)
UMSCC6
siACOT7 #1
siACOT7 #2
siCTRL

Figure 8

D

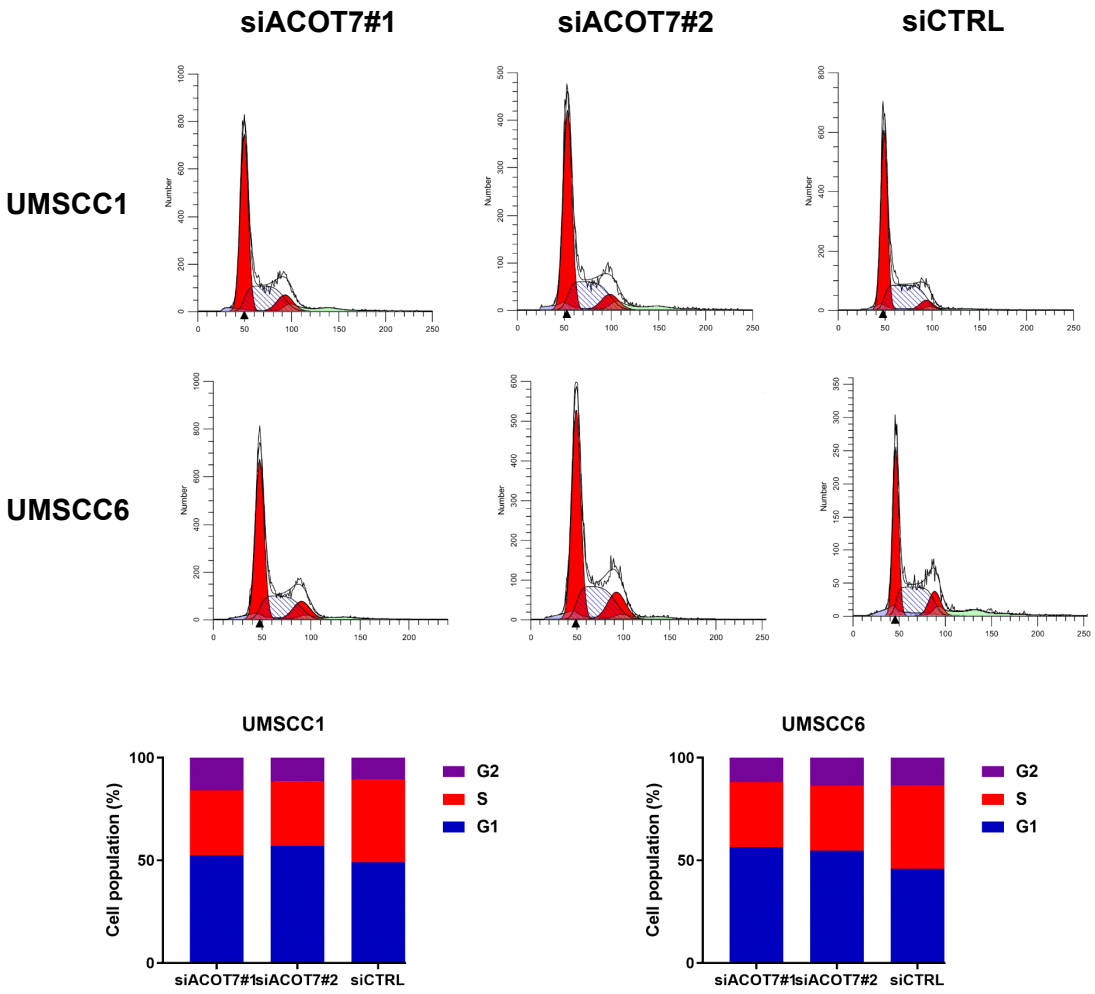
siACOT7#1
siACOT7#2
siCTRL
UMSCC1
UMSCC6
Number
UMSCC1
UMSCC6
Cell population (%)
100
50
0
G2
S
G1
siACOT7#1
siACOT7#2
siCTRL

Figure 8

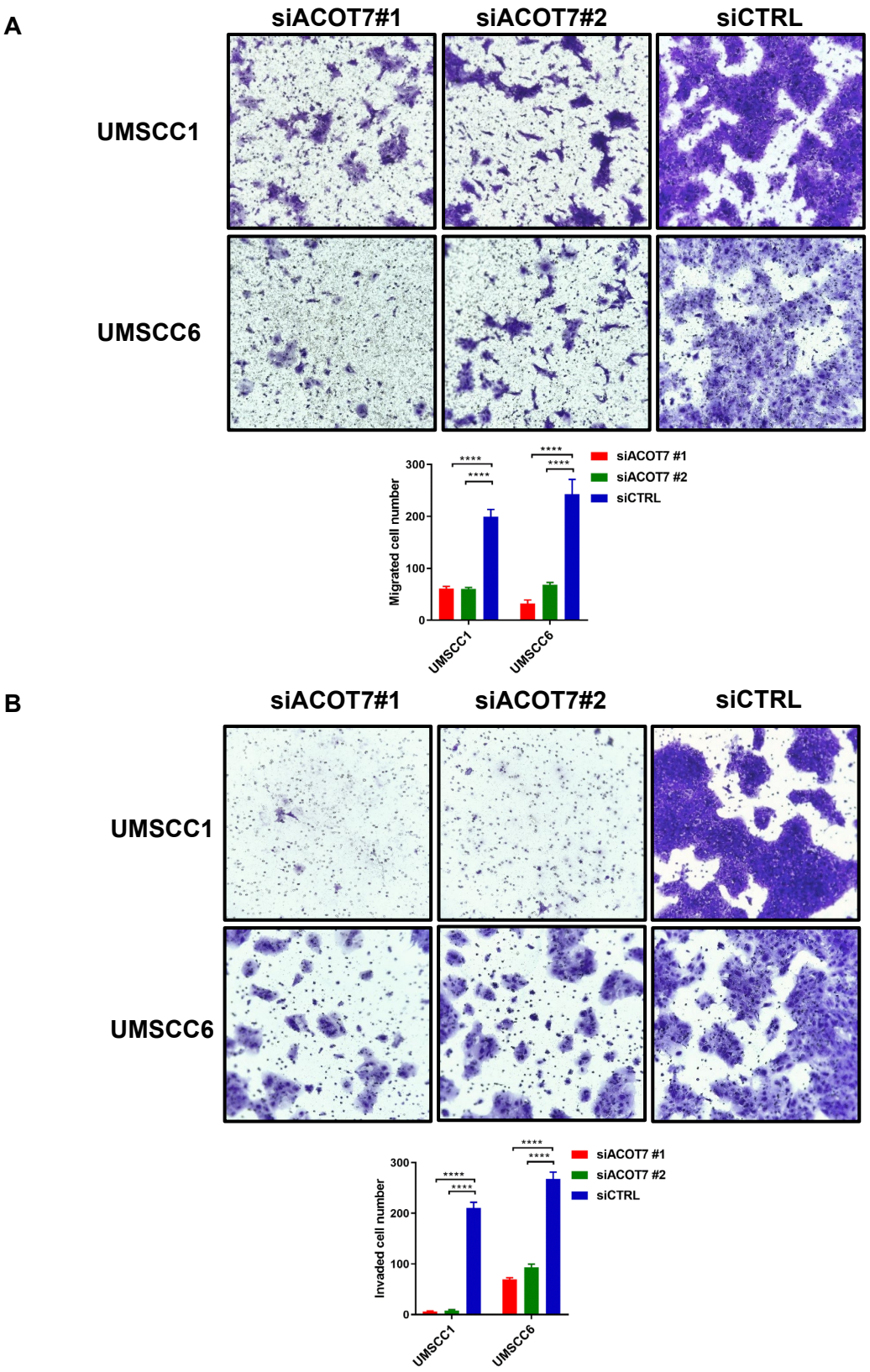
A
siACOT7#1
siACOT7#2
siCTRL
UMSCC1
UMSCC6
Migrated cell number
300
200
100
0
****
****
****
****
siACOT7 #1
siACOT7 #2
siCTRL
UMSCC1
UMSCC6
B
siACOT7#1
siACOT7#2
siCTRL
UMSCC1
UMSCC6
Invaded cell number
300
200
100
0
****
****
****
****
siACOT7 #1
siACOT7 #2
siCTRL
UMSCC1
UMSCC6

Figure 9

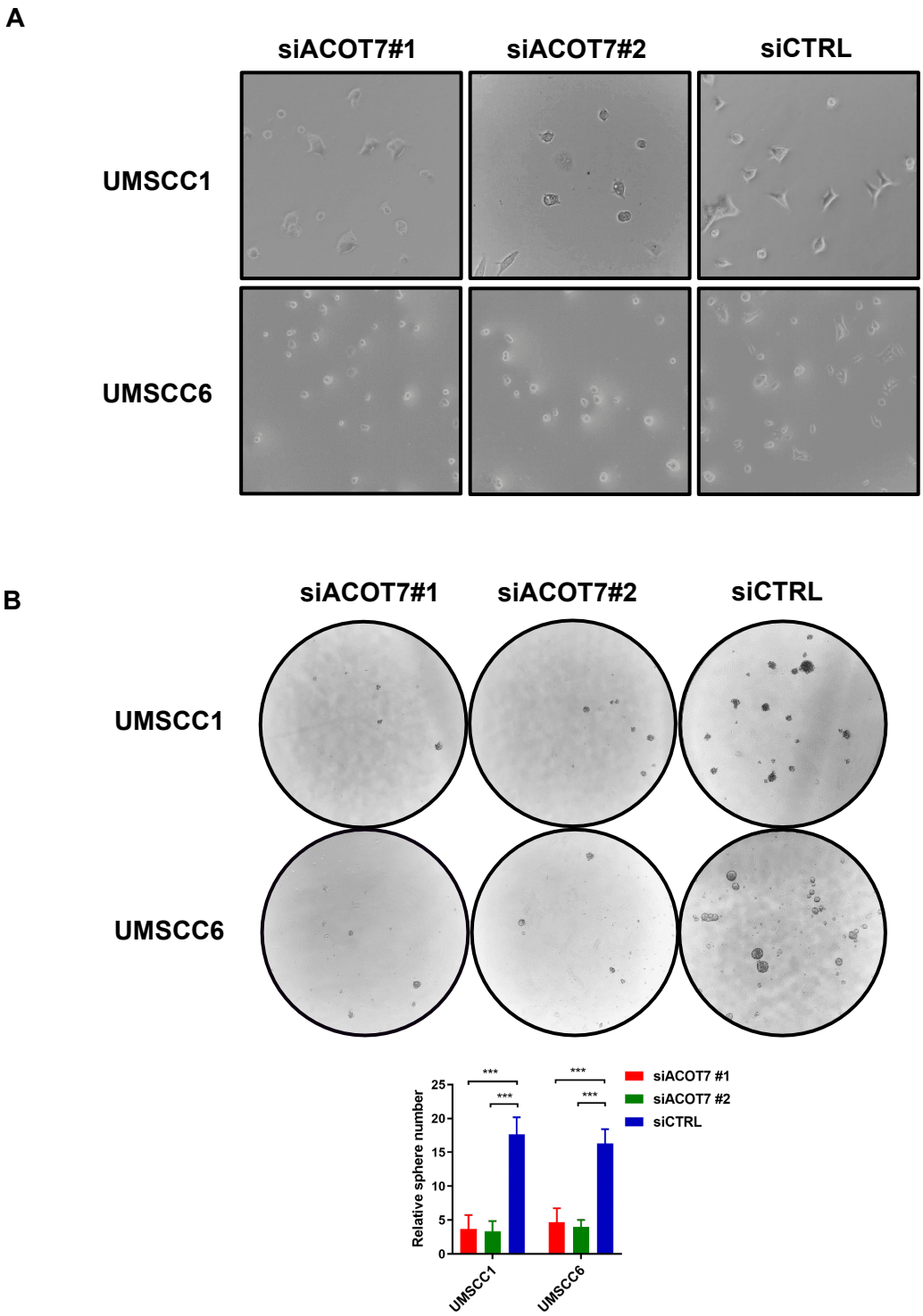
A
siACOT7#1
siACOT7#2
siCTRL
UMSCC1
UMSCC6
B
siACOT7#1
siACOT7#2
siCTRL
UMSCC1
UMSCC6
Relative sphere number
25
20
15
10
5
0
***
***
***
***
siACOT7 #1
siACOT7 #2
siCTRL
UMSCC1
UMSCC6

Figure 10

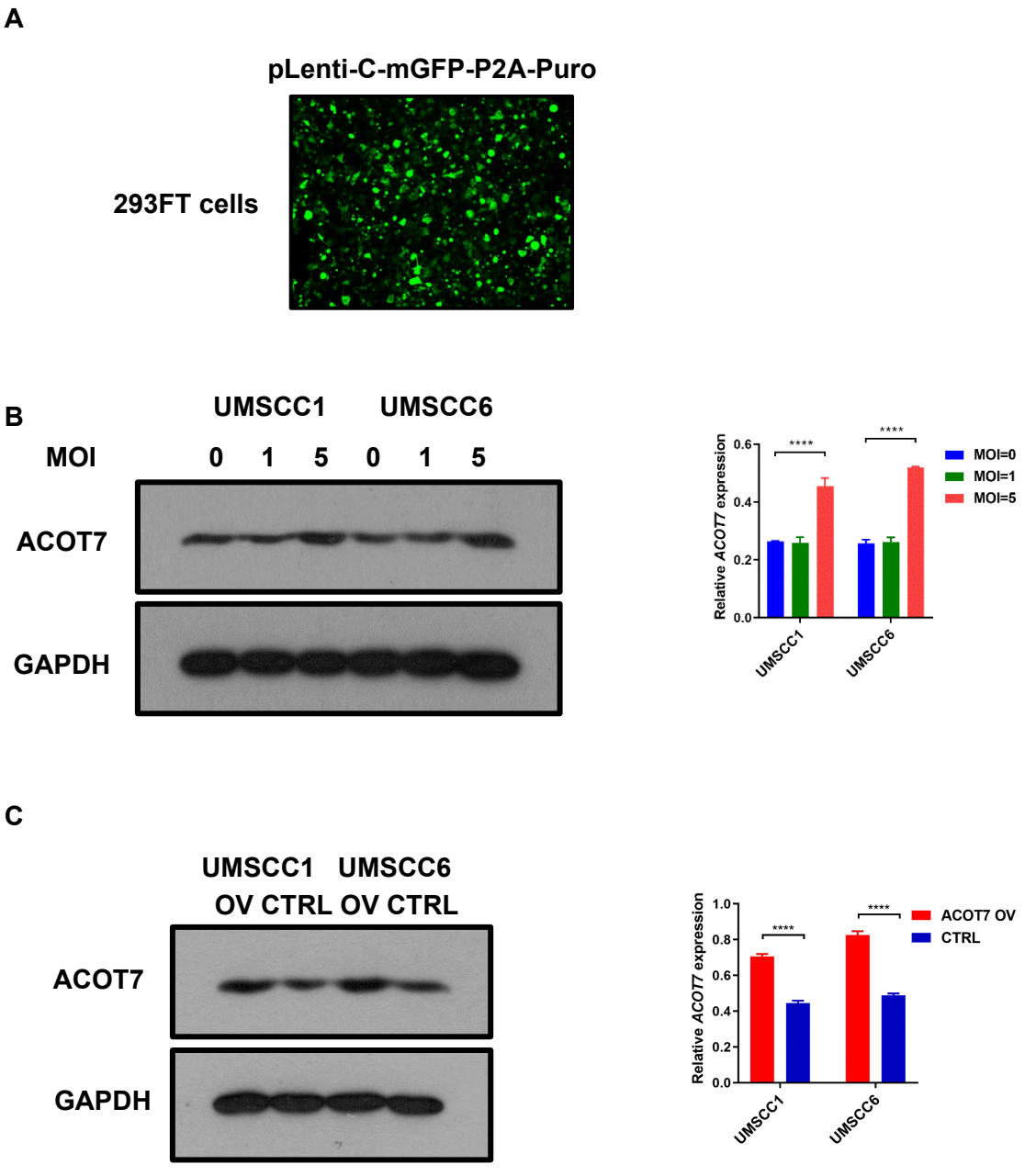
A
pLenti-C-mGFP-P2A-Puro
293FT cells
B
UMSCC1
UMSCC6
MOI
0 1 5 0 1 5
ACOT7
GAPDH
Relative ACOT7 expression
0.6
0.4
0.2
0.0
****
****
MOI=0
MOI=1
MOI=5
UMSCC1
UMSCC6
C
UMSCC1 UMSCC6
OV CTRL OV CTRL
ACOT7
GAPDH
Relative ACOT7 expression
1.0
0.8
0.6
0.4
0.2
0.0
****
****
ACOT7 OV
CTRL
UMSCC1
UMSCC6

Figure 11

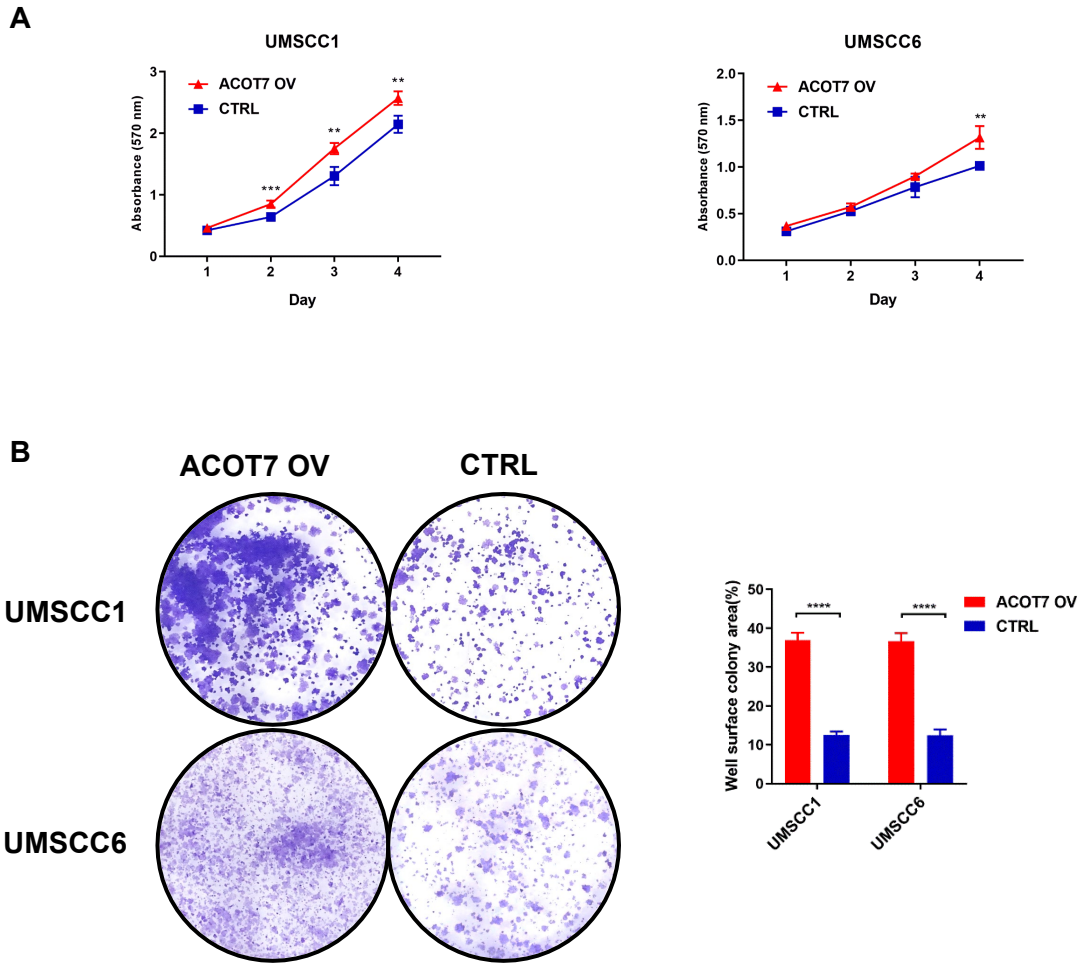
A
UMSCC1
ACOT7 OV
CTRL
Absorbance (570 nm)
Day
UMSCC6
ACOT7 OV
CTRL
Absorbance (570 nm)
Day
B
ACOT7 OV
CTRL
UMSCC1
UMSCC6
Well surface colony area(%)
ACOT7 OV
CTRL
UMSCC1
UMSCC6

Figure 12

C

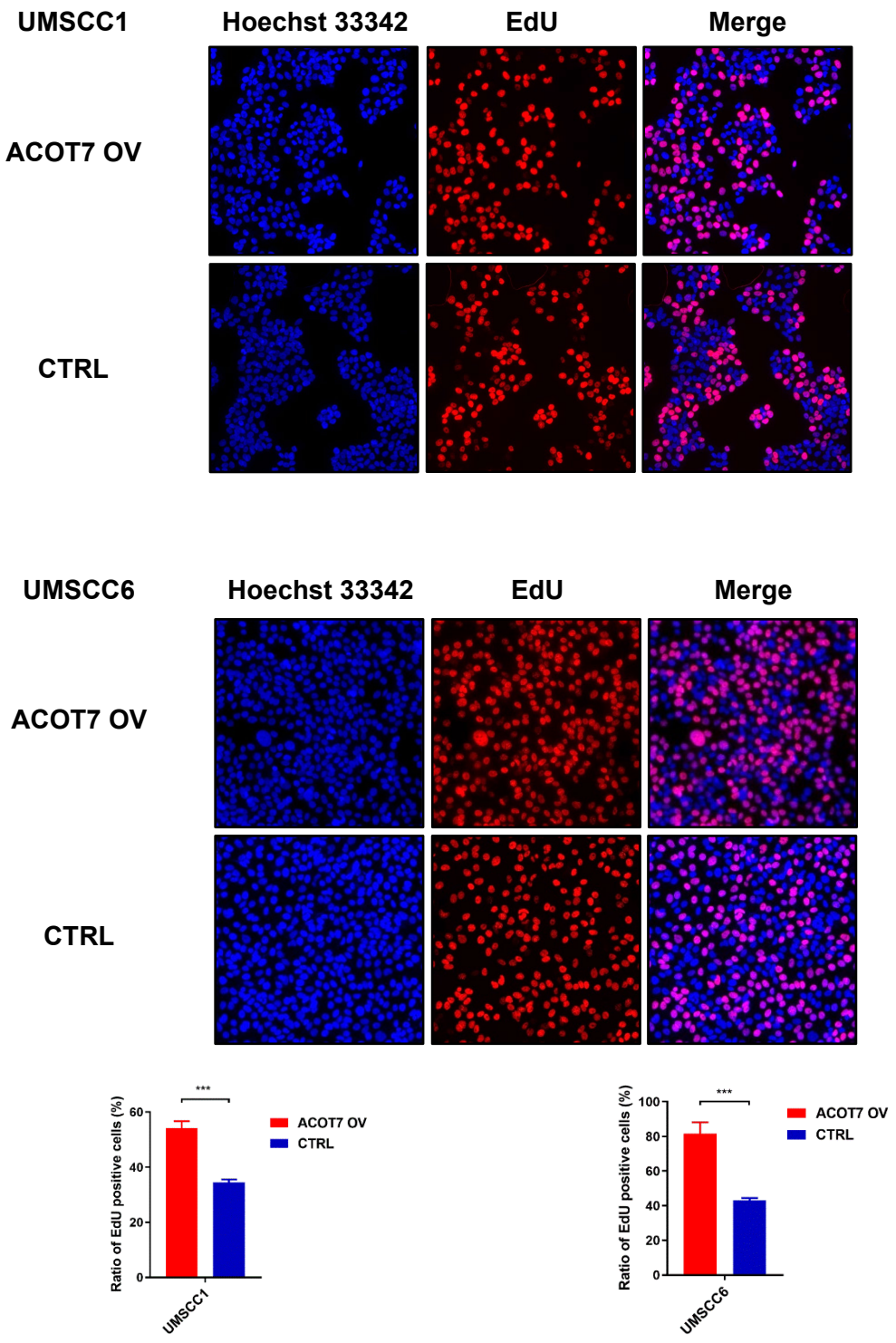
UMSCC1
Hoechst 33342
EdU
Merge
ACOT7 OV
CTRL
UMSCC6
Hoechst 33342
EdU
Merge
ACOT7 OV
CTRL
Ratio of EdU positive cells (%)
60
40
20
0
***
ACOT7 OV
CTRL
UMSCC1
Ratio of EdU positive cells (%)
100
80
60
40
20
0
***
ACOT7 OV
CTRL
UMSCC6

Figure 12

D

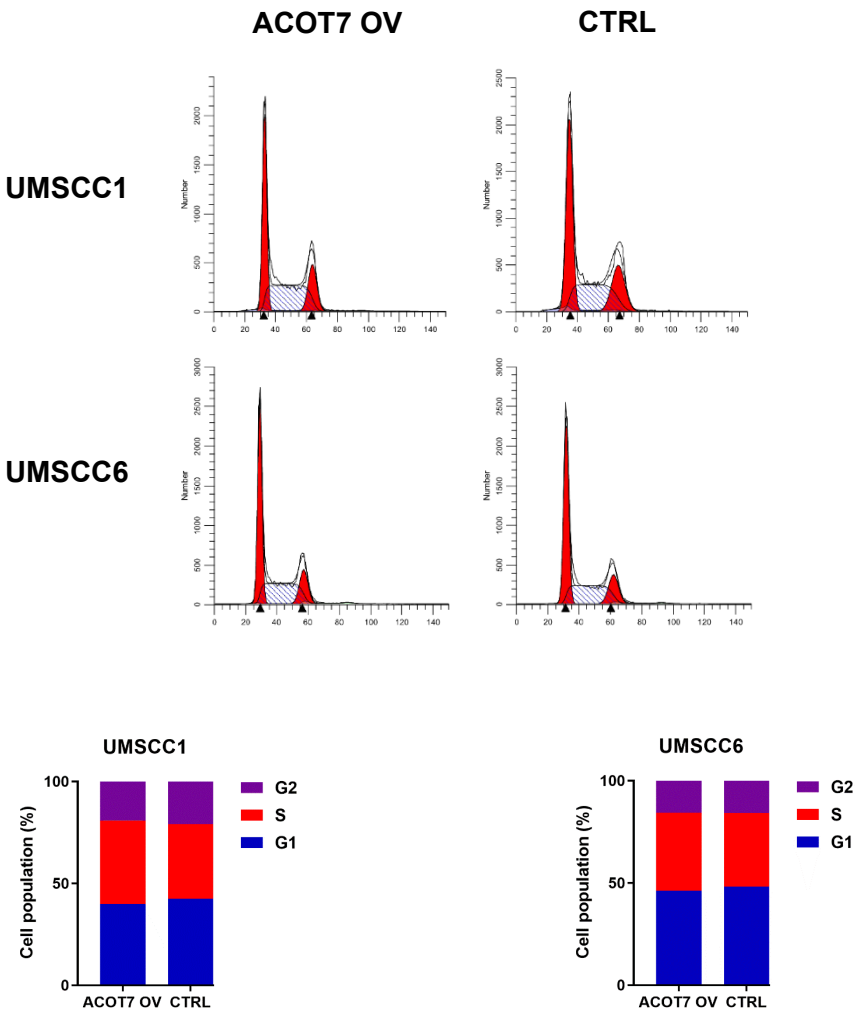
ACOT7 OV
CTRL
UMSCC1
UMSCC6
Number
UMSCC1
UMSCC6
Cell population (%)
100
50
0
G2
S
G1
ACOT7 OV
CTRL

Figure 12

A

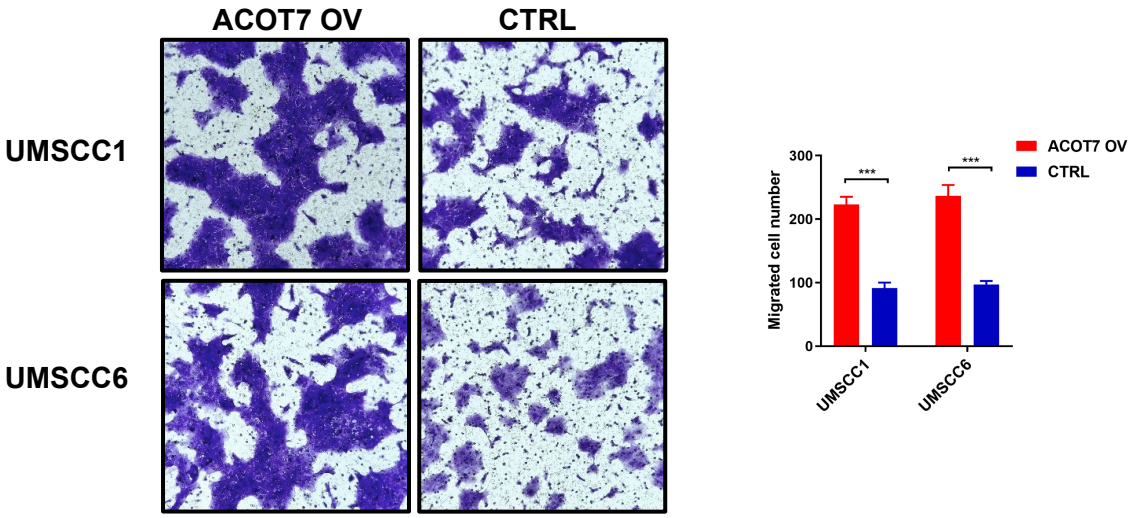
ACOT7 OV
CTRL
UMSCC1
UMSCC6
Migrated cell number
300
200
100
0
***
***
ACOT7 OV
CTRL
UMSCC1
UMSCC6

B

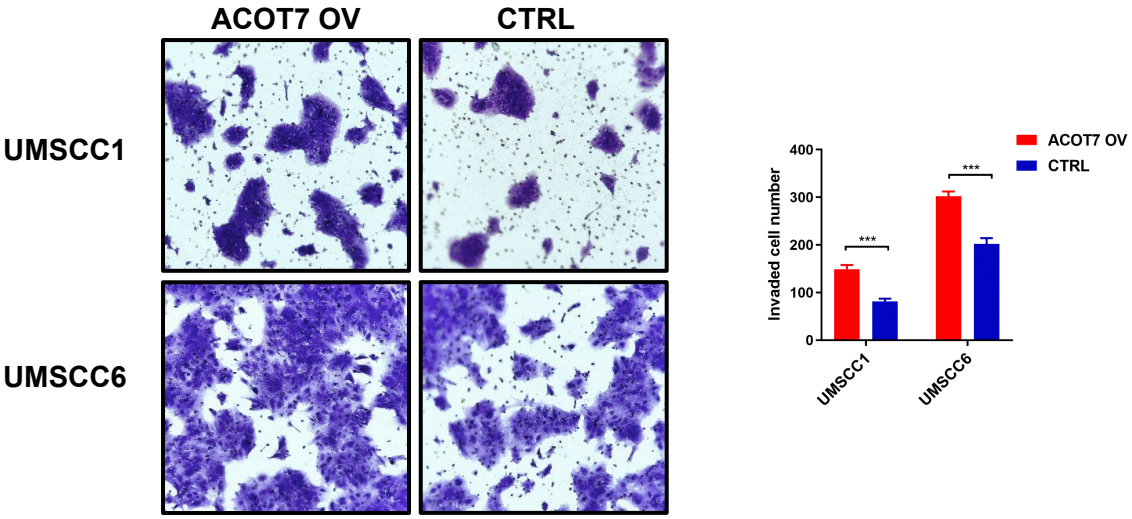
ACOT7 OV
CTRL
UMSCC1
UMSCC6
Invaded cell number
400
300
200
100
0
***
***
ACOT7 OV
CTRL
UMSCC1
UMSCC6

Figure 13

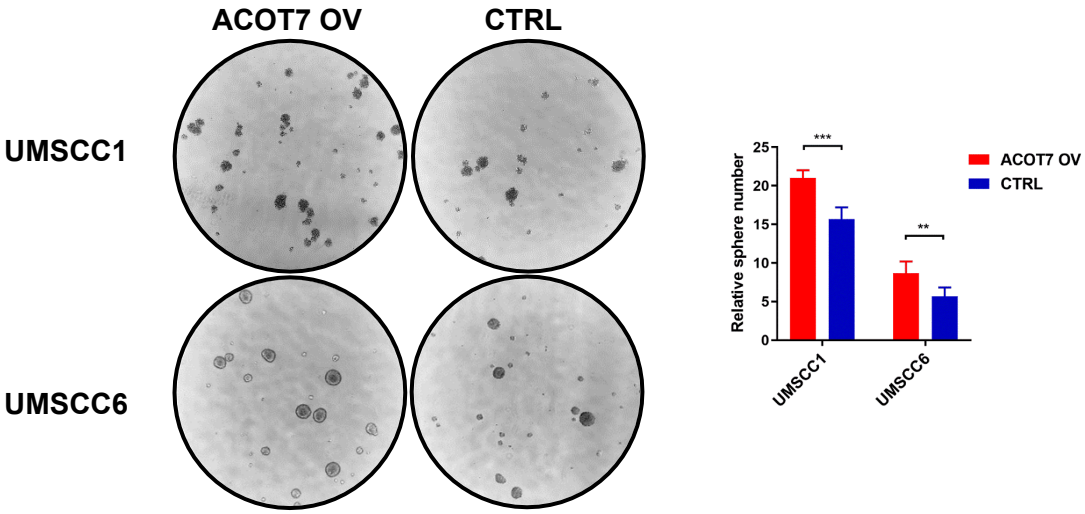
ACOT7 OV
CTRL
UMSCC1
UMSCC6
Relative sphere number
25
20
15
10
5
0
***
**
ACOT7 OV
CTRL
UMSCC1
UMSCC6

Figure 14

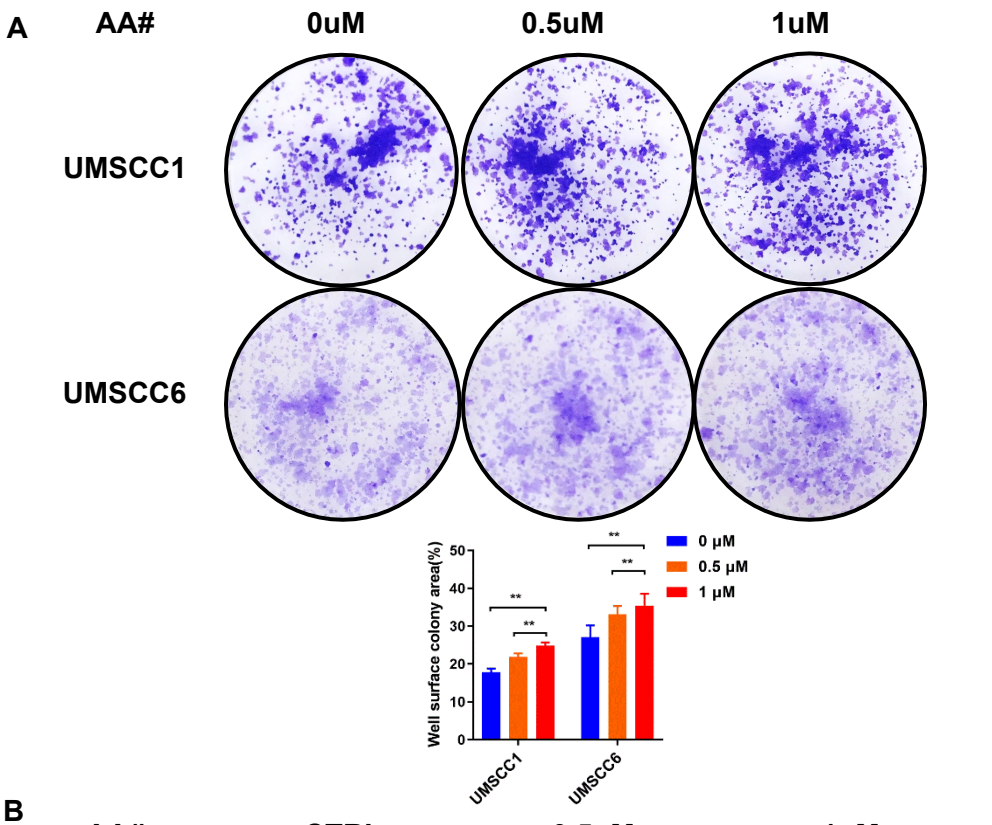
A
AA#
0uM
0.5uM
1uM
UMSCC1
UMSCC6
Well surface colony area(%)
0 μM
0.5 μM
1 μM
UMSCC1
UMSCC6

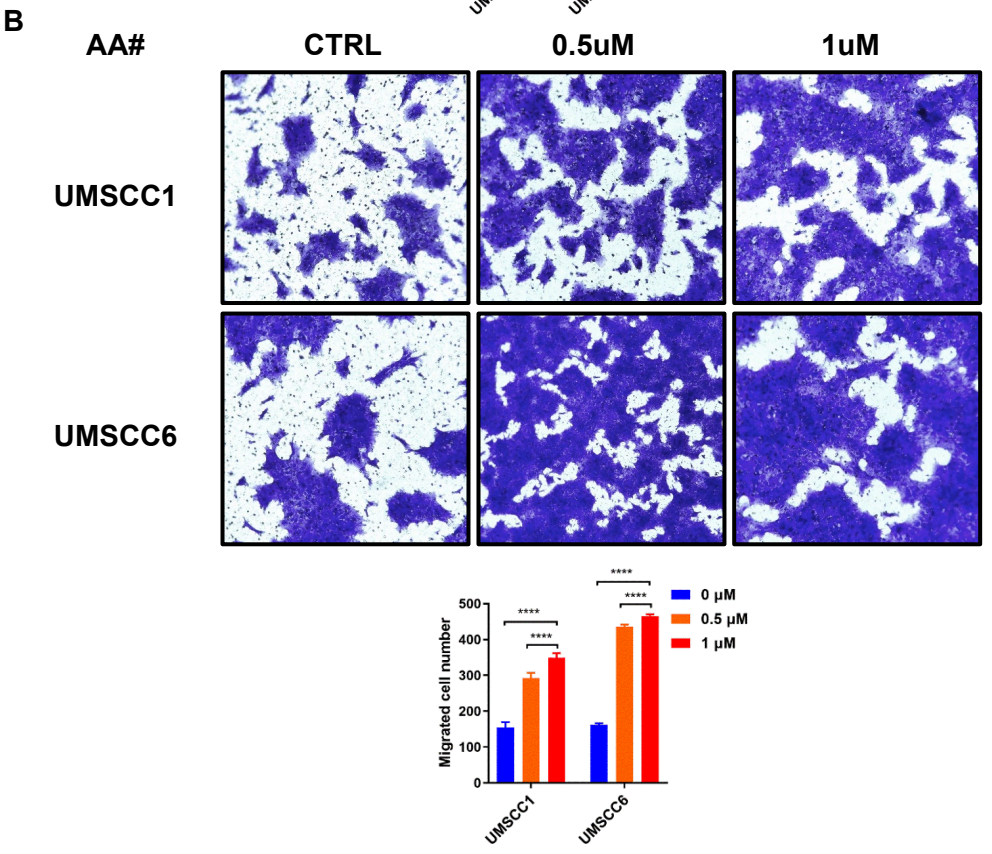
B
AA#
CTRL
0.5uM
1uM
UMSCC1
UMSCC6
Migrated cell number
0 μM
0.5 μM
1 μM
UMSCC1
UMSCC6

Figure 15

A


UMSCC1
****
Fold change
15
10
5
0
Negative Control
Anti-MYC
ACOT7 Promoter Expression
UMSCC6
****
Fold change
25
20
15
10
5
0
Negative Control
Anti-MYC
ACOT7 Promoter Expression

B

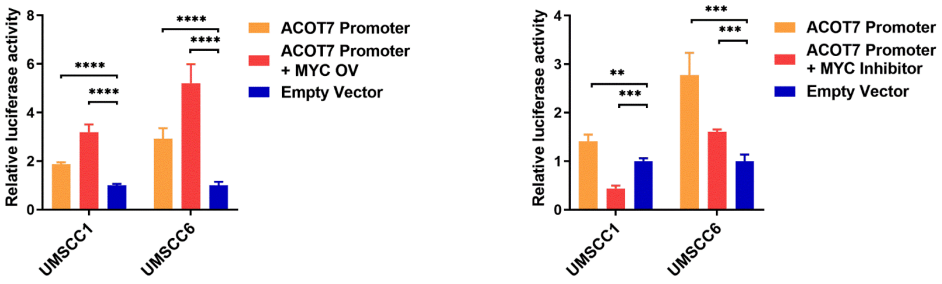
Relative luciferase activity
8
6
4
2
0
****
****
****
****
UMSCC1
UMSCC6
ACOT7 Promoter
ACOT7 Promoter
+ MYC OV
Empty Vector
Relative luciferase activity
4
3
2
1
0
**
***
***
***
UMSCC1
UMSCC6
ACOT7 Promoter
ACOT7 Promoter
+ MYC Inhibitor
Empty Vector

Figure 16

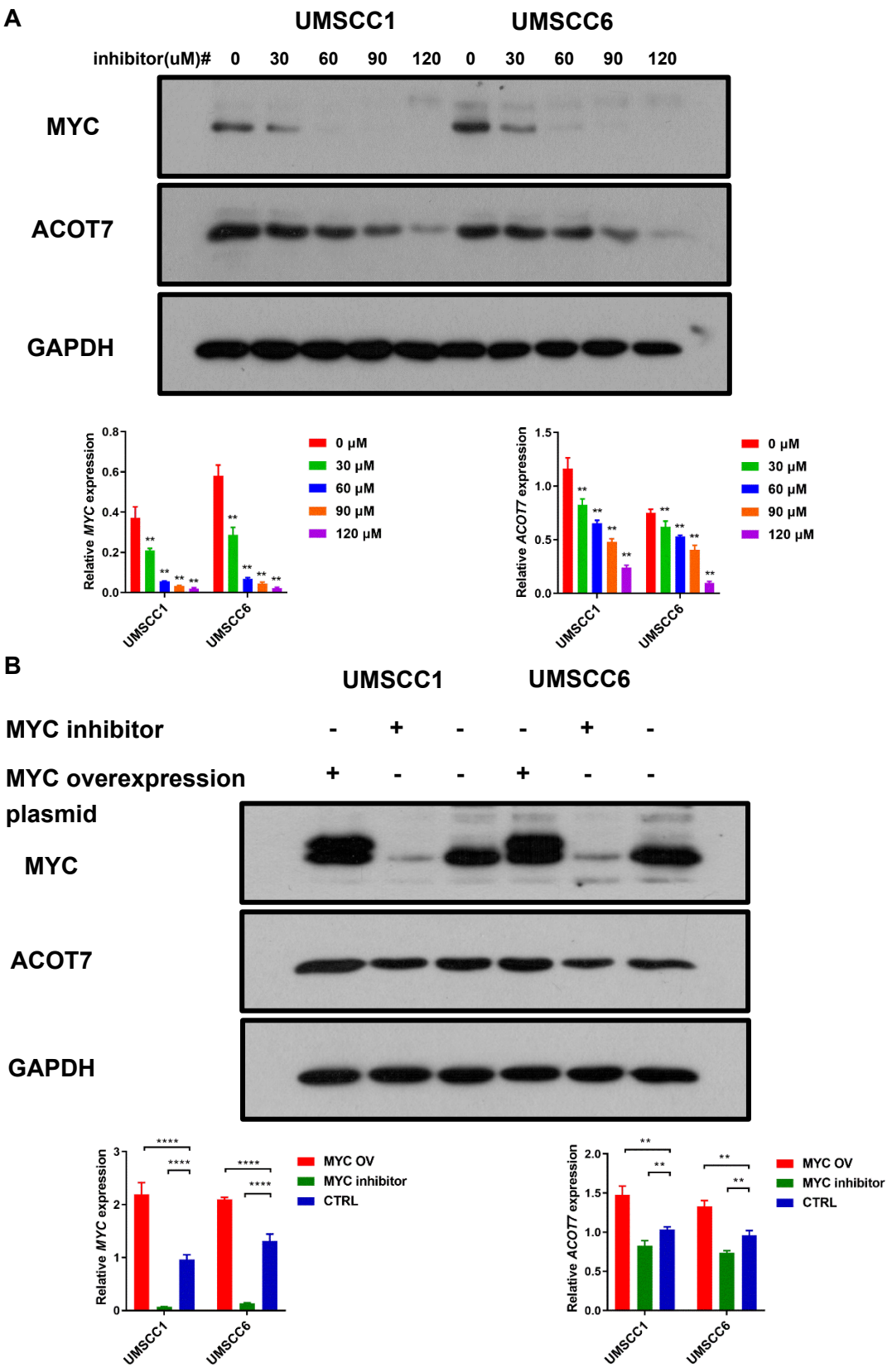
A
UMSCC1
UMSCC6
inhibitor(uM)# 0 30 60 90 120 0 30 60 90 120
MYC
ACOT7
GAPDH
Relative MYC expression
0 μM
30 μM
60 μM
90 μM
120 μM
UMSCC1
UMSCC6
Relative ACOT7 expression
B
UMSCC1
UMSCC6
MYC inhibitor - + - - + -
MYC overexpression plasmid + - - + - -
MYC
ACOT7
GAPDH
Relative MYC expression
MYC OV
MYC inhibitor
CTRL
Relative ACOT7 expression

Figure 17

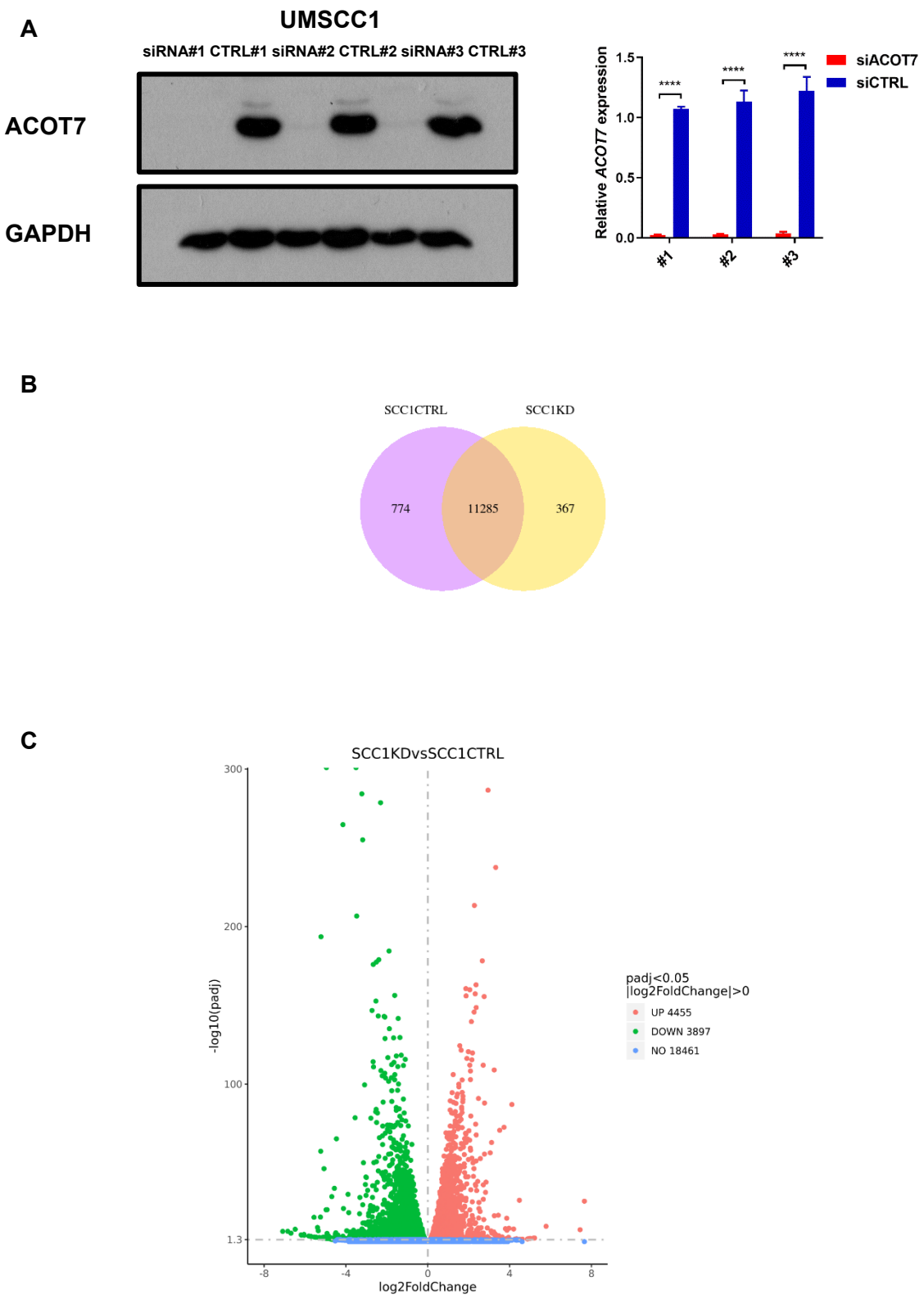
A
UMSCC1
siRNA#1 CTRL#1 siRNA#2 CTRL#2 siRNA#3 CTRL#3
ACOT7
GAPDH
Relative ACOT7 expression
siACOT7
siCTRL
****
#1
#2
#3
B
SCC1CTRL
SCC1KD
774
11285
367
C
SCC1KDvsSCC1CTRL
-log10(padj)
log2FoldChange
padj<0.05
|log2FoldChange|>0
UP 4455
DOWN 3897
NO 18461

Figure 18

D

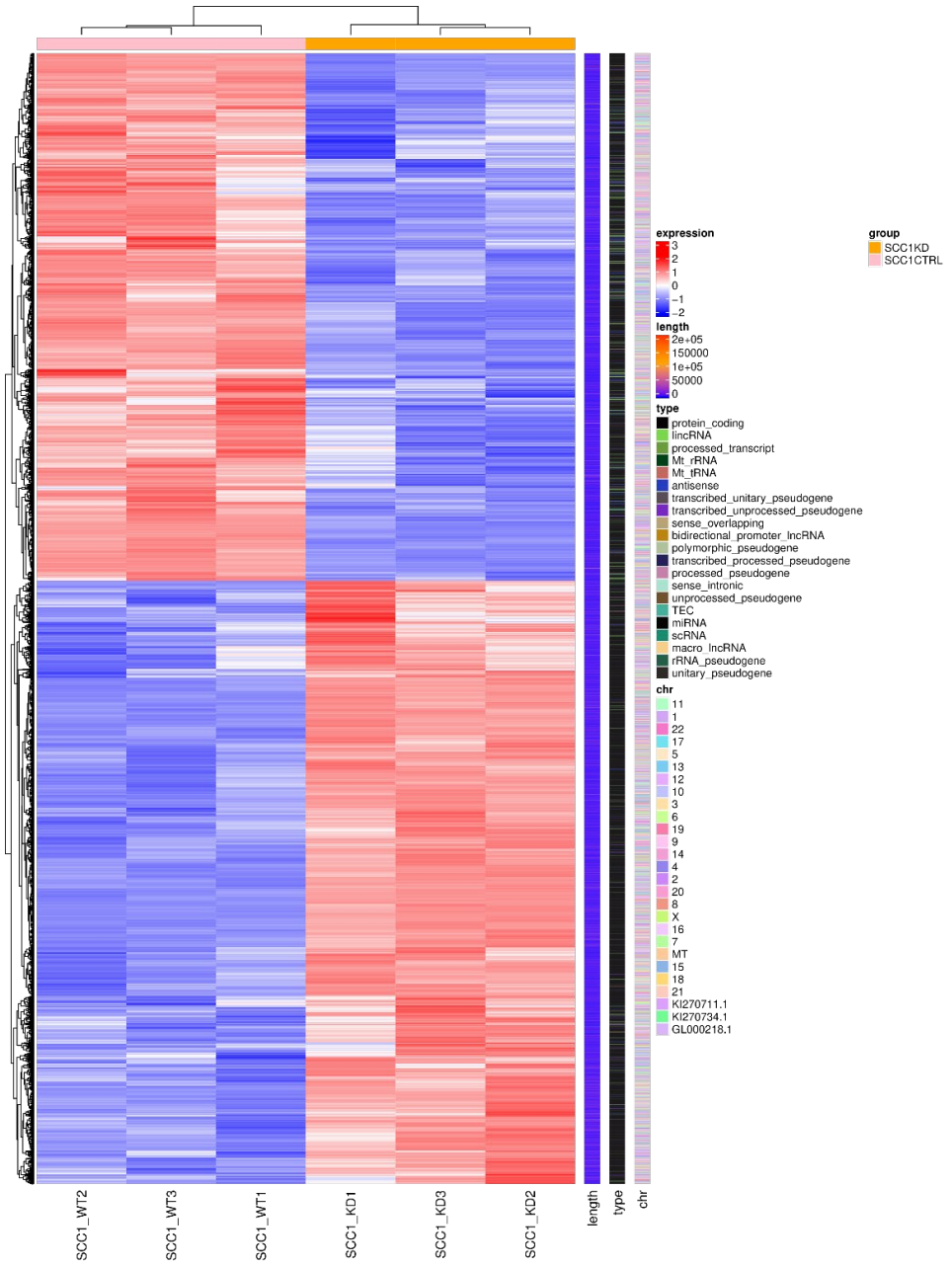
expression
3
2
1
0
−1
−2
length
2e+05
150000
1e+05
50000
0
type
protein_coding
lincRNA
processed_transcript
Mt_rRNA
Mt_tRNA
antisense
transcribed_unitary_pseudogene
transcribed_unprocessed_pseudogene
sense_overlapping
bidirectional_promoter_lncRNA
polymorphic_pseudogene
transcribed_processed_pseudogene
processed_pseudogene
sense_intronic
unprocessed_pseudogene
TEC
miRNA
scRNA
macro_lncRNA
rRNA_pseudogene
unitary_pseudogene
chr
11
1
22
17
5
13
12
10
3
6
19
9
14
4
2
20
8
X
16
7
MT
15
18
21
KI270711.1
KI270734.1
GL000218.1
group
SCC1KD
SCC1CTRL
SCC1_WT2
SCC1_WT3
SCC1_WT1
SCC1_KD1
SCC1_KD3
SCC1_KD2
length
type
chr

Figure 18

E

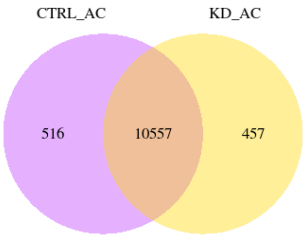
UMSCC23
CTRL_AC
KD_AC
516
10557
457

F

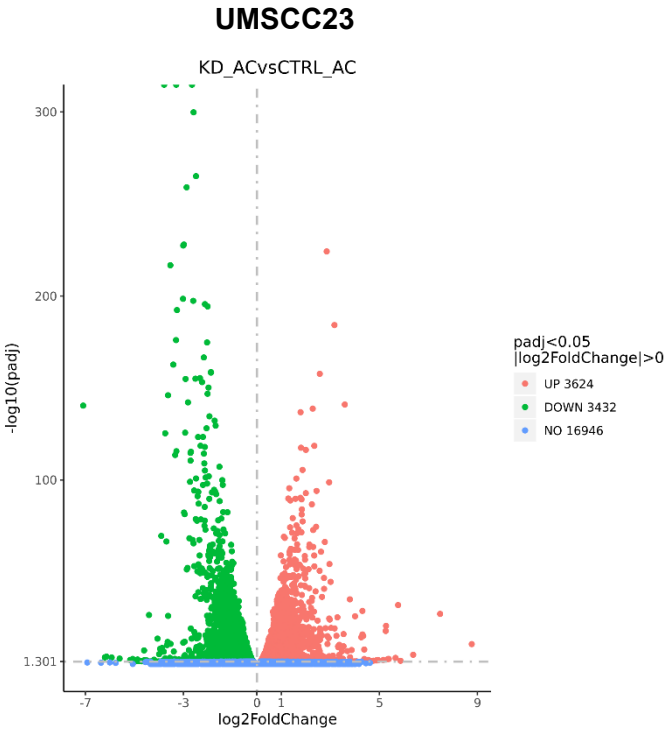
UMSCC23
KD_ACvsCTRL_AC
-log10(padj)
300
200
100
1.301
-7
-3
0
1
5
9
log2FoldChange
padj<0.05
|log2FoldChange|>0
UP 3624
DOWN 3432
NO 16946

Figure 18

G

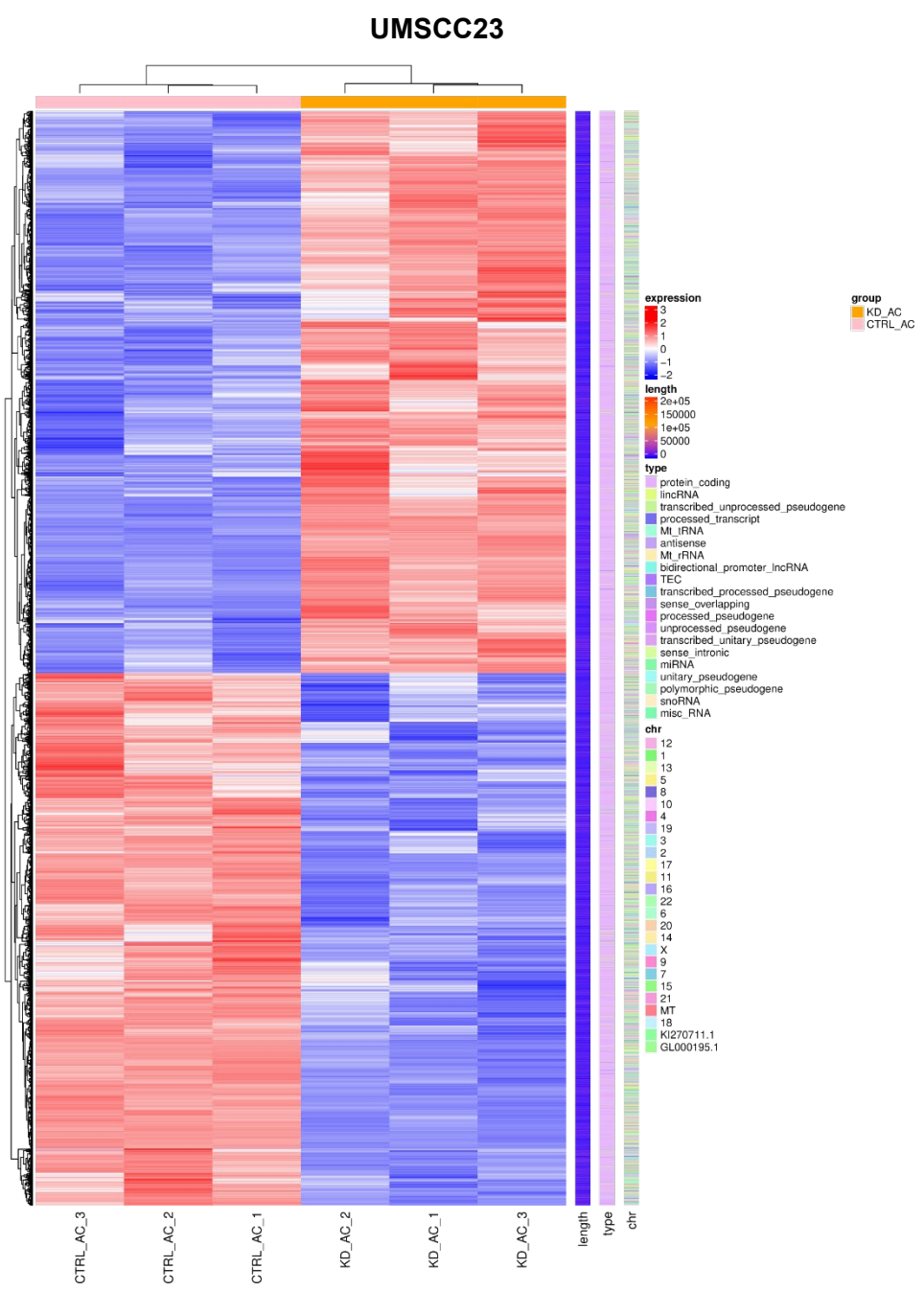
UMSCC23
expression
3
2
1
0
−1
−2
group
KD_AC
CTRL_AC
length
2e+05
150000
1e+05
50000
0
type
protein_coding
lincRNA
transcribed_unprocessed_pseudogene
processed_transcript
Mt_tRNA
antisense
Mt_rRNA
bidirectional_promoter_lncRNA
TEC
transcribed_processed_pseudogene
sense_overlapping
processed_pseudogene
unprocessed_pseudogene
transcribed_unitary_pseudogene
sense_intronic
miRNA
unitary_pseudogene
polymorphic_pseudogene
snoRNA
misc_RNA
chr
12
1
13
5
8
10
4
19
3
2
17
11
16
22
6
20
14
X
9
7
15
21
MT
18
KI270711.1
GL000195.1
CTRL_AC_3
CTRL_AC_2
CTRL_AC_1
KD_AC_2
KD_AC_1
KD_AC_3
length
type
chr

Figure 18

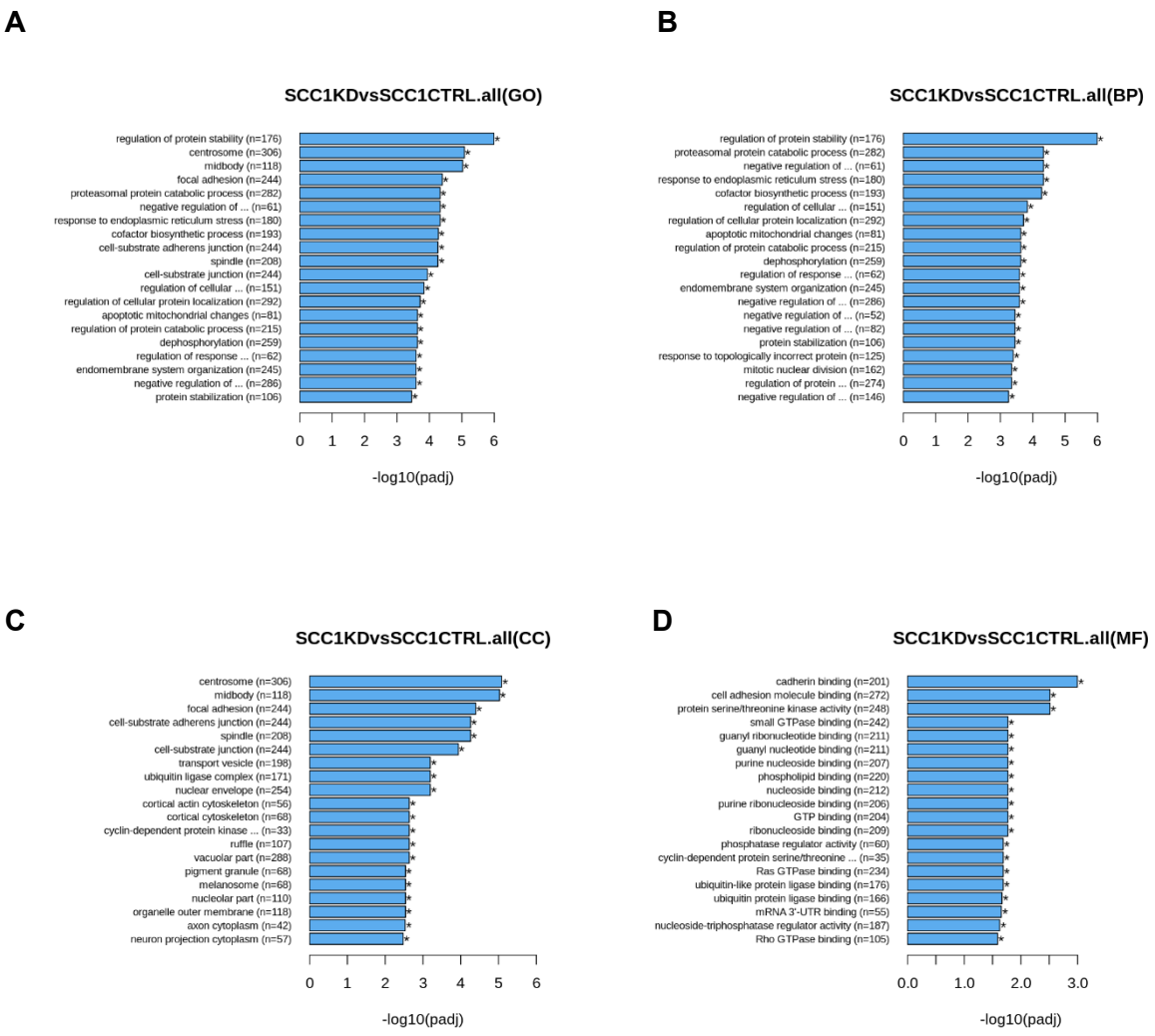
A
SCC1KDvsSCC1CTRL.all(GO)
regulation of protein stability (n=176)
centrosome (n=306)
midbody (n=118)
focal adhesion (n=244)
proteasomal protein catabolic process (n=282)
negative regulation of ... (n=61)
response to endoplasmic reticulum stress (n=180)
cofactor biosynthetic process (n=193)
cell-substrate adherens junction (n=244)
spindle (n=208)
cell-substrate junction (n=244)
regulation of cellular ... (n=151)
regulation of cellular protein localization (n=292)
apoptotic mitochondrial changes (n=81)
regulation of protein catabolic process (n=215)
dephosphorylation (n=259)
regulation of response ... (n=62)
endomembrane system organization (n=245)
negative regulation of ... (n=286)
protein stabiiization (n=106)
0 1 2 3 4 5 6
-log10(padj)
B
SCC1KDvsSCC1CTRL.all(BP)
regulation of protein stability (n=176)
proteasomal protein catabolic process (n=282)
negative regulation of ... (n=61)
response to endoplasmic reticulum stress (n=180)
cofactor biosynthetic process (n=193)
regulation of cellular ... (n=151)
regulation of cellular protein localization (n=292)
apoptotic mitochondrial changes (n=81)
regulation of protein catabolic process (n=215)
dephosphorylation (n=259)
regulation of response ... (n=62)
endomembrane system organization (n=245)
negative regulation of ... (n=286)
negative regulation of ... (n=52)
negative regulation of ... (n=82)
protein stabilization (n=106)
response to topologically incorrect protein (n=125)
mitotic nuclear division (n=162)
regulation of protein ... (n=274)
negative regulation of ... (n=146)
0 1 2 3 4 5 6
-log10(padj)
C
SCC1KDvsSCC1CTRL.all(CC)
centrosome (n=306)
midbody (n=118)
focal adhesion (n=244)
cell-substrate adherens junction (n=244)
spindle (n=208)
cell-substrate junction (n=244)
transport vesicle (n=198)
ubiquitin ligase complex (n=171)
nuclear envelope (n=254)
cortical actin cytoskeleton (n=56)
cortical cytoskeleton (n=68)
cyclin-dependent protein kinase ... (n=33)
ruffle (n=107)
vacuolar part (n=288)
pigment granule (n=68)
melanosome (n=68)
nucleolar part (n=110)
organelle outer membrane (n=118)
axon cytoplasm (n=42)
neuron projection cytoplasm (n=57)
0 1 2 3 4 5 6
-log10(padj)
D
SCC1KDvsSCC1CTRL.all(MF)
cadherin binding (n=201)
cell adhesion molecule binding (n=272)
protein serine/threonine kinase activity (n=248)
small GTPase binding (n=242)
guanyl ribonucleotide binding (n=211)
guanyl nucleotide binding (n=211)
purine nucleoside binding (n=207)
phospholipid binding (n=220)
nucleoside binding (n=212)
purine ribonucleoside binding (n=206)
GTP binding (n=204)
ribonucleoside binding (n=209)
phosphatase regulator activity (n=60)
cyclin-dependent protein serine/threonine ... (n=35)
Ras GTPase binding (n=234)
ubiquitin-like protein ligase binding (n=176)
ubiquitin protein ligase binding (n=166)
mRNA 3'-UTR binding (n=55)
nucleoside-triphosphatase regulator activity (n=187)
Rho GTPase binding (n=105)
0.0 1.0 2.0 3.0
-log10(padj)

Figure 19

A

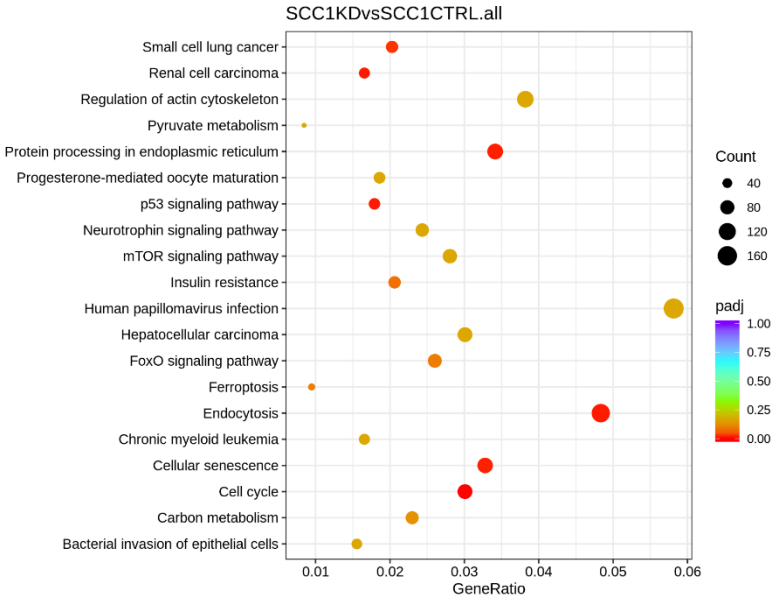
SCC1KDvsSCC1CTRL.all
Small cell lung cancer
Renal cell carcinoma
Regulation of actin cytoskeleton
Pyruvate metabolism
Protein processing in endoplasmic reticulum
Progesterone-mediated oocyte maturation
p53 signaling pathway
Neurotrophin signaling pathway
mTOR signaling pathway
Insulin resistance
Human papillomavirus infection
Hepatocellular carcinoma
FoxO signaling pathway
Ferroptosis
Endocytosis
Chronic myeloid leukemia
Cellular senescence
Cell cycle
Carbon metabolism
Bacterial invasion of epithelial cells
0.01
0.02
0.03
0.04
0.05
0.06
GeneRatio
Count
40
80
120
160
padj
1.00
0.75
0.50
0.25
0.00

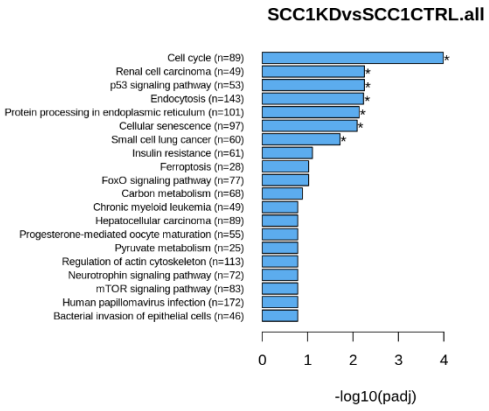
SCC1KDvsSCC1CTRL.all
Cell cycle (n=89)
Renal cell carcinoma (n=49)
p53 signaling pathway (n=53)
Endocytosis (n=143)
Protein processing in endoplasmic reticulum (n=101)
Cellular senescence (n=97)
Small cell lung cancer (n=60)
Insulin resistance (n=61)
Ferroptosis (n=28)
FoxO signaling pathway (n=77)
Carbon metabolism (n=68)
Chronic myeloid leukemia (n=49)
Hepatocellular carcinoma (n=89)
Progesterone-mediated oocyte maturation (n=55)
Pyruvate metabolism (n=25)
Regulation of actin cytoskeleton (n=113)
Neurotrophin signaling pathway (n=72)
mTOR signaling pathway (n=83)
Human papillomavirus infection (n=172)
Bacterial invasion of epithelial cells (n=46)
0
1
2
3
4
-log10(padj)

Figure 20

B

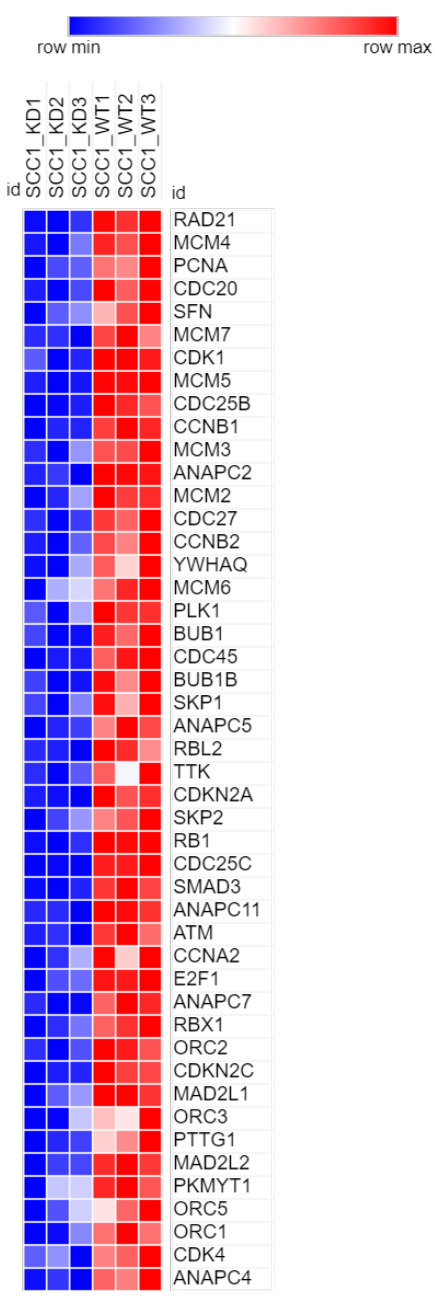
row min
row max
id
SCC1_KD1
SCC1_KD2
SCC1_KD3
SCC1_WT1
SCC1_WT2
SCC1_WT3
id
RAD21
MCM4
PCNA
CDC20
SFN
MCM7
CDK1
MCM5
CDC25B
CCNB1
MCM3
ANAPC2
MCM2
CDC27
CCNB2
YWHAQ
MCM6
PLK1
BUB1
CDC45
BUB1B
SKP1
ANAPC5
RBL2
TTK
CDKN2A
SKP2
RB1
CDC25C
SMAD3
ANAPC11
ATM
CCNA2
E2F1
ANAPC7
RBX1
ORC2
CDKN2C
MAD2L1
ORC3
PTTG1
MAD2L2
PKMYT1
ORC5
ORC1
CDK4
ANAPC4

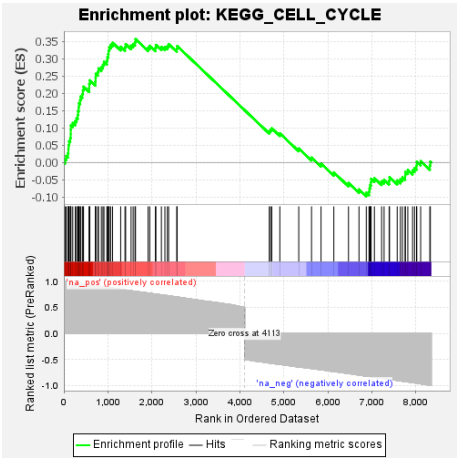
Enrichment plot: KEGG_CELL_CYCLE
Enrichment score (ES)
0.35
0.30
0.25
0.20
0.15
0.10
0.05
0.00
-0.05
-0.10
Ranked list metric (PreRanked)
1.0
0.5
0.0
-0.5
-1.0
'na_pos' (positively correlated)
Zero cross at 4113
'na_neg' (negatively correlated)
0
1,000
2,000
3,000
4,000
5,000
6,000
7,000
8,000
Rank in Ordered Dataset
Enrichment profile
Hits
Ranking metric scores

Figure 20

C

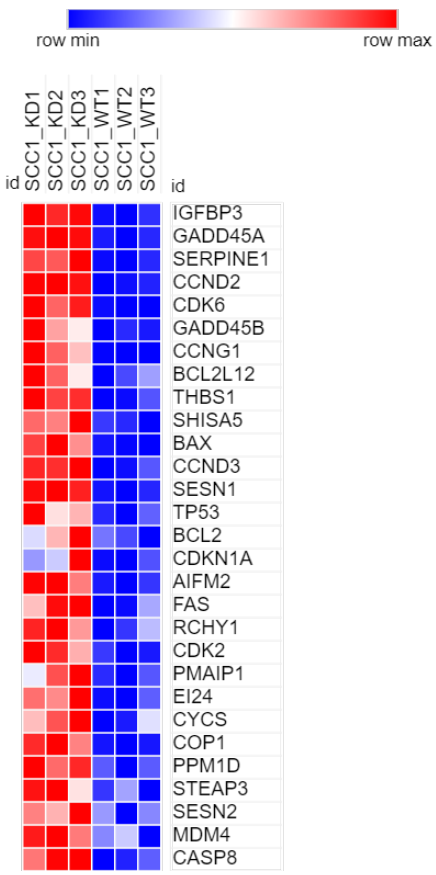
row min
row max
id
SCC1_KD1
SCC1_KD2
SCC1_KD3
SCC1_WT1
SCC1_WT2
SCC1_WT3
id
IGFBP3
GADD45A
SERPINE1
CCND2
CDK6
GADD45B
CCNG1
BCL2L12
THBS1
SHISA5
BAX
CCND3
SESN1
TP53
BCL2
CDKN1A
AIFM2
FAS
RCHY1
CDK2
PMAIP1
EI24
CYCS
COP1
PPM1D
STEAP3
SESN2
MDM4
CASP8

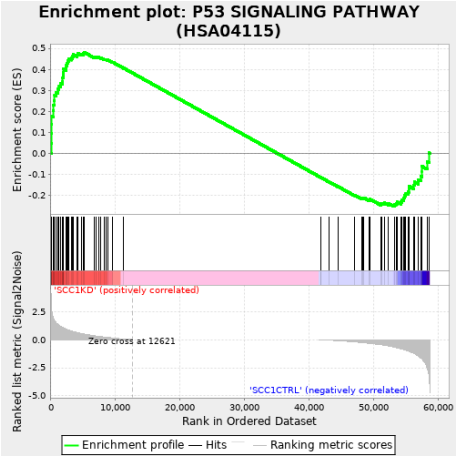
Enrichment plot: P53 SIGNALING PATHWAY (HSA04115)
Enrichment score (ES)
'SCC1KD' (positively correlated)
Ranked list metric (Signal2Noise)
Zero cross at 12621
'SCC1CTRL' (negatively correlated)
Rank in Ordered Dataset
Enrichment profile
Hits
Ranking metric scores

Figure 20

D

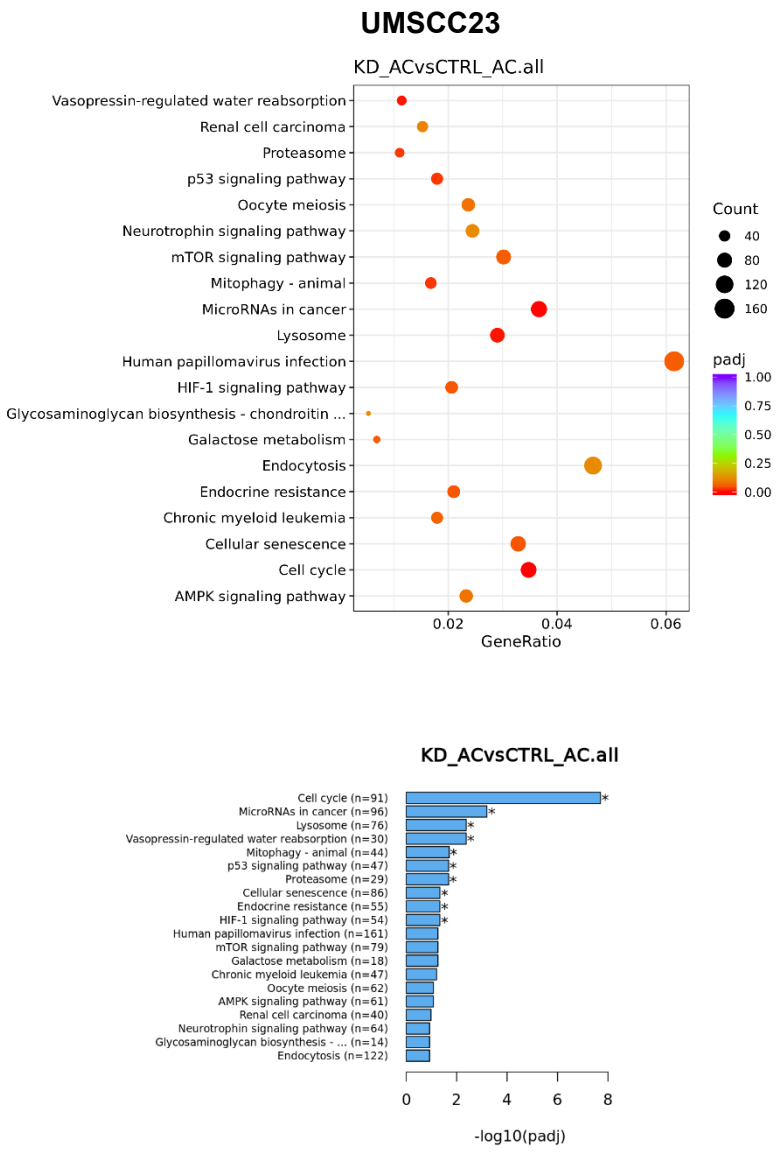
UMSCC23
KD_ACvsCTRL_AC.all
Vasopressin-regulated water reabsorption
Renal cell carcinoma
Proteasome
p53 signaling pathway
Oocyte meiosis
Neurotrophin signaling pathway
mTOR signaling pathway
Mitophagy - animal
MicroRNAs in cancer
Lysosome
Human papillomavirus infection
HIF-1 signaling pathway
Glycosaminoglycan biosynthesis - chondroitin ...
Galactose metabolism
Endocytosis
Endocrine resistance
Chronic myeloid leukemia
Cellular senescence
Cell cycle
AMPK signaling pathway
0.02
0.04
0.06
GeneRatio
Count
40
80
120
160
padj
1.00
0.75
0.50
0.25
0.00
KD_ACvsCTRL_AC.all
Cell cycle (n=91)
MicroRNAs in cancer (n=96)
Lysosome (n=76)
Vasopressin-regulated water reabsorption (n=30)
Mitophagy - animal (n=44)
p53 signaling pathway (n=47)
Proteasome (n=29)
Cellular senescence (n=86)
Endocrine resistance (n=55)
HIF-1 signaling pathway (n=54)
Human papillomavirus infection (n=161)
mTOR signaling pathway (n=79)
Galactose metabolism (n=18)
Chronic myeloid leukemia (n=47)
Oocyte meiosis (n=62)
AMPK signaling pathway (n=61)
Renal cell carcinoma (n=40)
Neurotrophin signaling pathway (n=64)
Glycosaminoglycan biosynthesis - ... (n=14)
Endocytosis (n=122)
0
2
4
6
8
-log10(padj)

Figure 20

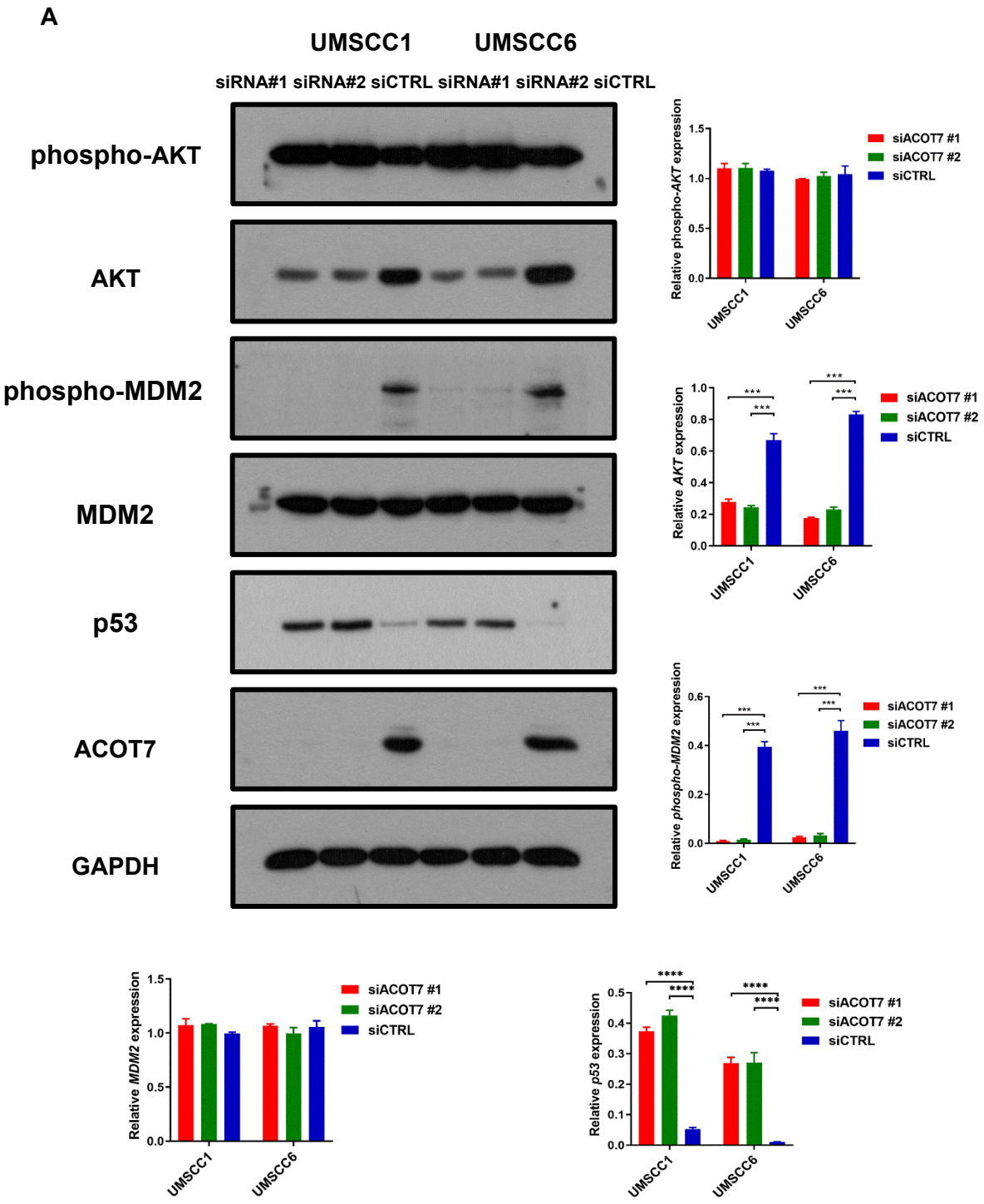
A
UMSCC1
UMSCC6
siRNA#1 siRNA#2 siCTRL siRNA#1 siRNA#2 siCTRL
phospho-AKT
AKT
phospho-MDM2
MDM2
p53
ACOT7
GAPDH
Relative phospho-AKT expression
Relative AKT expression
Relative phospho-MDM2 expression
Relative MDM2 expression
Relative p53 expression
siACOT7 #1
siACOT7 #2
siCTRL
UMSCC1
UMSCC6

Figure 21

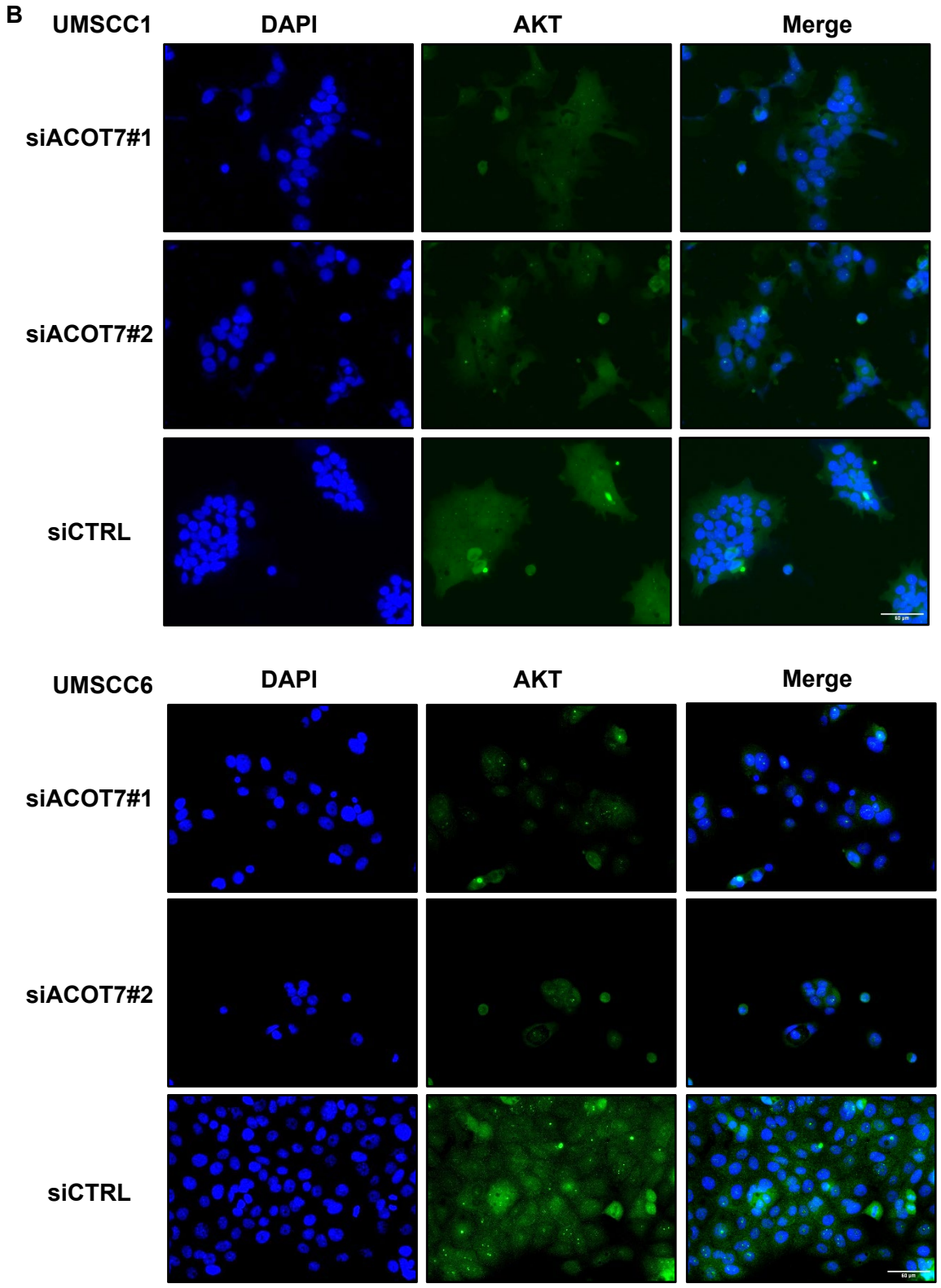
B
UMSCC1
DAPI
AKT
Merge
siACOT7#1
siACOT7#2
siCTRL
UMSCC6
DAPI
AKT
Merge
siACOT7#1
siACOT7#2
siCTRL

Figure 21

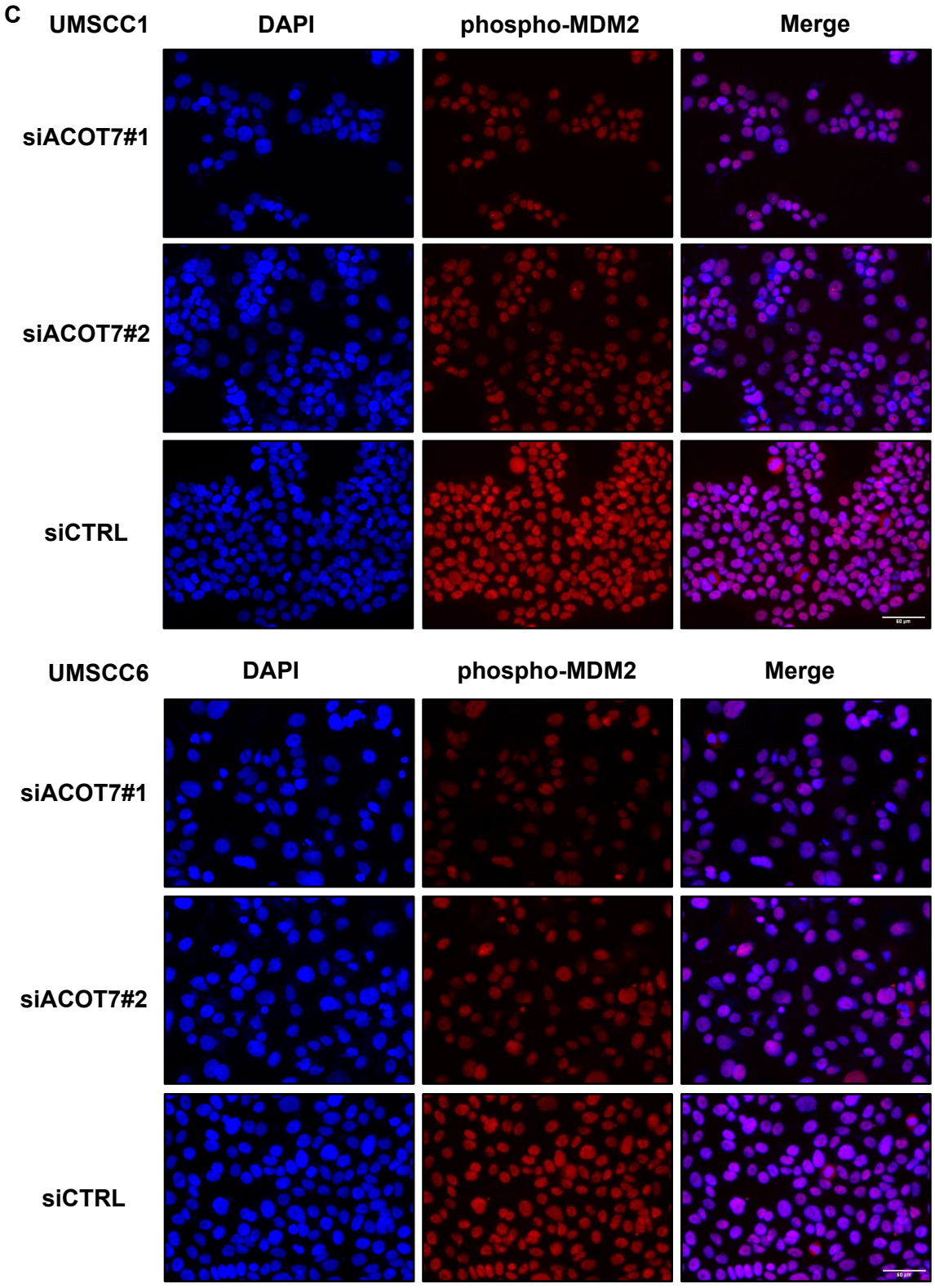
C
UMSCC1
DAPI
phospho-MDM2
Merge
siACOT7#1
siACOT7#2
siCTRL
UMSCC6
DAPI
phospho-MDM2
Merge
siACOT7#1
siACOT7#2
siCTRL

Figure 21

D

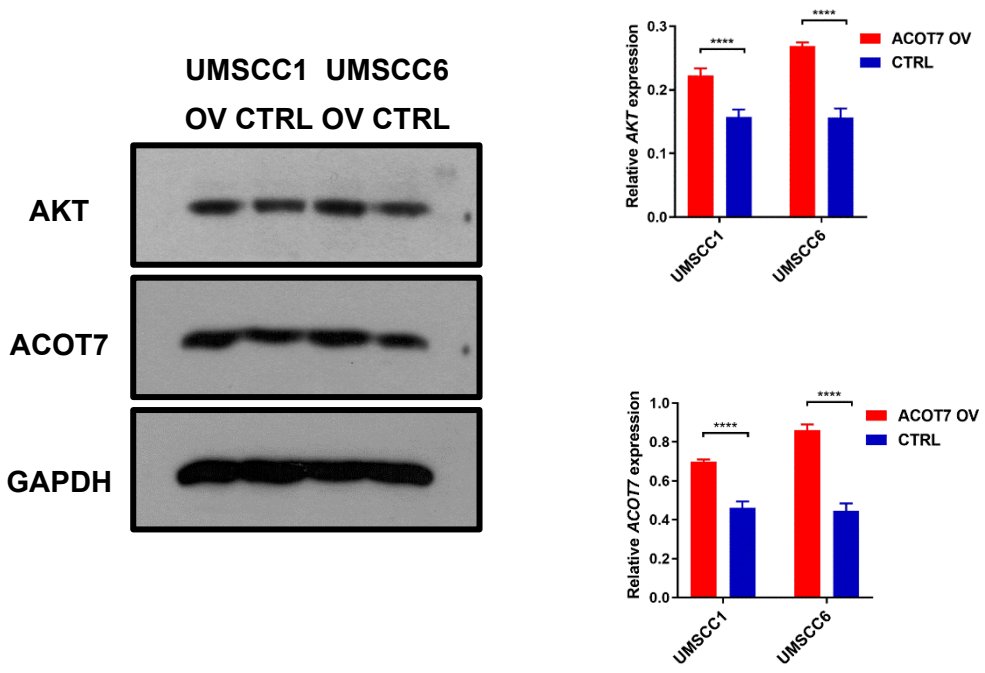
UMSCC1 UMSCC6
OV CTRL OV CTRL
AKT
ACOT7
GAPDH
Relative AKT expression
0.3
0.2
0.1
0.0
****
****
ACOT7 OV
CTRL
UMSCC1
UMSCC6
Relative ACOT7 expression
1.0
0.8
0.6
0.4
0.2
0.0
****
****
ACOT7 OV
CTRL
UMSCC1
UMSCC6

Figure 21

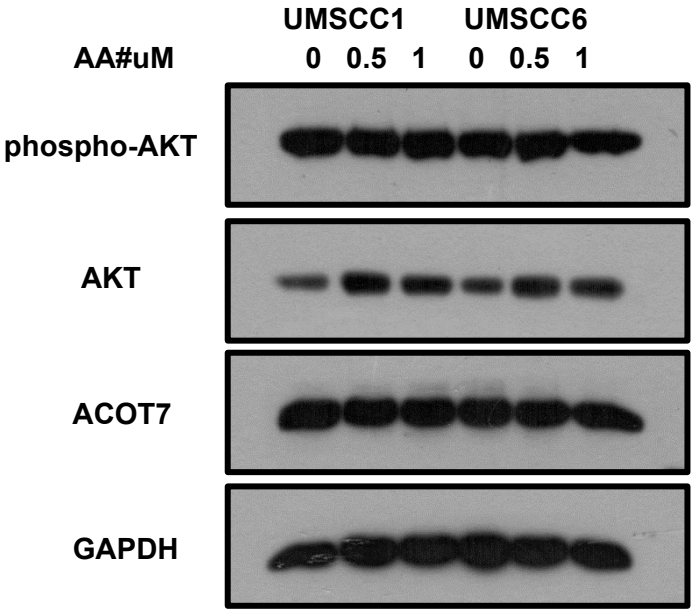
UMSCC1
UMSCC6
AA#uM
0 0.5 1 0 0.5 1
phospho-AKT
AKT
ACOT7
GAPDH

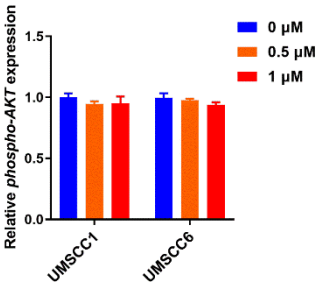
Relative phospho-AKT expression
0 μM
0.5 μM
1 μM
UMSCC1
UMSCC6

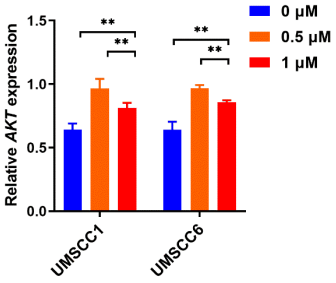
Relative AKT expression
0 μM
0.5 μM
1 μM
**
UMSCC1
UMSCC6

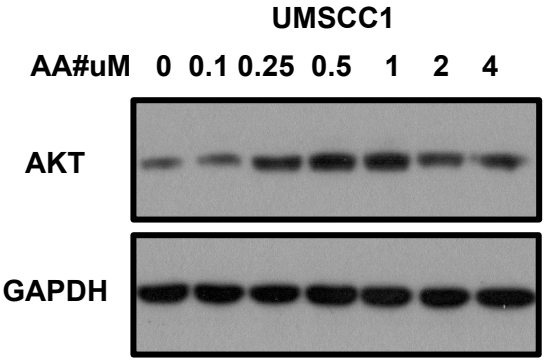
UMSCC1
AA#uM 0 0.1 0.25 0.5 1 2 4
AKT
GAPDH

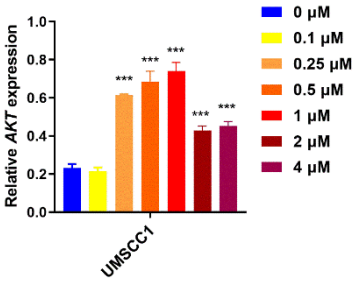
Relative AKT expression
0 μM
0.1 μM
0.25 μM
0.5 μM
1 μM
2 μM
4 μM
***
UMSCC1

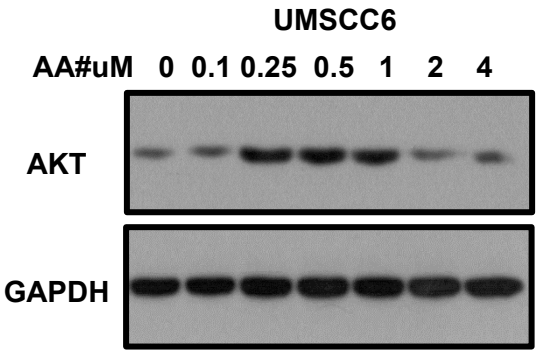
UMSCC6
AA#uM 0 0.1 0.25 0.5 1 2 4
AKT
GAPDH

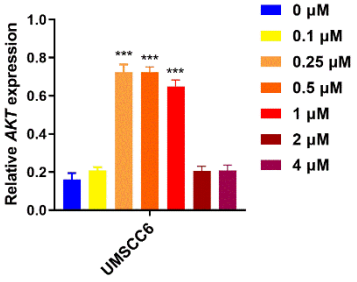
Relative AKT expression
0 μM
0.1 μM
0.25 μM
0.5 μM
1 μM
2 μM
4 μM
***
UMSCC6

Figure 22

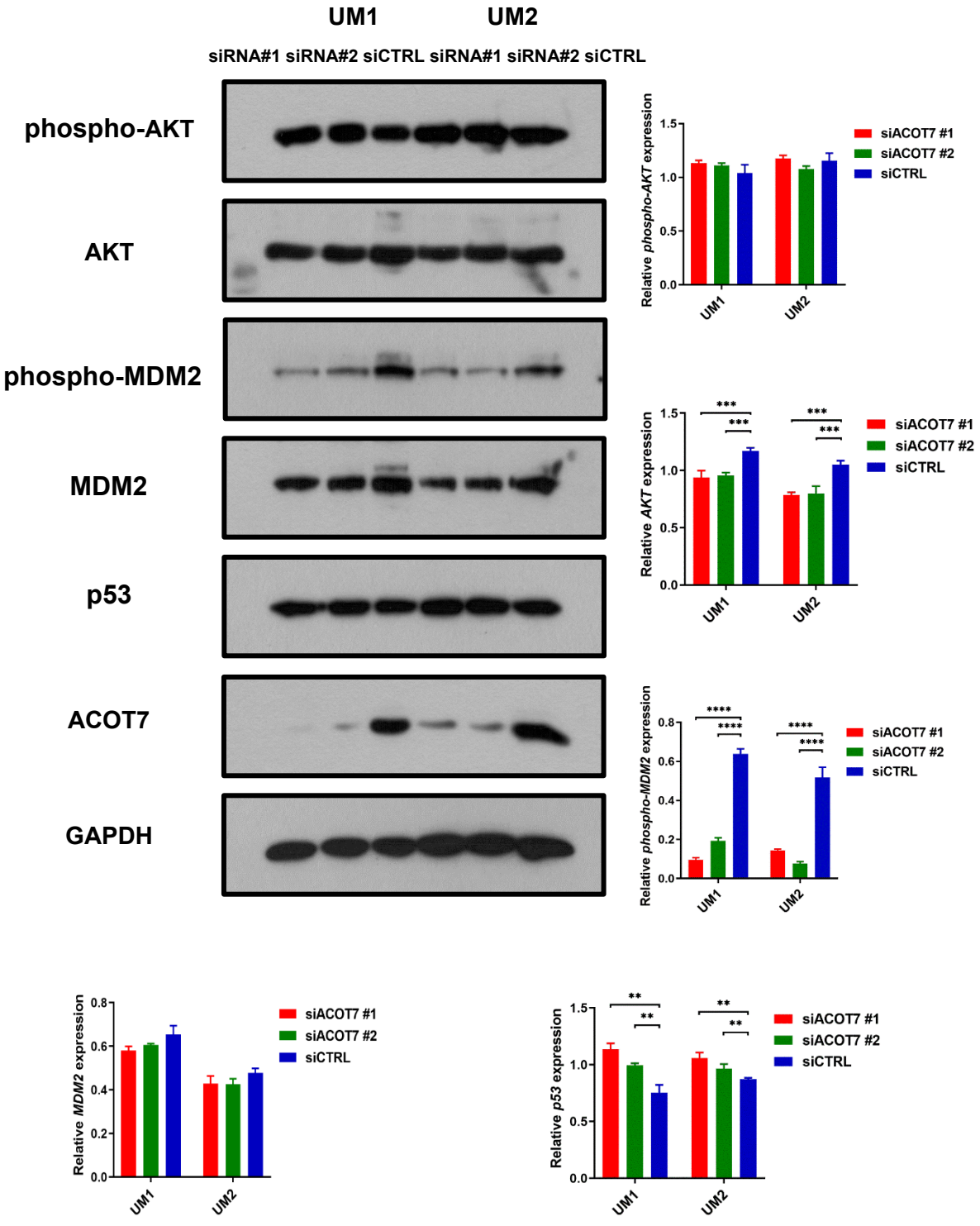
UM1
UM2
siRNA#1 siRNA#2 siCTRL siRNA#1 siRNA#2 siCTRL
phospho-AKT
AKT
phospho-MDM2
MDM2
p53
ACOT7
GAPDH
Relative phospho-AKT expression
Relative AKT expression
Relative phospho-MDM2 expression
Relative MDM2 expression
Relative p53 expression
siACOT7 #1
siACOT7 #2
siCTRL
UM1
UM2

Figure 23

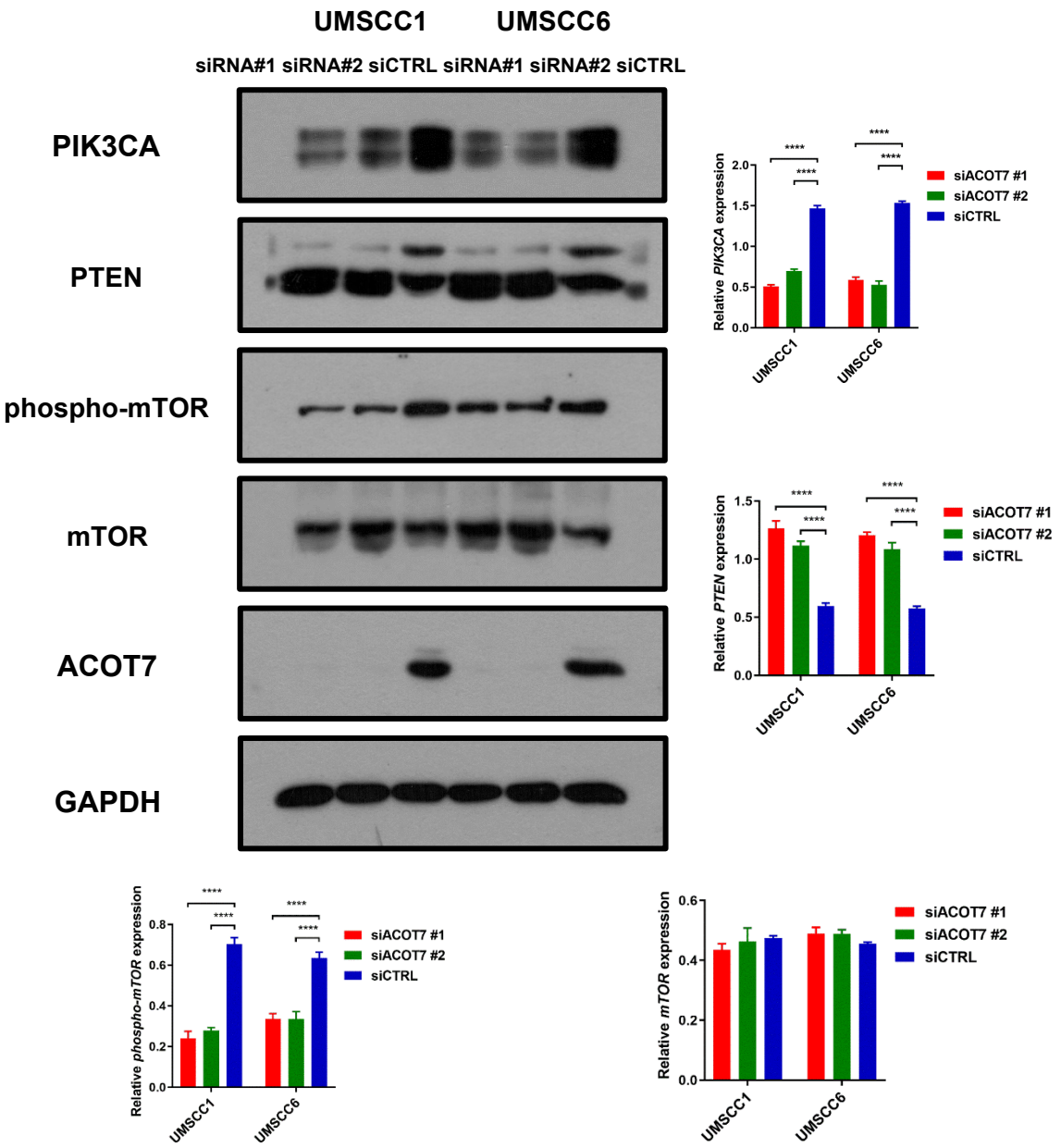
UMSCC1
UMSCC6
siRNA#1 siRNA#2 siCTRL siRNA#1 siRNA#2 siCTRL
PIK3CA
PTEN
phospho-mTOR
mTOR
ACOT7
GAPDH
Relative PIK3CA expression
Relative PTEN expression
Relative phospho-mTOR expression
Relative mTOR expression
siACOT7 #1
siACOT7 #2
siCTRL
UMSCC1
UMSCC6
****

Figure 24

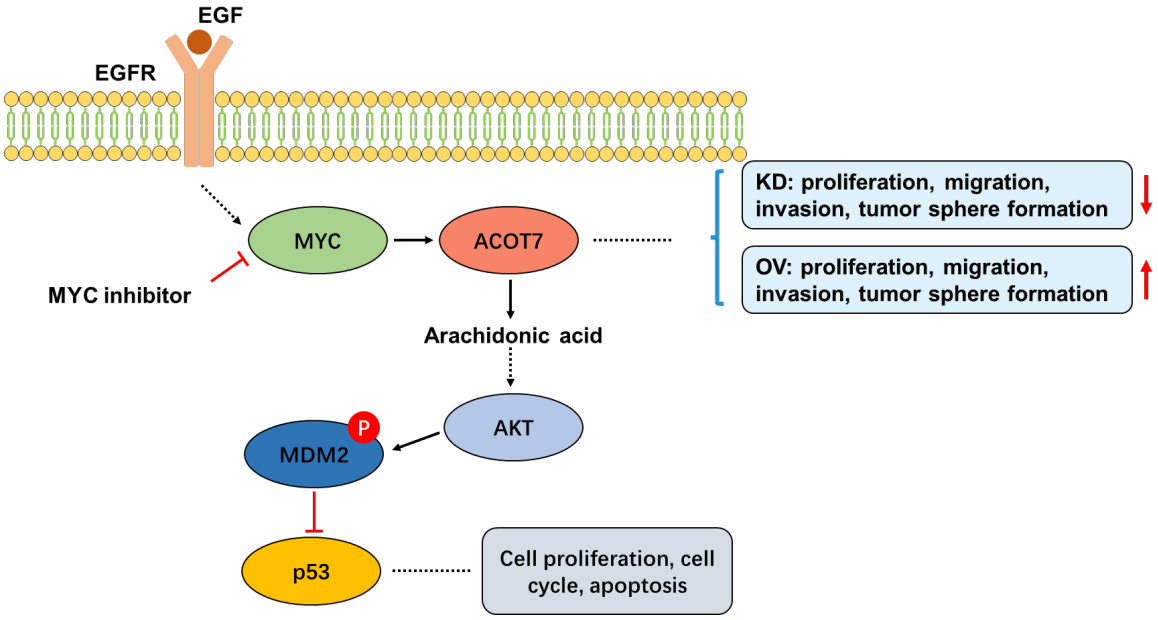
EGF
EGFR
MYC
ACOT7
MYC inhibitor
KD: proliferation, migration, invasion, tumor sphere formation
OV: proliferation, migration, invasion, tumor sphere formation
Arachidonic acid
AKT
P
MDM2
p53
Cell proliferation, cell cycle, apoptosis

Figure 25

SUPPLEMENTARY MATERIALS

Table 1. Primers used in this project.

Gene	Sequence
ACOT7 Promoter Forward	TCTCCCTTCTTGGGTGTTTTT
ACOT7 Promoter Reverse	CTTTTACTGGGAGCGCTGAG

Table 2. Antibodies used in this project.

Primary Antibodies	Species	Type	Supplier
ACOT7	Rabbit	Polyclonal	Proteintech Group, Inc
ACOT7	Rabbit	Polyclonal	Invitrogen
MYC	Mouse	Monoclonal	Santa Cruz Biotechnology, Inc.
AKT	Rabbit	Polyclonal	Proteintech Group, Inc
Phospho-AKT	Rabbit	Monoclonal	Cell Signaling Technology
MDM2	Mouse	Monoclonal	Proteintech Group, Inc
Phospho-MDM2	Rabbit	Polyclonal	Invitrogen
p53	Rabbit	Polyclonal	Proteintech Group, Inc
PI3KCA	Mouse	Monoclonal	Proteintech Group, Inc
PTEN	Rabbit	Polyclonal	Proteintech Group, Inc
Phospho-mTOR	Mouse	Monoclonal	Proteintech Group, Inc
mTOR	Mouse	Monoclonal	Proteintech Group, Inc

Table 3. A list of top 20 upregulated/ downregulated genes list following ACOT7 downregulation in UMSCC1 cells.

Top 20 upregulated genes	Top 20 downregulated genes
ANKRD1	RAB7B
NPPB	KNDC1
SLC2A3	BGN
MFAP5	CALML3
RUBCNL	SOX21-AS1
FOXJ1	AL365356.3
AP001271.2	LINC01348
AC109588.1	GPR85
LINC02474	LINC00475
PDE3A	TMEM173
LINC00824	CLCA2
CDH5	PRODH
TPM3P6	CCDC8
AC005392.1	ELFN1
VSTM1	ANXA10
TGFB2-AS1	IGSF10
TGFB2	AC009630.2
PI3	COX7A1
KRTAP2-3	BBOX1
AP000892.3	LINC01546

Table 4. A list of top 20 upregulated/ downregulated genes following ACOT7 downregulation in UMSCC23 cells.

Top 20 upregulated genes	Top 20 downregulated genes
RSAD2	ACOT7
SLC2A3	SCGB1A1
NPPB	AC114550.1
FP671120.1	AP003390.1
IFI44L	AL078590.2
AC108515.1	CHRNA9
RBMS1P1	AC114550.3
VIL1	AC046185.3
CMPK2	AL355388.2
ANKRD1	PABPC4L
MYL7	RF00410
IGSF23	RASGEF1B
AP000892.3	RN7SL151P
HIF1A-AS2	MMP9
AC105411.1	AL160408.1
GRIP2	AVPR2
AC011448.1	ITGA7
SMCO2	NPR2
RGS6	GMNC
LINC00520	LINC01958

REFERENCES

1. Price, K.A. and E.E. Cohen, *Current treatment options for metastatic head and neck cancer.* Curr Treat Options Oncol, 2012. **13**(1): p. 35-46.
2. Son, E., et al., *Cancers of the Major Salivary Gland.* J Oncol Pract, 2018. **14**(2): p. 99-108.
3. Siegel, R.L., et al., *Cancer Statistics, 2021.* CA Cancer J Clin, 2021. **71**(1): p. 7-33.
4. Bray, F., et al., *Global estimates of cancer prevalence for 27 sites in the adult population in 2008.* Int J Cancer, 2013. **132**(5): p. 1133-45.
5. Lambert, R., et al., *Epidemiology of cancer from the oral cavity and oropharynx.* Eur J Gastroenterol Hepatol, 2011. **23**(8): p. 633-41.
6. DeSantis, C., D. Naishadham, and A. Jemal, *Cancer statistics for African Americans, 2013.* CA Cancer J Clin, 2013. **63**(3): p. 151-66.
7. Sadri, G. and H. Mahjub, *Tobacco smoking and oral cancer: a meta-analysis.* J Res Health Sci, 2007. **7**(1): p. 18-23.
8. Hashim, D., et al., *Head and neck cancer prevention: from primary prevention to impact of clinicians on reducing burden.* Ann Oncol, 2019. **30**(5): p. 744-756.
9. Chaturvedi, A.K., et al., *Human papillomavirus and rising oropharyngeal cancer incidence in the United States.* J Clin Oncol, 2011. **29**(32): p. 4294-301.
10. Adelstein, D.J., et al., *Head and neck squamous cell cancer and the human papillomavirus: summary of a National Cancer Institute State of the Science Meeting,*

November 9-10, 2008, Washington, D.C. Head Neck, 2009. **31**(11): p. 1393-422.

11. Boffetta, P., et al., *Occupation and larynx and hypopharynx cancer: an international case-control study in France, Italy, Spain, and Switzerland.* Cancer Causes Control, 2003. **14**(3): p. 203-12.

12. Chien, Y.C., et al., *Serologic markers of Epstein-Barr virus infection and nasopharyngeal carcinoma in Taiwanese men.* N Engl J Med, 2001. **345**(26): p. 1877-82.

13. Yu, M.C. and J.M. Yuan, *Epidemiology of nasopharyngeal carcinoma.* Semin Cancer Biol, 2002. **12**(6): p. 421-9.

14. Beltz, A., et al., *[Staging of oropharyngeal carcinomas : New TNM classification as a challenge for head and neck cancer centers].* HNO, 2018. **66**(5): p. 375-382.

15. Glastonbury, C.M., *Critical Changes in the Staging of Head and Neck Cancer.* Radiol Imaging Cancer, 2020. **2**(1): p. e190022.

16. Deshpande, A.M. and D.T. Wong, *Molecular mechanisms of head and neck cancer.* Expert Rev Anticancer Ther, 2008. **8**(5): p. 799-809.

17. Johnson, D.E., et al., *Head and neck squamous cell carcinoma.* Nat Rev Dis Primers, 2020. **6**(1): p. 92.

18. Reinhardt, H.C. and B. Schumacher, *The p53 network: cellular and systemic DNA damage responses in aging and cancer.* Trends Genet, 2012. **28**(3): p. 128-36.

19. Zhou, G., Z. Liu, and J.N. Myers, *TP53 Mutations in Head and Neck Squamous Cell Carcinoma and Their Impact on Disease Progression and Treatment Response.* J Cell

Biochem, 2016. **117**(12): p. 2682-2692.

20. Kriegs, M., et al., *Analyzing expression and phosphorylation of the EGF receptor in HNSCC.* Sci Rep, 2019. **9**(1): p. 13564.

21. Kalyankrishna, S. and J.R. Grandis, *Epidermal growth factor receptor biology in head and neck cancer.* J Clin Oncol, 2006. **24**(17): p. 2666-72.

22. Herrero, R., *Chapter 7: Human papillomavirus and cancer of the upper aerodigestive tract.* J Natl Cancer Inst Monogr, 2003(31): p. 47-51.

23. Furniss, C.S., et al., *Human papillomavirus 16 and head and neck squamous cell carcinoma.* Int J Cancer, 2007. **120**(11): p. 2386-92.

24. Chai, R.C., et al., *Current trends in the etiology and diagnosis of HPV-related head and neck cancers.* Cancer Med, 2015. **4**(4): p. 596-607.

25. Monnier, Y. and C. Simon, *Surgery Versus Radiotherapy for Early Oropharyngeal Tumors: a Never-Ending Debate.* Curr Treat Options Oncol, 2015. **16**(9): p. 42.

26. Marur, S. and A.A. Forastiere, *Head and Neck Squamous Cell Carcinoma: Update on Epidemiology, Diagnosis, and Treatment.* Mayo Clin Proc, 2016. **91**(3): p. 386-96.

27. Zhao, X. and L. Cui, *A robust six-miRNA prognostic signature for head and neck squamous cell carcinoma.* J Cell Physiol, 2020.

28. Hunt, M.C. and S.E. Alexson, *The role Acyl-CoA thioesterases play in mediating intracellular lipid metabolism.* Prog Lipid Res, 2002. **41**(2): p. 99-130.

29. Jung, S.H., et al., *Acyl-CoA thioesterase 7 is involved in cell cycle progression via*

regulation of PKCzeta-p53-p21 signaling pathway. Cell Death Dis, 2017. **8**(5): p. e2793.

30. Kang, H.W., et al., *Thioesterase superfamily member 2/acyl-CoA thioesterase 13 (Them2/Acot13) regulates hepatic lipid and glucose metabolism.* FASEB J, 2012. **26**(5): p. 2209-21.

31. Kirkby, B., et al., *Functional and structural properties of mammalian acyl-coenzyme A thioesterases.* Prog Lipid Res, 2010. **49**(4): p. 366-77.

32. Svensson, L.T., S.E.H. Alexson, and J.K. Hiltunen, *Very Long-Chain and Long-Chain Acyl-Coa Thioesterases in Rat-Liver Mitochondria - Identification, Purification, Characterization, and Induction by Peroxisome Proliferators.* Journal of Biological Chemistry, 1995. **270**(20): p. 12177-12183.

33. Westin, M.A., S.E. Alexson, and M.C. Hunt, *Molecular cloning and characterization of two mouse peroxisome proliferator-activated receptor alpha (PPARalpha)-regulated peroxisomal acyl-CoA thioesterases.* J Biol Chem, 2004. **279**(21): p. 21841-8.

34. Lindquist, P.J., L.T. Svensson, and S.E. Alexson, *Molecular cloning of the peroxisome proliferator-induced 46-kDa cytosolic acyl-CoA thioesterase from mouse and rat liver--recombinant expression in Escherichia coli, tissue expression, and nutritional regulation.* Eur J Biochem, 1998. **251**(3): p. 631-40.

35. Hunt, M.C., et al., *A revised nomenclature for mammalian acyl-CoA thioesterases/hydrolases.* J Lipid Res, 2005. **46**(9): p. 2029-32.

36. Brocker, C., et al., *Evolutionary divergence and functions of the human acyl-CoA*

thioesterase gene (ACOT) family. Hum Genomics, 2010. **4**(6): p. 411-20.

37. Tillander, V., S.E.H. Alexson, and D.E. Cohen, *Deactivating Fatty Acids: Acyl-CoA Thioesterase-Mediated Control of Lipid Metabolism.* Trends Endocrinol Metab, 2017. **28**(7): p. 473-484.

38. Yamada, J., *Long-chain acyl-CoA hydrolase in the brain.* Amino Acids, 2005. **28**(3): p. 273-8.

39. Yamada, J., et al., *Long-chain acyl-CoA hydrolase from rat brain cytosol: purification, characterization, and immunohistochemical localization.* Arch Biochem Biophys, 1996. **326**(1): p. 106-14.

40. Zhang, X., et al., *Expression level of ACOT7 influences the prognosis in acute myeloid leukemia patients.* Cancer Biomark, 2019. **26**(4): p. 441-449.

41. Ellis, J.M., G.W. Wong, and M.J. Wolfgang, *Acyl coenzyme A thioesterase 7 regulates neuronal fatty acid metabolism to prevent neurotoxicity.* Mol Cell Biol, 2013. **33**(9): p. 1869-82.

42. Sakuma, S., et al., *Simultaneous measurement of prostaglandin and arachidonoyl CoA formed from arachidonic acid in rabbit kidney medulla microsomes: the roles of Zn2+ and Cu2+ as modulators of formation of the two products.* Prostaglandins Leukotrienes and Essential Fatty Acids, 1999. **61**(2): p. 105-112.

43. Bagci, O. and S. Kurtgoz, *Amplification of Cellular Oncogenes in Solid Tumors.* N Am J Med Sci, 2015. **7**(8): p. 341-6.

44. Yamada, J., et al., *Purification, molecular cloning, and genomic organization of human brain long-chain acyl-CoA hydrolase.* J Biochem, 1999. **126**(6): p. 1013-9.

45. Wang, Z., M.A. Jensen, and J.C. Zenklusen, *A Practical Guide to The Cancer Genome Atlas (TCGA).* Methods Mol Biol, 2016. **1418**: p. 111-41.

46. Seiler, M., et al., *Somatic Mutational Landscape of Splicing Factor Genes and Their Functional Consequences across 33 Cancer Types.* Cell Reports, 2018. **23**(1): p. 282-+.

47. Barrett, T., et al., *NCBI GEO: archive for functional genomics data sets--update.* Nucleic Acids Res, 2013. **41**(Database issue): p. D991-5.

48. Barrett, T., et al., *NCBI GEO: archive for functional genomics data sets--10 years on.* Nucleic Acids Res, 2011. **39**(Database issue): p. D1005-10.

49. Wang, F., et al., *ACOT1 expression is associated with poor prognosis in gastric adenocarcinoma.* Human Pathology, 2018. **77**: p. 35-44.

50. Ni, C., et al., *ACOT4 accumulation via AKT-mediated phosphorylation promotes pancreatic tumourigenesis.* Cancer Lett, 2021. **498**: p. 19-30.

51. Xu, C.L., et al., *Acyl-CoA Thioesterase 8 and 11 as Novel Biomarkers for Clear Cell Renal Cell Carcinoma.* Frontiers in Genetics, 2020. **11**.

52. Lu, M., et al., *ACOT12-Dependent Alteration of Acetyl-CoA Drives Hepatocellular Carcinoma Metastasis by Epigenetic Induction of Epithelial-Mesenchymal Transition.* Cell Metab, 2019. **29**(4): p. 886-900 e5.

53. Feng, H.Q. and X.J. Liu, *Interaction between ACOT7 and LncRNA NMRAL2P via*

Methylation Regulates Gastric Cancer Progression. Yonsei Medical Journal, 2020. **61**(6): p. 471-481.

54. Ma, B., et al., *Transcriptome Analyses Identify a Metabolic Gene Signature Indicative of Dedifferentiation of Papillary Thyroid Cancer.* J Clin Endocrinol Metab, 2019. **104**(9): p. 3713-3725.

55. Liu, K.T., et al., *Regulatory mechanism of fatty acid-CoA metabolic enzymes under endoplasmic reticulum stress in lung cancer.* Oncology Reports, 2018. **40**(5): p. 2674-2682.

56. Sumantran, V.N., P. Mishra, and N. Sudhakar, *Microarray analysis of differentially expressed genes regulating lipid metabolism during melanoma progression.* Indian J Biochem Biophys, 2015. **52**(2): p. 125-31.

57. Zhang, T., et al., *Identification of Mitochondrial-Related Prognostic Biomarkers Associated With Primary Bile Acid Biosynthesis and Tumor Microenvironment of Hepatocellular Carcinoma.* Front Oncol, 2021. **11**: p. 587479.

58. Dang, C.V., A. Le, and P. Gao, *MYC-induced cancer cell energy metabolism and therapeutic opportunities.* Clin Cancer Res, 2009. **15**(21): p. 6479-83.

59. Baltaci, E., et al., *CT120: A New Potential Target for c-Myc in Head and Neck Cancers.* J Cancer, 2017. **8**(5): p. 880-886.

60. Stine, Z.E., et al., *MYC, Metabolism, and Cancer.* Cancer Discov, 2015. **5**(10): p. 1024-39.

61. Casciano, J.C., et al., *MYC regulates fatty acid metabolism through a multigenic program in claudin-low triple negative breast cancer.* Br J Cancer, 2020. **122**(6): p. 868-884.

62. Field, J.K., et al., *Elevated expression of the c-myc oncoprotein correlates with poor prognosis in head and neck squamous cell carcinoma.* Oncogene, 1989. **4**(12): p. 1463-8.

63. Xu, B., et al., *c-MYC depletion potentiates cisplatin-induced apoptosis in head and neck squamous cell carcinoma: involvement of TSP-1 up-regulation.* Ann Oncol, 2010. **21**(3): p. 670-672.

64. Edmunds, L.R., et al., *c-Myc programs fatty acid metabolism and dictates acetyl-CoA abundance and fate.* J Biol Chem, 2015. **290**(33): p. 20100.

65. Zirath, H., et al., *MYC inhibition induces metabolic changes leading to accumulation of lipid droplets in tumor cells.* Proc Natl Acad Sci U S A, 2013. **110**(25): p. 10258-63.

66. Gupta, A., et al., *PAK2-c-Myc-PKM2 axis plays an essential role in head and neck oncogenesis via regulating Warburg effect.* Cell Death Dis, 2018. **9**(8): p. 825.

67. Rizzo, M.T., *The role of arachidonic acid in normal and malignant hematopoiesis.* Prostaglandins Leukot Essent Fatty Acids, 2002. **66**(1): p. 57-69.

68. Villegas-Comonfort, S., et al., *Arachidonic acid promotes migration and invasion through a PI3K/Akt-dependent pathway in MDA-MB-231 breast cancer cells.* Prostaglandins Leukotrienes and Essential Fatty Acids, 2014. **90**(5): p. 169-177.

69. Neufeld, E.J., et al., *High-Affinity Esterification of Eicosanoid Precursor Fatty-Acids by Platelets.* Journal of Clinical Investigation, 1983. **72**(1): p. 214-220.

70. Needleman, P., et al., *Arachidonic acid metabolism.* Annu Rev Biochem, 1986. **55**: p. 69-102.

71. McCarty, M.F. and J.J. DiNicolantonio, *Minimizing Membrane Arachidonic Acid Content as a Strategy for Controlling Cancer: A Review.* Nutrition and Cancer-an International Journal, 2018. **70**(6): p. 840-850.

72. Tang, N.T., et al., *Fatty-Acid Uptake in Prostate Cancer Cells Using Dynamic Microfluidic Raman Technology.* Molecules, 2020. **25**(7).

73. Tawadros, T., et al., *Ligand-independent activation of EphA2 by arachidonic acid induces metastasis-like behaviour in prostate cancer cells.* Br J Cancer, 2012. **107**(10): p. 1737-44.

74. Gottlieb, T.M., et al., *Cross-talk between Akt, p53 and Mdm2: possible implications for the regulation of apoptosis.* Oncogene, 2002. **21**(8): p. 1299-1303.

75. Sherr, C.J., *Tumor surveillance via the ARF-p53 pathway.* Genes Dev, 1998. **12**(19): p. 2984-91.

76. Ogawara, Y., et al., *Akt enhances Mdm2-mediated ubiquitination and degradation of p53.* J Biol Chem, 2002. **277**(24): p. 21843-50.

77. Woods, D.B. and K.H. Vousden, *Regulation of p53 function.* Exp Cell Res, 2001. **264**(1): p. 56-66.

78. Fuchs, S.Y., et al., *Mdm2 association with p53 targets its ubiquitination.* Oncogene, 1998. **17**(19): p. 2543-7.

79. Zhou, B.P., et al., *HER-2/neu induces p53 ubiquitination via Akt-mediated MDM2 phosphorylation.* Nat Cell Biol, 2001. **3**(11): p. 973-82.

80. Mayo, L.D. and D.B. Donner, *A phosphatidylinositol 3-kinase/Akt pathway promotes translocation of Mdm2 from the cytoplasm to the nucleus.* Proc Natl Acad Sci U S A, 2001. **98**(20): p. 11598-603.

81. Hughes-Fulford, M., et al., *Arachidonic acid activates phosphatidylinositol 3-kinase signaling and induces gene expression in prostate cancer.* Cancer Res, 2006. **66**(3): p. 1427-33.

82. Lee, S.H., M.Y. Lee, and H.J. Han, *Short-period hypoxia increases mouse embryonic stem cell proliferation through cooperation of arachidonic acid and PI3K/Akt signalling pathways.* Cell Prolif, 2008. **41**(2): p. 230-47.

83. Wang, L., et al., *DEGseq: an R package for identifying differentially expressed genes from RNA-seq data.* Bioinformatics, 2010. **26**(1): p. 136-8.

84. Kanehisa, M. and S. Goto, *KEGG: kyoto encyclopedia of genes and genomes.* Nucleic Acids Res, 2000. **28**(1): p. 27-30.

85. Chen, H., H.D. Liu, and G.L. Qing, *Targeting oncogenic Myc as a strategy for cancer treatment.* Signal Transduction and Targeted Therapy, 2018. **3**.

86. Meyer, N. and L.Z. Penn, *Reflecting on 25 years with MYC.* Nat Rev Cancer, 2008.

8(12): p. 976-90.

87. Blackwood, E.M. and R.N. Eisenman, *Max - a Helix-Loop-Helix Zipper Protein That Forms a Sequence-Specific DNA-Binding Complex with Myc.* Science, 1991. **251**(4998): p. 1211-1217.

88. Nie, Z.Q., et al., *c-Myc Is a Universal Amplifier of Expressed Genes in Lymphocytes and Embryonic Stem Cells.* Cell, 2012. **151**(1): p. 68-79.

89. Bretones, G., M.D. Delgado, and J. Leon, *Myc and cell cycle control.* Biochim Biophys Acta, 2015. **1849**(5): p. 506-16.

90. Claassen, G.F. and S.R. Hann, *A role for transcriptional repression of p21CIP1 by c-Myc in overcoming transforming growth factor beta -induced cell-cycle arrest.* Proc Natl Acad Sci U S A, 2000. **97**(17): p. 9498-503.

91. Vlach, J., et al., *Growth arrest by the cyclin-dependent kinase inhibitor p27(Kip1) is abrogated by c-Myc.* Embo Journal, 1996. **15**(23): p. 6595-6604.

92. Zeller, K.I., et al., *Global mapping of c-Myc binding sites and target gene networks in human B cells.* Proc Natl Acad Sci U S A, 2006. **103**(47): p. 17834-9.

93. Li, Z., et al., *A global transcriptional regulatory role for c-Myc in Burkitt's lymphoma cells.* Proc Natl Acad Sci U S A, 2003. **100**(14): p. 8164-9.

94. McMahon, S.B., *MYC and the control of apoptosis.* Cold Spring Harb Perspect Med, 2014. **4**(7): p. a014407.

95. Wang, R., et al., *The transcription factor Myc controls metabolic reprogramming upon T*

lymphocyte activation. Immunity, 2011. **35**(6): p. 871-82.

96. Sakai, M., et al., *Arachidonic acid and cancer risk: a systematic review of observational studies.* BMC Cancer, 2012. **12**: p. 606.

97. Ghosh, J. and C.E. Myers, *Arachidonic acid stimulates prostate cancer cell growth: critical role of 5-lipoxygenase.* Biochem Biophys Res Commun, 1997. **235**(2): p. 418-23.

98. Wang, B., et al., *Metabolism pathways of arachidonic acids: mechanisms and potential therapeutic targets.* Signal Transduct Target Ther, 2021. **6**(1): p. 94.

99. Xin, C., et al., *Expression of Cytosolic Phospholipase A2 (cPLA2)-Arachidonic Acid (AA)-Cyclooxygenase-2 (COX-2) Pathway Factors in Lung Cancer Patients and Its Implication in Lung Cancer Early Detection and Prognosis.* Med Sci Monit, 2019. **25**: p. 5543-5551.

100. Angelucci, A., et al., *Arachidonic acid modulates the crosstalk between prostate carcinoma and bone stromal cells.* Endocrine-Related Cancer, 2008. **15**(1): p. 91-100.

101. Fresno Vara, J.A., et al., *PI3K/Akt signalling pathway and cancer.* Cancer Treat Rev, 2004. **30**(2): p. 193-204.

102. Shi, Y., et al., *Optimal classes of chemotherapeutic agents sensitized by specific small-molecule inhibitors of akt in vitro and in vivo.* Neoplasia, 2005. **7**(11): p. 992-1000.

103. Cantley, L.C. and B.G. Neel, *New insights into tumor suppression: PTEN suppresses tumor formation by restraining the phosphoinositide 3-kinase AKT pathway.* Proceedings of the National Academy of Sciences of the United States of America, 1999. **96**(8): p. 4240-4245.

104. Parcellier, A., et al., *PKB and the mitochondria: AKTing on apoptosis.* Cell Signal, 2008. **20**(1): p. 21-30.

105. Zhou, H.L., et al., *Akt regulates cell survival and apoptosis at a postmitochondrial level.* Journal of Cell Biology, 2000. **151**(3): p. 483-494.

106. Wee, K.B. and B.D. Aguda, *Akt versus p53 in a network of oncogenes and tumor suppressor genes regulating cell survival and death.* Biophys J, 2006. **91**(3): p. 857-65.

107. Levine, A.J., *p53, the cellular gatekeeper for growth and division.* Cell, 1997. **88**(3): p. 323-31.

108. Chen, J., *The Cell-Cycle Arrest and Apoptotic Functions of p53 in Tumor Initiation and Progression.* Cold Spring Harb Perspect Med, 2016. **6**(3): p. a026104.

109. Riley, T., et al., *Transcriptional control of human p53-regulated genes.* Nat Rev Mol Cell Biol, 2008. **9**(5): p. 402-12.

110. Lacroix, M., et al., *Metabolic functions of the tumor suppressor p53: Implications in normal physiology, metabolic disorders, and cancer.* Mol Metab, 2020. **33**: p. 2-22.

111. Goldstein, I. and V. Rotter, *Regulation of lipid metabolism by p53 - fighting two villains with one sword.* Trends Endocrinol Metab, 2012. **23**(11): p. 567-75.

112. Oren, M., *Decision making by p53: life, death and cancer.* Cell Death Differ, 2003. **10**(4): p. 431-42.